



Heinrich Heine
Universität
Düsseldorf



Institut für
Quantitative & Theoretische
Biologie



Studying Multiple Growth Phases of *E. coli* on Minimal Medium with Experiment and Theory

Heinrich-Heine-Universität Düsseldorf

Institute for Quantitative and Theoretical Biology

Institute for Synthetic Microbiology

Bachelor Thesis

Submitted by:
Tobias Pfennig
Mat. No. 2779012

September 6, 2020

Primary Reviewer: Prof. Dr. Oliver Ebenhöh
Secondary Reviewer: Prof. Dr. Ilka Maria Axmann

Abstract

German

Escherichia coli (*E. coli*) zeigt komplexes Verhalten, das schon auf Minimalmedium mit einer einzelnen Kohlenstoff- und Energiequelle auftritt. Ein solches Wachstum wurde hier mit modernen Kultivierungs- und Monitoringverfahren untersucht.

E. coli Stamm W3110Z1 wurde auf M9 Minimalmedium mit Zusatz von Glukose oder Acetat angezogen. Entsprechende Batch-Kultivierungen wurden in einem BioLector Pro Bioreaktor mit Online-Überwachung durchgeführt. Dieses System ermöglicht die spektrometrische Messung verschiedener Kulturparameter (Optische Dichte, pH, gelöster Sauerstoff und Fluoreszenz bei verschiedenen Wellenlängen, beispielsweise zur Quantifizierung von NADH). Bis zu 48 Kulturen werden parallel, in Echtzeit und ohne Probenentnahme überwacht.

Charakteristische Entwicklungen der oben genannten Parameter zeigten getrennte Wachstumsphasen auf. In allen Experimenten begleitete den initialen Lag eine hohe spezifische respirative Aktivität bei nur geringem Anstieg der Biomasse. Die Stationärphase mit stationären Kulturparametern war ebenso in jedem Experiment anzutreffen. Jedoch hing das Verhalten in dem dazwischenliegenden, exponentiellen Wachstum stark von der Art und der Menge der Kohlenstoffquelle sowie der initialen Zelldichte ab.

Bei ausreichendem Glukose-Level wuchs *E. coli* in zwei separaten, exponentiellen Wachstumsphasen. Das Glukose-getriebene Wachstum war von der Ansäuerung des Mediums gezeichnet. Die pH Senkung wurde vermutlich durch Auscheidung von Acetat im Zusammenhang mit Überflussmetabolismus hervorgerufen. Der erneute, leichte Anstieg des pH-Wertes in der folgenden, exponetuellen Phase zeigte möglicherweise den Verbrauch des ausgeschiedenen Acetates an, ging jedoch nur mit geringer Produktion von Biomasse einher. Dieser vermutete Wechsel zwischen Acetat Erzeugung und Verbrauch, genannt *acetat switch*, wurde von einem starken Abfall des Rückstreuungssignals begleitet. Ein ähnlicher Einbruch des Rückstreuungssignals erschien zu Beginn der Stationärphase. Man kann vermuten, dass diese Streuungseinbrüche auf starke Veränderungen in der Zellform oder im Glykogenmetabolismus zurückgehen, als Reaktion der Zellen auf das Aufbrauchen der jeweiligen Kohlenstoffquelle (Glucose oder Acetat).

Zudem deutete ein Wechsel in Wachstumsraten und zellulärer Aktivität darauf hin, dass das Wachstum mit Glukose-Verbrauch ebenfalls in zwei Subphasen unterteilt ist. Auf die Lagphase folgend, wuchs *E. coli* langsam und unter Anhäufung von NADH, jedoch ohne starke Ansäuerung des Mediums als Anzeichen von Acetatausscheidung. Wohlmöglich durch das steigende NADH/NAD⁺-Verhältnis schien der Überflussmetabolismus anschließend eingeleitet zu werden, was zu höheren gemessenen Wachstumsraten und der vermuteten Produktion von Acetat führte.

Ein erster Versuch dieses Wachstumsverhalten zu modellieren war nicht erfolgreich. Abweichungen der Daten von einem quantitativ kaliberten ODE Modell auf Basis der Monod-Gleichung zeigten auf, dass weitreichendere Modelle benötigt werden um solch komplexes Verhalten zu beschreiben. Das exponentielle Wachstum von Zellen auf Acetat als einziger Kohlenstoffquelle war ebenso heterogen. Diese Beobachtungen zeigen die Vielschichtigkeit, die bereits im grundlegenden Metabolismus einzelliger Organismen liegt.

English

Escherichia coli (*E. coli*) shows complex growth behavior that can arise even on minimal synthetic media with a single carbon and energy source. Here, this growth was studied using modern cultivation and monitoring methods.

E. coli strain W3110Z1 was grown on M9 minimal medium with supplemented glucose or acetate. Batch growth experiments were performed in a BioLector Pro bioreactor with online monitoring. This system allows for the spectroscopic measurement of different culture parameters (optical density, pH, dissolved oxygen, and fluorescence at different wavelengths, e.g. to quantify NADH). Up to 48 cultures can be measured in parallel, in real-time and without the need for sampling. Characteristic developments in these parameters showed distinct phases during growth. In all experiments, the initial lag phase was accompanied by strong specific respiratory activity with an only minor increase in biomass. Stationary phases with mostly static culture parameters were also ubiquitous at the end. However, the intermediate, exponential growth depended strongly on the kind and amount of carbon source and the initial cell density.

For sufficient glucose levels, *E. coli* grew in two separate, exponential growth phases. Glucose-fueled growth was accompanied by acidification of the medium, presumably caused by acetate excretion in the process of overflow metabolism. A slight increase of pH in the following exponential phase possibly stemmed from the subsequent consumption of this excreted acetate. However, during the alkalization only little biomass was produced. This shift of acetate production and usage, called acetate switch, was marked by a strong drop in backscattering signal. A similar drop of backscattering appeared at the onset of the stationary phase. These scatter-drops were theorized as changes in cell-shape or glycogen metabolism in reaction to the depletion of the respective carbon source (glucose or acetate).

Importantly, a switch in growth rates and metabolic activities indicated that the growth with uptake of glucose was also divided into two exponential sub-phases. Following the lag phase, *E. coli* first grew slowly with the accumulation of NADH but no acidification of the medium as a sign of acetate production. Possibly triggered by the rising NADH/NAD⁺ ratio, overflow metabolism seemed to be then induced afterward and caused higher growth rates and acetate excretion.

A first attempt at modeling this growth behavior was not successful. Deviations of the data from a quantitatively calibrated ODE Model based on the Monod equation pointed to the need for extended growth models to capture such complex behaviour. The exponential growth of cells grown with acetate as the sole carbon source was heterogeneous as well. These observations show the intricacy that lies even in the basic metabolism of single-celled organisms.

Introduction

Escherichia coli (*E. coli*) is widely utilized in both industry and academic research. Its uses span from the production of biological components to the representation of general single-celled systems as a model organism (Valgepea et al., 2010; Hobman, Penn, and Pallen, 2007). Especially where the efficient and error-free synthesis of components is desired, the used strain of *E. coli* has to be finely described for the used growing environment. Unexpected behavior of the cells may lead to an impaired production up to the emergence of byproducts harming the production strain (Valgepea et al., 2010). This could be detrimental, especially in the synthesis of e.g. medical compounds like insulin (Swartz, 2001). For the use as a model organism, this need for characterization also arises naturally. A solution could be the detailed and quantitative experimental characterization and mathematical modelling of *E. coli* growth dynamics and metabolism. This way, predictions could be made regarding the behavior of *E. coli* in different environments or regarding behavior resulting from modifications of *E. coli* cells (Orth, Palsson, and Fleming, 2010).

1.0.0.1 Diauxie on Glucose

E. coli shows selectivity when provided with multiple potential carbon sources. The underlying principle is known as carbon catabolite repression (CCR), where there is a strict order of preferred carbon sources and the consumption of one source mostly represses the consumption of others (O’Beirne and Hamer, 2000; Loomis and Magasanik, 1967). These phases of each substrates’ consumption are also often separated by lag phases with little to no growth (O’Beirne and Hamer, 2000). Due to this regulatory system, in media with two or more such carbon sources the consumption of each substrate usually causes a separate phase of growth until the particular substrate is exhausted. This effect is known as diauxic growth (Monod, 1949).

Interestingly, even in well aerated culture supplemented with only glucose at higher concentrations a diauxie-like growth can be

observed. This is caused by *E. coli* excreting part of the glucose-supplied carbon as acetate (Wolfe, 2005; Enjalbert et al., 2015; O’Beirne and Hamer, 2000; Andersen and Von Meyenburg, 1980). To achieve this, many enzymes of the tricarboxylic acid (TCA) cycle are down-regulated (Wolfe, 2005; Vemuri et al., 2006). Normally, glucose is metabolized beginning with the glycolysis and resulting in acetyl-coenzyme A (acetyl-CoA) as an intermediate product. This acetyl-CoA is then used by the TCA cycle to generate CO₂, ATP and reduced nicotinamide adenine dinucleotide (NADH). With lowered TCA cycle activity, however, a part of the acetyl-CoA pool is redirected over the pathway formed by the phosphate acetyl-transferase (Pta) and acetate kinase (AckA). This results in acetate excretion (for pathway overview see Fig. 1.1)(Wolfe, 2005; Enjalbert et al., 2015). While typical for anaerobic fermentation, acetate production also occurs under aerobic conditions at high glucose concentrations or, more generally, an imbalance between the carbon/energy source and other nutrients such as the nitrogen source. This process is also well studied in budding yeast (Brauer et al., 2005; Aon and Cortassa, 2001). In *E. coli* the production of acetate during the growth with glucose is called overflow metabolism and can lead to the excretion of up to 15 % of carbon uptake (Wolfe, 2005; Enjalbert et al., 2015). It has been hypothesized that the partial metabolization of glucose that is caused by this process enables *E. coli* to grow more rapidly. The acetyl-CoA redirection both decreases the usage of oxidized nicotinamide adenine dinucleotide (NAD⁺) in the TCA cycle and frees bound CoA. This effectively increases cofactor availability for glycolysis (NAD⁺) and the remaining TCA cycle (CoA-SH). This, in turn, allows for higher metabolic fluxes and thus an increased production of central metabolites (Wolfe, 2005).

As a result of the acetate excretion, *E. coli* induces a second phase of growth after the initial growth on glucose, metabolizing the newly

excreted acetate. The switching between both phases, acetate excretion and assimilation, is known as acetate switch (Wolfe, 2005) and very similar to what is known as the diauxic shift in budding yeast (Brauer et al., 2005). The second growth phase using acetate is characterized by a strongly reduced growth rate in comparison to growth on glucose or acetate alone. As for regular diauxie, both growth phases are also often separated by a lag phase with suspended growth (Enjalbert et al., 2015).

Since acetate is cytotoxic (Wolfe, 2005) and the excretion results in wasteful substrate usage, both overflow metabolism and acetate switch are of interest. This is the case for bioreactor experiments as well as industrial bioreactors, where glucose is a widely used supplement.

1.0.0.2 The BioLector

Modern measurement techniques aid in elucidating such cellular phenomena and in furthering the goal for data-driven modeling. Specialized reactor systems can provide detailed online measurements, i.e. real-time parameter measurements of active bacterial cultures without the need for interruption of the reactor (m2p-labs GmbH, n.d.). Monitoring physiological parameters this way while keeping the environment tightly controlled may give clues about the states of *E. coli* cells at each timepoint (see e.g. Andersen and Von Meyenburg, 1980). This way, the timings, triggers, magnitudes, and phenotypic effects of cellular changes may be examined. This includes overflow metabolism and acetate switch. Additionally, a theorized model may be validated on the data, as it should be able to reproduce such cellular changes and the observed parameter behavior.

A reactor capable of such measurements is the BioLector Pro ("BioLector") by m2p-labs. It is a plate-reader system for liquid cultures with LED-based online measurements, temperature, humidity, and gas control. It allows for up to 48 simultaneously observed cultures, each having a volume of ca. 1 ml. The system was designed to be scalable i.e. the culture-environment is controlled to be similar to large-scale bioreactor setups. This way,

culture-behavior can be expected to be similar as well. The built-in optical measurement system can track the 180° scatter ("scatter"), riboflavin- and NADH-fluorescences, as well as O₂ saturation and pH of the growth medium by utilizing sensor-polymer fluorescence (m2p-labs GmbH, n.d.). The 180° scatter is measured by passing a beam of light into the sample in which this beam is then scattered. The intensity of the scattered light returning to the beams' entry point is recorded. This is used to asses the concentration of biomass, alternatively to measuring optical density (OD). Riboflavin, its derivatives, and NADH are essential molecules of the central metabolism of *E. coli*. Their individual fluorescence is, thus, used to gain an insight into the state of this metabolic network. Riboflavin was also proposed by the manufacturer as an alternative biomass measurement. Observing O₂ saturation and pH levels gives an insight into the culture environment and how it is influences by *E. coli*.

When complemented by appropriate plate layouts and supplementary offline experiments, the BioLector's online measurements allow for a comprehensive view of the growth of *E. coli*.

1.0.0.3 Modeling

Early approaches to generalized, phenotypical models observed the linkage of bacterial growth rate to substrate quantity, ribosomal efficiency, as well as other factors (Scott and Hwa, 2011). This led to the phrasing of so-called growth laws, mathematical descriptions of these empirical findings (Scott and Hwa, 2011). These "laws" provide a framework for cell- to population-level modeling, as new models should be able to show the growth laws' regularities.

One such growth law is the nutrient law proposed by Jacques Monod in 1949. It describes the basic dependency of bacterial growth rate of biomass μ_{BM} on (carbon-) substrate concentration c_S (variable names adjusted for consistency):

$$\mu_{BM} = \mu_{BM,max} \cdot \frac{c_S}{K_S + c_S} \quad (1.1)$$

Where $\mu_{BM,max}$ is the maximal observed growth rate and K_S specifies the substrate concen-

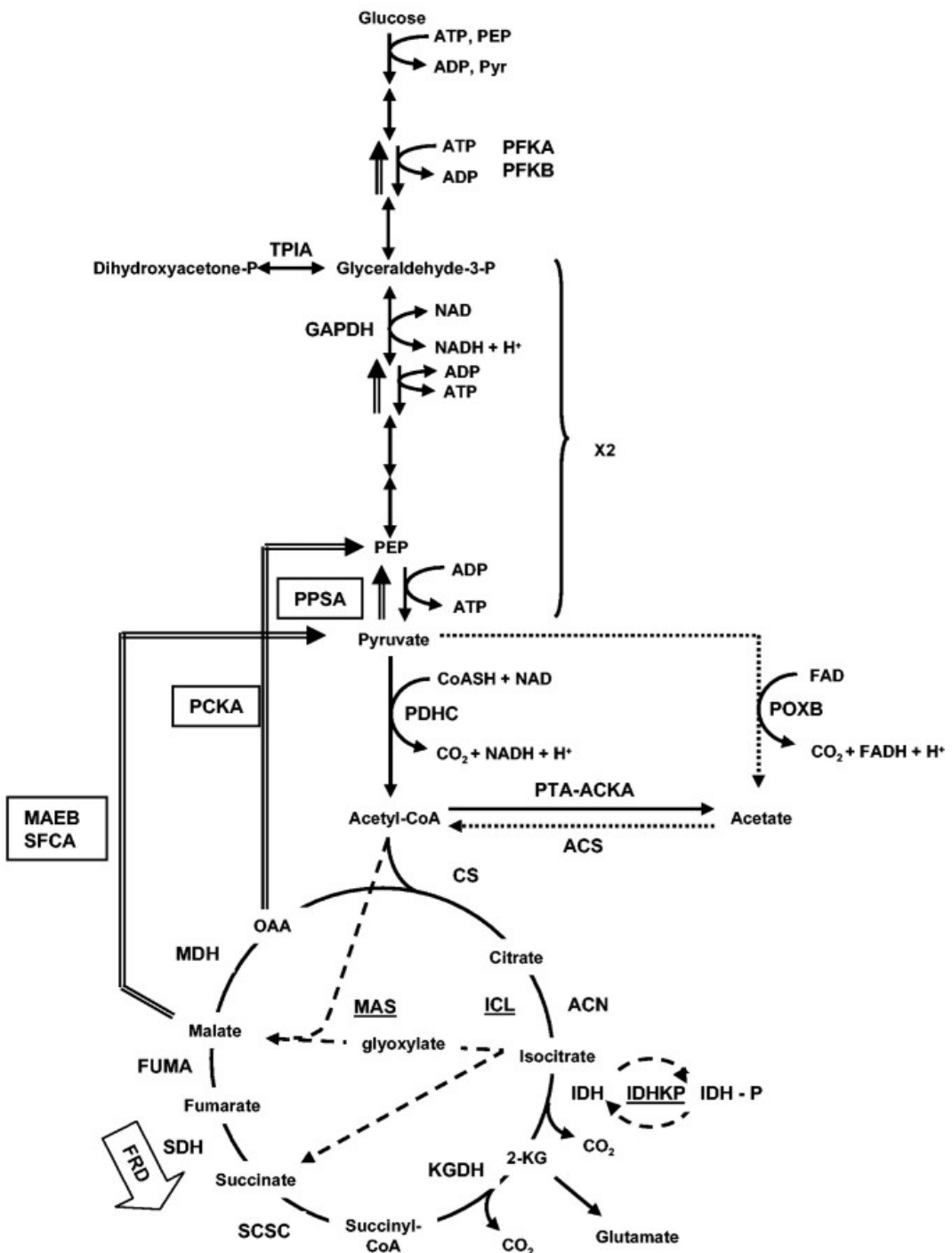


Figure 1.1: **The pathways of central metabolism.** Taken from Wolfe, 2005. Only some of the intermediates and enzymes of glycolysis are noted. PEP, phosphoenolpyruvate; Pyr, pyruvate; PFK, phosphofructokinase; TPIA, triosephosphate isomerase; GAPDH, glyceraldehyde-3-phosphate dehydrogenase; PDHC, pyruvate dehydrogenase complex. For acetate metabolism: POXB, pyruvate oxidase; PTA-ACKA, phosphotransacetylase-acetate kinase pathway; ACS, AMP-forming acetyl-CoA synthetase. The dotted arrows denote the proposed PDHC bypass formed by POXB and AMP-ACS. For the TCA cycle: CS, citrate synthase; ACN, aconitase; IDH, isocitrate dehydrogenase; 2-KG, 2-ketoglutarate; KGDH, 2-ketoglutarate dehydrogenase; SCSC, succinyl-CoA synthetase complex; SDH, succinate dehydrogenase; FUMA, fumarase; MDH, malate dehydrogenase; OAA, oxaloacetate. FRD, fumarate reductase, expressed under anaerobic conditions, bypasses SDH. For the glyoxylate bypass: ICL, isocitrate lyase; MAS, malate synthase; IDHK/P, isocitrate dehydrogenase kinase/phosphatase. Underlines and dashed arrows denote enzymes and steps unique to the glyoxylate bypass. For gluconeogenesis: PPSA, PEP synthase; PCKA, pyruvate carboxylase; MAEB and SFCA, malic enzymes. Boxes and double-lined arrows denote enzymes and steps unique to gluconeogenesis.

tration where μ_{BM} reaches its half-maximal value (Monod, 1949). K_S is specific to each strain-environment combination. The yield Y of biomass from a given substrate is another growth constant:

$$Y = \frac{c_{BM,max} - c_{BM,0}}{c_{S,0}} \quad (1.2)$$

With the biomass concentration c_{BM} , its initial value $c_{BM,0}$ at the start of the experiment and its maximum throughout the experiment $c_{BM,max}$. $c_{S,0}$ is the initial substrate concentration.

With μ_{BM} and Y , a model of ordinary differential equations (ODEs, section 2.9.6) can be constructed as a fundamental bacterial growth model (Herbert, Elsworth, and Telling, 1956). However, ODEs have the potential for much larger and more complex models, tracking single metabolites, enzymes or pathways with integrated knowledge about enzyme kinetics and metabolic regulation (Kremling et al., 2018). Modeling *E. coli* using such models may provide further insights into the interplay of pathways and the logic behind the observed phenotypical behavior.

1.0.0.4 Objective

The aim of this work is the examination of the growth of *E. coli* on glucose or acetate supplemented minimal medium. Using modern online measurement techniques, parameters surrounding the growth of *E. coli* are collected for different experimental setups and joined with supplementary offline measurements. Notable events during the growth are investigated and their causes hypothesized. Finally, the gained information is combined with the modeling of the cellular system of *E. coli*.

Contents

1	Introduction	1
2	Materials & Methods	8
2.1	Strain & Precultures	8
2.2	Ex. HighGA: Glucose vs. Acetate	9
2.3	Ex. BMG: Glucose Dry Mass Weighing	10
2.4	Ex. HighG: Glucose Revision	11
2.5	Ex. BMA: Acetate Dry Mass Weighing	11
2.6	Ex. LowG: Small Glucose Gradient	12
2.7	Ex. InocG: Inoculation Gradient	12
2.8	Ex. HighA: Acetate Revision	12
2.9	Data Handling	12
2.9.1	Importing Data	12
2.9.2	Determining Scatter Drops	12
2.9.3	Manual Annotation	13
2.9.4	Biomass Equivalent	13
2.9.5	Derived Measured Variables	14
2.9.6	Modeling	15
3	Results	16
3.1	Preculture Similarity	16
3.2	Biomass Estimation	16
3.2.1	Filter Weights	16
3.2.2	Estimation Model	16
3.3	Points and Phases	20
3.3.1	Glucose	20
3.3.2	Acetate	27
3.4	Various	32
3.4.1	Glucose	32
3.4.2	Acetate	32
3.4.3	Outliers	32
3.5	Modeling	33
3.5.1	Growth Constants	33
3.5.2	Monod Model	34
4	Discussion	38
4.1	Multiple Growth Phases	38
4.1.1	The Lag Phase	38
4.1.2	The End of Lag	38
4.1.3	The Growth Phases	40
4.1.4	The First Growth Phase	40
4.1.5	The First Scatter-Drop	42
4.1.6	The Second Growth Phase	43
4.1.7	The Second Scatter Drop	43
4.1.8	The Stationary Phase	44

4.2	Growth on Acetate	44
4.2.1	The Lag Phase	44
4.2.2	The End of Lag	44
4.2.3	The Growth Phase	44
4.2.4	The Scatter-Drop	45
4.2.5	The Unknown Phase	46
4.3	The Monod Model	46
4.4	Discussion of Errors	47
4.5	Future Outlook	47
References		51
5 Appendix		52
6 Acknowledgements		75
7 Selbstständigkeitserklärung — Declaration of Academic Honesty		76

Table 1.1: **Common abbreviations and symbols used in this work.** For points-of-interest the substrate is noted in parentheses. SI units are used conventionally. Parameters are instead defined in Tab. S5

Abbreviation	description
Ace	Acetate
AU	Arbitrary unit
AckA	Acetate kinase
BM	Biomass
C-molarity	Carbon molarity
C-mol l^{-1} / C-M	Moles of carbon per liter, used with metric prefixes
Ex./ Exs.	Experiment(s), labels specific experiments
EOL	End-of-lag point (acetate & glucose)
FHP	Five-hour-point (glucose)
FMN	Flavin mononucleotide
FAD	Flavin adenine dinucleotide
Glc	Glucose
GRD	Growth decrease point (acetate)
GRI	Growth increase point (acetate)
MilliQ	Ultrapure water
MSE	Mean squared error
M9	Pure M9 minimal medium (Tab. S2)
M9S	M9 minimal medium with additives
M9A	M9 minimal medium with additives & 66 mM acetate
M9G	M9 minimal medium with additives & 22 mM glucose
$\text{NAD}^+ / \text{NADH}$	Nicotinamide adenine dinucleotide, oxidized or reduced
Norm.	Normalized by biomass weight in g
$\text{OD}_{600} / \text{OD}$	Optical density at 600 nm wavelength
O2D	O_2 -dip (acetate)
OTR	Oxygen transfer rate
POI	Point-of-interest
Pta	Phosphate acetyl-transferase
Ribof	Riboflavin
RSE	Residual standard error
Scat	Scatter
S_d / σ	Standard deviation
SD1/ SD2	Scatter-drop 1 or 2 (glucose)
SDA	Scatter-drop acetate
T	Temperature
t	Time
TCA	Tricarboxylic acid cycle
$\mu_{\text{BM}} / \mu_{\text{scat}} / \mu_{\text{ribof}}$	Growth rate of biomass, riboflavin or scatter
$q_{\text{O}_2} / (\frac{\widehat{dc}_{\text{O}_2}}{dt})_{\text{resp}}$	Normalized oxygen consumption rate, also respiration
$\frac{\widehat{dc}_{\text{H}^+}}{dt}$	Normalized alteration rate of H^+ concentration
$\frac{\widehat{dNADH}}{dt}$	Normalized alteration rate of NADH fluorescence
\widehat{NADH}	Normalized NADH fluorescence
$\widehat{\text{ribof}}$	Normalized riboflavin fluorescence

Materials & Methods

A series of experiments utilizing the BioLector was conducted. *E. coli* was grown in M9 medium with variable concentrations of either glucose or acetate. The starting optical density of *E. coli* was also varied. For biomass estimation from BioLector data, time-series measurements of dry mass were conducted. The measured data was then computationally evaluated and following fit using a mathematical model.

If not denoted otherwise, all samples and solutions were stored in either Eppendorf tubes (Eppendorf AG, Hamburg, Germany), or Falcon centrifuge tubes (Thermo Fisher Scientific Inc., Schwerte, Germany) of appropriate volume. Low-volume manual pipetting was performed using the following pipettes: Eppendorf reference 2 (Eppendorf AG, Hamburg, Germany), VITLAB Micropipette (VITLAB GmbH, Grossostheim, Germany) or Rainin Pipet-Lite XLS (Mettler-Toledo GmbH, Giessen, Germany) with ratiolab pipette tips (ratiolab GmbH, Dreireich, Germany). For higher volumes, a pipetting aid accu-jet pro (BRAND GMBH + CO KG, Wertheim, Germany) with SARSTEDT Serological pipettes (SARSTEDT AG & Co. KG, Nümbrecht, Germany) was used. Ultrapure lab water (further "MilliQ") was produced using a MilliQ Academic (Merck KGaA, Darmstadt, Germany) water purification system.

All well plate layouts involving gradients were pipetted using an OT-2 pipetting robot (Opentrons, New York, USA).

2.1 Strain & Precultures

A small sample of *Escherichia coli* strain W3110Z1 (genotype: *lacI*^q, PN25-tetrR, Sp^R, IN(rrnD-rrnE)1, rph-1, (see: ATCC 39936); received from: Expressys (Dr. Rolf Lutz), Bammental, Germany) was taken from -80 °C storage ("cryo-culture"). For the precultures of experiments ("Ex." or "Exs.") HighGA - HighG, the cells were first transferred into liquid LB medium (20 g l⁻¹ LB Broth (Lennox); Carl Roth GmbH + Co. KG, Karlsruhe,

Germany) with 100 µg ml⁻¹ spectinomycin and incubated at 250 rpm and 37 °C in a New Brunswick Innova 42 (Eppendorf AG, Hamburg, Germany) incubator shaker. After one change of medium, they were plated on an agarose Petri dish containing 35 g l⁻¹ LB broth and 100 µg ml⁻¹ spectinomycin (a Petri dish with LB-Medium and spectinomycin is further called "plate"). The inoculated plate was left to incubate at 37 °C overnight in a Model KB 53 (BINDER GmbH, Tuttlingen, Germany) cooling incubator. This resulted in a dense bacterial lawn. To achieve single, monoclonal colonies for the following experiments, a small amount of this bacterial matter was spread onto another plate and again left to incubate at 37 °C. An isolated colony was picked from this plate and spread onto a fresh one. After another 24 h of incubation at 37 °C, the plate (further "source-plate I") was placed in refrigeration and used as the source for all initial inoculations of liquid media for Exs. HighGA, BMG, and HighG.

Between the previous experiments and Exs. BMA to HighA, a three-months laboratory lockdown took place due to the COVID-19 pandemic. Therefore, a second source plate ("source-plate II") was created since the first one was no longer viable. The plate was directly inoculated from the same cryo-culture and also incubated at 37 °C for 24 h. The plate was then also refrigerated. Inoculation of liquid media first occurred after several days of refrigeration. Because media and solutions used for Exs. HighGA – HighG were running low, all media (M9, M9S, M9A, M9G) were newly made.

Liquid cultures were created by picking a colony from the respective source-plate and transferring it into 5 ml of minimal M9 medium with growth-supporting supplements, antibiotics, and 66 mM (0.4 % w/v) acetate or 22 mM (0.4 % w/v) glucose ("M9A" or "M9G", Tab. S2), depending on the experiment. Yeast extract was also added to the medium to a concentration of 1 g l⁻¹. This liquid culture was then incubated at 250 rpm and 37 °C. Every

two to seven days, 50 μ l of this liquid culture were transferred into 5 ml of fresh M9G or M9A medium and continued to be incubated. For the following experiments, the respectively newest liquid culture was used. In instances, where the liquid culture did not recover after transfer to fresh medium, a new liquid preculture was inoculated from the respective source plate.

2.2 Ex. HighGA: Glucose vs. Acetate

One day before the experiment, the liquid culture growing on M9G with yeast extract was again renewed by transferring 50 μ l of the newest liquid culture into fresh medium with following shaking and incubation. For preparation, first, the optical density at 600 nm wavelength (OD_{600} , here "OD" is used synonymously) of a 1:4 dilution of culture with MilliQ was determined. 1 ml of diluted culture was measured using a NanoDrop 2000c (Thermo Fisher Scientific Inc., Schwerte, Germany) spectrophotometer in cuvette mode and semi-micro PS disposable cuvettes (VWR International GmbH, Darmstadt, Germany) cuvettes. Then, to achieve 5 ml of inoculation solution with 1 OD, a volume

$$V = \frac{V_{end} \cdot 1 \text{ OD}}{4 \cdot OD_{600}^{1:4}} \quad (2.1)$$

with final volume $V_{end} = 5 \text{ ml}$ was taken from the undiluted culture and centrifuged at 4500 rpm for 5 min in a Thermo Scientific Heraeus Multifuge X3R (Thermo Fisher Scientific Inc., Schwerte, Germany). The supernatant was discarded and 5 ml of fresh M9 medium with growth-supporting additives and antibiotics ("M9S", Tab. S2) were added again. Cells were resuspended by pipetting the solution with a 1 ml micropipette until reaching homogeneity. Each 50 ml of M9S, M9G, and M9A media, as well as the 5 ml of 1 OD cell solution were placed in an OT-2 pipetting robot with P300 pipette module (Opentrons, New York, USA) and ratiolab pipette tips. Using the OT2 API v1 (Opentrons, New York, USA) open-source *python* API, the robot was programmed to fill a 48-well MTP-48-BOH well plate

("FlowerPlate"; m2p-labs GmbH, Baesweiler, Germany). The pipetting layout included seven-step gradients of both glucose and acetate (further also "glc" and "ace" respectively) with equal carbon-molarity. Carbon molarity ("C-molarity") or carbon concentration, here c^C , denotes the concentration of the referenced organic compound (in mol/l) multiplied with the average number of carbon atoms per molecule (derived base unit: C-mol/l or C-M, used with metric prefixes):

$$c_{glc}^C = c_{glc} \cdot 6 \quad (2.2)$$

$$c_{ace}^C = c_{ace} \cdot 2 \quad (2.3)$$

The gradients were created by diluting either M9A or M9G with M9S. They ranged from 0 to 119.88 C-mM and included 3 replicates per step and carbon source. The last columns' 6 wells were used as blanks. They were filled with low, medium, and high concentrations of glucose or acetate and were not inoculated. Before cells were added, the FlowerPlate was shortly refrigerated. This served to reduce the growth of cells in the wells before the start of the BioLector run. Refrigeration was performed for all experiments. However, the duration of cooling varied and, thus, the temperature of the medium. All wells were filled with a total of 1 ml with non-blank wells containing 100 μ l of cell solution. This gave an inoculation OD of 0.1.

The finished FlowerPlate was sealed using the gas permeable and evaporation reducing sealing foil F-GPR48-10 (m2p-labs GmbH, Baesweiler, Germany) and was placed in the BioLector. Measurements were made at 900 rpm shaking speed, 85 % humidity, and 37 °C for ca. 70 h. The sealing procedure, as well as shaking speed, humidity, and temperature during the run were alike for all experiments. The optical online-measurements were (gain settings in parenthesis): scatter (3, also "scat"), riboflavin fluorescence (6, also "riboflavin" or "ribof"), pH (7), O₂ saturation (7) and NADH fluorescence (1) (see Tab. 2.1 for filter module specifications). Because of their similar absorption and fluorescence spectra (Drössler et al., 2003) the riboflavin measurement likely also detects fluo-

rescence of flavin mononucleotide (FMN) and partially of flavin adenine dinucleotide (FAD). All measurements were taken continuously with ca. 8 min per measuring cycle.

Table 2.1: Used Filter modules. Product ID, excitation and emission wavelengths are given. All stated wavelengths have a bandpass of 10 nm. No fluorescence emission takes place for the scatter measurement, it is measured at the excitation wavelength.

Measured	ID	Excitation	Emission
Scatter	201	620 nm	-
Riboflavin	227	436 nm	540 nm
pH	202	470 nm	525 nm
O ₂ saturation	203	520 nm	600 nm
NADH	405	365 nm	450 nm

2.3 Ex. BMG: Glucose Dry Mass Weighing

Seven ReliaDisc Non-sterile Membrane Filtration Media (Ahlstrom-Munksjö, Helsinki, Finland) cellulose-acetate filters with 0.2 µm pore size were placed in Petri dishes and dried for 24 h at 60 °C in an emptied PEQLAB PerfectBlot hybridization oven (VWR International GmbH, Darmstadt, Germany). They were then left to cool to room temperature (RT) and weighed in five cycles on an Analytical balance ABP 100-4M (KERN & SOHN GmbH, Balingen, Germany) with 1 mg verification value. After initial calibration, the filters were placed with a small overhang directly on the outside of the scales weighing pan to allow for better picking up. This weighing protocol was later seen to cause enlarged variance in the weights (section 3.2.1). Since very low cell masses were expected, the error-prone 0.1 mg decimal was also used. Multiple, repeated measurements of each filter served to estimate this error.

Again, a 1 OD cell solution was prepared from a 24 h old M9G and yeast extract liquid culture (see Ex. HighGA). The hand-pipetted layout exclusively used M9 medium with 119.88 C-mM glucose as growth medium. All wells were inoculated with M9G culture to a 0.1 OD

except for three non-inoculated blanks. To examine the biomass during growth, each 6 wells of the plate were sampled at 7 time-points during the online measurement. The first sample was taken when a mean raw scatter of 1.5 AU was reached after ca. 5.5 h. At this scatter value, a weighable cell mass was expected. For sampling, the BioLector run was temporarily paused. Then, using a microliter pipette, the sealing foil on the respective wells was pierced and as much cell solution as possible was pipetted from one full plate column into a falcon tube. The incentive was to gain at least 5 ml of cell solution. The speed of this step differed greatly between samplings and meanwhile the run was paused for up to 10 min per sampling.

5 ml of the sampled cell solution were taken using a Multipette stream (Eppendorf AG, Hamburg, Germany) with a 5 ml Combitip advanced (Eppendorf AG, Hamburg, Germany). Then one of the pre-weighed filters was fixated in a Thermo Scientific Nalgene reusable bottle top filter (Thermo Fisher Scientific Inc., Schwerite, Germany) and the cell solution was poured on the filter. Afterward a 450 mbar pressure was applied using a vacuum pump system SC 950 (KNF DAC GmbH, Hamburg, Germany). After the solution was filtered through, three washing steps were performed by each pouring 5 ml of MilliQ into the filter and then applying the vacuum. The filter was then put back into the respective Petri dish and placed in the hybridization oven for drying at 60 °C.

The rest of the seven samples were taken in intervals of approximately 1 h and each treated as explained. During the second sampling ca. 90 µl of cell solution were filtered extra. This was noted and considered during data analysis. After 24 h and 48 h all filters were weighed in three or five cycles respectively. Despite intermediate drying the weights after 48 h collectively laid above those 24 h prior so no further weighing was conducted. After three months the filters were weighed again with 2, 5, and 8 d of drying at 60 °C. This was done to investigate the final weights of the filters again,

since weighings during Ex. BMA suggested that full drying of the filters could take more than 2 days. For the remeasured 5 d and 8 d weighings a corrected weighing protocol was used. Here, the filters were instead placed in weighing-boats of ca. 2 g tare weight and in the center of the scale. This was intended to avoid position dependence of the weight data and reduce the variance of the repetitive measurements. Independently from that change, however, the remeasured weights showed an unexpected increase and were not further considered.

The same online measurement settings were used as in Ex. HighGA with exception of NADH fluorescence, where a gain of 7 was employed. These gain-settings were used for all following experiments. During the active BioLector run all wells were continuously monitored. For data analysis and creation of a biomass model, though, only two non-sampled wells were taken into account.

2.4 Ex. HighG: Glucose Revision

Ex. HighG mostly repeated the protocol of Ex. HighGA. However the FlowerPlate was pipetted without an acetate gradient, but instead with six technical replicates per glucose concentration. Only three blank wells were used. This left three wells which were additionally pipetted with the highest glucose concentration. All wells except for blanks were inoculated with M9G culture as before.

2.5 Ex. BMA: Acetate Dry Mass Weighing

For Ex. BMA and following experiments, source-plate II was used together with newly mixed media and solutions. 13 cellulose-acetate filters were dried at 60 °C for over 24 h. Meanwhile, a FlowerPlate was pipetted similarly to Ex. BMG, with the exception that all wells contained 119.88 C-mM acetate instead of glucose. Again, all wells but three blanks were inoculated to a starting OD of 0.1. The BioLector run was started overnight to allow

for *E. coli* to grow to a raw scatter of 1.5 AU. The cells grew more slowly than expected for acetate cultures and the first samples was taken only ca. 19 h after the start of the run. Therefore, it was already late in the day and after four hourly samplings, the experiment was suspended for the rest of the day. The remaining three samples were then taken the next day in intervals of 1 h. This lead to a time range surrounding the scatter-drop of ca. 10 h not being sampled (Figs. S9 & S10).

Samples were treated similarly to Ex. BMG for the filtering and drying of biomass: 5 ml of cell solution were drawn through a dried cellulose-acetate filter, washed with 3 x 5 ml MilliQ and subsequently dried at 60 °C in the hybridization oven. Additionally, each three of the empty and dried filters were treated with M9A and M9G media in the same manner as FlowerPlate samples. This served to evaluate if the media alone had measurable effects on the weights of the filters. All filters were weighed after 1, 2, 3, 5, 8, and 11 d of drying. Initially, the weighing was also done similarly to Ex. BMG where the filters were placed directly on the rim of the weighing pan. For part of the 3 d measurements the corrected weighing protocol (see Ex. BMG) was used to test if this change would produce notable weight differences. Since no differences were measured but a decrease in variance was expected, measurements 5 d - 11 d also used the corrected weighing protocol. Following the 5 d measurement, however, filter weights experienced an unexpected and strong increase. Other samples and media were also stored in the hybridization oven. Therefore, it was hypothesized that water was drawn into the filters from these sources. Nevertheless, adding a Petri dish of CaCl₂ for desiccation resulted in only a minor reduction of filter weights. Further attempts to find the reason for this sudden increase were also not successful. Thus, these increased measurements were not used further. For data analysis only the three non-sampled wells were considered. Also, per Ex. BMG only weights with 2 d of drying were used for biomass estimation.

2.6 Ex. LowG: Small Glucose Gradient

For the better resolution of the low substrate concentration range a FlowerPlate was pipetted with 15-step glucose gradients between 0 and 39.96 mM. The OT-2 was employed again. Each concentration-step included three replicates. All wells except for three blanks were inoculated with M9G culture to a 0.1 OD. The blanks were also set up with a 3-step concentration gradient.

2.7 Ex. InocG: Inoculation Gradient

To differentiate between culture effects caused by growth time and cell density, a high-glucose (119.88 C-mM) FlowerPlate was inoculated to different initial ODs with M9G culture. First, a 1 OD cell solution was produced by spinning down an appropriate amount of preculture and adding 5 ml of M9G medium. Next, 15-step inoculation gradients were employed by varying the amounts of cell solution and M9G medium per well. Throughout the gradients the initial OD was varied between 0.02 and 0.5 in log-spaced intervals. This corresponded to $\pm 500\%$ of the regular inoculation OD of 0.1. For this, the OT-2 was employed. Again, three blanks were left without inoculation.

2.8 Ex. HighA: Acetate Revision

Similar to Ex. HighG, a FlowerPlate was laid out with only acetate gradients ranging from 0 to 119.88 C-mM and six replicates per step. Again, the OT-2 was used for pipetting. As opposed to Exs. HighGA and BMA however, an M9A culture was used to inoculate all wells but the three blanks.

2.9 Data Handling

Most data analysis was performed in *R* (v. 4.0.2, R Core Team, 2020) using an RStudio environment (v. 1.2.5033, RStudio Team, 2019).

Python 3 ("python", v. 3.7.7, Python Software Foundation, 2020) with Spyder environment (v. 3.3.6., Raybaut and Cordoba, 2020) was used for programming of the OT-2. A list of used packages can be found in Tab. S3. Important function parameters that were set to values other than their default are collected in Tab. S4. References and explanations of constants used in this work can also be found in Tab. S5.

2.9.1 Importing Data

BioLector data including all timepoints was saved as a CSV file using BioLector 3 software (v. 3.16.74.0, m2p-labs GmbH, 2011). It was then imported into *R* and automatically blank-corrected using a modified version of *platexpress::readExperiment*. The modification allowed for the import of temperature, user comments, and system events, along with the raw online measurements. Then an upper cut-off for the BioLector run time ("time" or "t") was set for each experiment using *platexpress::cutData*. The cut-off was manually set to include all timepoints with notable changes in the online measurements and an additional surplus of > 1 h into the time ranges with stationary data. Furthermore, an arbitrary 2 h time range at the beginning of each data set was ignored for many evaluations, since many measurements varied strongly there (section 3.4.3, 2 h timepoints are annotated as a dotted line in most plots).

The maximal O₂ saturation values which were reached shortly after starting the run varied slightly around the expected 100 %. Therefore, the data for each well was normalized to 100 % with respect to the highest measured saturation value of the run.

2.9.2 Determining Scatter Drops

The well-wise drops in scatter were computationally determined. The scatter-drops annotated in this way were initially meant to be used for visualization. Thus a quick and approximative method was used for searching. A drop was defined as a sudden and strong decrease of scatter signal when compared to the rest of the curve. Therefore, strongly negative first

derivatives were determined. For that the data was first smoothed using `pspline::sm.smooth` with `norder = 4`. Then the first and second derivatives of this scatter-smoothing ($\frac{dscat}{dt}$ and $\frac{d^2scat}{dt^2}$) were predicted at all timepoints using `predict` with `nderiv = 1` or `nderiv = 2` respectively. It was assumed that these slopes would be random and normally distributed if the scatter signal was mostly stationary and noisy. Strong increases or decreases in scatter for the actual signal would therefore appear as outliers in such a distribution. This was expected to apply to the second derivative as well, which should revolve around 0 in a random signal. Subsequently, normal distributions of the first and second scatter derivatives were defined. Their determining parameters mean (μ) and sd (σ) were calculated using the functions `mean` and `sd` on the whole of predicted first- or second derivative values, respectively. The outlier slopes were then determined in a three step fashion using significance-like thresholds (θ) from the normal distribution quantile function `qnorm`:

$$\theta_{\frac{dscat}{dt},req} = qnorm(0.1, \mu_{\frac{dscat}{dt}}, \sigma_{\frac{dscat}{dt}}) \quad (2.4)$$

$$\theta_{\frac{dscat}{dt},suf} = qnorm(0.05, \mu_{\frac{dscat}{dt}}, \sigma_{\frac{dscat}{dt}}) \quad (2.5)$$

$$\theta_{\frac{d^2scat}{dt^2},low} = qnorm(0.05, \mu_{\frac{d^2scat}{dt^2}}, \sigma_{\frac{d^2scat}{dt^2}}) \quad (2.6)$$

$$\theta_{\frac{d^2scat}{dt^2},high} = qnorm(0.95, \mu_{\frac{d^2scat}{dt^2}}, \sigma_{\frac{d^2scat}{dt^2}}) \quad (2.7)$$

In the first step $\theta_{\frac{dscat}{dt},req}$ was used as a threshold to determine outliers of the first derivatives. All timepoints with predicted $\frac{dscat}{dt} \leq \theta_{\frac{dscat}{dt},req}$ were considered to belong to a drop and all consecutive such points were grouped into one drop. However, only those groups with at least one included $\frac{dscat}{dt} \leq \theta_{\frac{dscat}{dt},suf}$ were considered further. Drops that were partially less steep, especially at their respective beginnings and endings, were still found to be one consecutive drop this way. Additionally, the bordering timepoints left of each drop were tested to have a $\frac{d^2scat}{dt^2} \leq \theta_{\frac{d^2scat}{dt^2},low}$ and the right hand points to have a $\frac{d^2scat}{dt^2} \geq \theta_{\frac{d^2scat}{dt^2},high}$. If so they were considered to also belong to the respective drops. This measure was taken to also allow for

the inclusion of the bordering points, where the drop connects the rest of the curve. Since these connections often appeared as peaks or valleys, their respective $\frac{dscat}{dt}$ should approach 0 and their $\frac{d^2scat}{dt^2} \neq 0$. These points would therefore escape the search concerning $\frac{dscat}{dt}$, but would usually be included in the drops if manually annotated. Thus, this exception was made. Then all replicate wells of one condition (carbon source and molarity or initial cell density) were grouped. Overlapping drops were combined with the lowest beginning time and the highest ending time describing the grouped drop. The automatic determination of these scatter-drops led to some particularly noisy time ranges being wrongfully marked as drops. In other cases some subtle changes were not recognized or their borders were set differently than if placed manually. As a countermeasure rough time ranges, where drops were expected, were set as a search range for each experiment. Overall, the grouped scatter-drops were generally considered acceptable.

2.9.3 Manual Annotation

For visualization and comparability between experiments points-of-interest were also manually annotated. These short time ranges with characteristically changing measurements, such as scatter-drops, were used to characterize the growth of *E. coli* (section 3.3).

2.9.4 Biomass Equivalent

The filter weights measured before ("pre") and after ("post") the application and drying of biomass samples were compared. First, all weights were normalized by the applied volume of cell culture, in most cases 5 ml. Then the means of these normalized weights were calculated. The weight changes between pre and 48 h samples were deemed the dry mass (further also "biomass" or "BM").

For unit-consistency between biomass (c_{BM}) and substrates the dry mass concentration was converted into a C-molarity:

$$c_{BM}^C = c_{BM} \cdot f_{BM}^C \cdot M_C \quad (2.8)$$

With the mass fraction $f_{BM}^C \approx 0.474$ (Folsom and Carlson, 2015) of carbon in *E. coli* dry matter and the molar mass $M_C = 12 \text{ g mol}^{-1}$ of ^{12}C (see also Tab. S5).

To express the uncertainty of the measured dry masses, a normally distributed stochastic error was assumed in all 48 h samples. Thus, the respective standard deviation ("sd" or " σ ") for the dry mass measured from a filter belonging to sample i at sampling time t_i was computed. This followed the propagation of uncertainty as

$$\sigma_{BM,i} = \sqrt{\sigma_{pre,i}^2 + \sigma_{post_{48\text{ h}},i}^2} \quad (2.9)$$

where $\sigma_{pre,i}^2$ and $\sigma_{post_{48\text{ h}},i}^2$ mark the variances of the repeated pre and post measurements, respectively.

To allow for the estimation of biomass from the online data, the dry mass measurements were paired with online measurements of scatter and riboflavin. The pairing was done by taking the time-wise closest online measurements for each sampling time, respectively. Then the dry mass vs. scatter or riboflavin data set was fit with linear models (Fig. 3.3). Additionally, glucose and acetate samples were also fit with other, different models that better describes their respective dry mass behaviors:

Both scatter and riboflavin fluorescence were not directly proportional to the biomasses of glucose samples and especially differed between timepoints preceding and following the first scatter-drop (section 3.3.1). Therefore, a well specific function was developed to calibrate both time ranges by separate linear models (Fig. 3.3, see section 3.2.2 for details). The model resulting from this function was called a concatenated model and showed a good fit to the riboflavin data (red line in Fig. 3.3b). It was subsequently used for biomass estimation with *E. coli* growing on glucose. Those wells which did not show a scatter-drop instead only used a single riboflavin linear model for estimation.

The dry mass for growth on acetate was treated similarly. Among riboflavin and scatter, the scatter data was chosen as the basis for biomass estimation. However, only the data points in the growth phase preceding the scatter-drop

could be fitted sensibly by a linear model or a combination of such. The biomass model used linear modeling with a forced zero-ordinate (Fig. 3.3d). Subsequently, biomass estimations were only performed up until the beginning of the scatter drop.

Normalized ("norm.") versions of all online measurements were also calculated with respect this estimated biomass weight (in g) at every timepoint (further marked with $\hat{\cdot}$).

2.9.5 Derived Measured Variables

As used for the determination of the scatter-drops all online measurements were smoothed with *pspline::sm.smooth* (*norder* = 3), allowing for the prediction of their time derivatives ("alteration rates"). Norm. rates were calculated by normalizing the alteration rate to the estimated biomass weight (in g) and are denoted as $\frac{d}{dt}$.

Additionally, the H^+ concentration c_{H^+} was inferred from the measured pH as

$$c_{\text{H}^+} = 10^{(\text{pH})} \quad (2.10)$$

where the unit of c_{H^+} is mol l^{-1} .

Furthermore, the concentration of dissolved O_2 c_{O_2} was calculated from the measured O_2 saturation:

$$c_{\text{O}_2,\text{max}} = H_{\text{cp}}(T) \cdot p_{\text{O}_2} \quad (2.11)$$

$$c_{\text{O}_2} = c_{\text{O}_2,\text{max}} \cdot \frac{O_2}{100} \quad (2.12)$$

with the maximal O_2 concentration in water $c_{\text{O}_2,\text{max}}$ and measured O_2 saturation O_2 (in %). $c_{\text{O}_2,\text{max}}$ was calculated according to Henry's law (Sander, 2015) with O_2 partial pressure $p_{\text{O}_2} = 1 \text{ atm} \cdot 21 \% \approx 21278.25 \text{ Pa}$ and Henry constant $H_{\text{cp}}(T)$ at temperature $T = 310.15 \text{ K}$. Henry constants are often stated at standard temperature $T_{\text{std}} = 298.15 \text{ K}$ ($H_{\text{cp}}(T_{\text{std}}) \approx 1.3 \cdot 10^{-5} \text{ mol m}^{-3} \text{ Pa}^{-1}$; Sander, 2015) and can in certain temperature ranges be converted using

$$H_{\text{cp}}(T) = H_{\text{cp}}(T_{\text{std}}) \cdot e^{\frac{-\Delta_{\text{sol}}H}{R} \cdot (T^{-1} - T_{\text{std}}^{-1})} \quad (2.13)$$

where the value $\frac{-\Delta_{\text{sol}}H}{R} \approx 1508 \text{ K}$ describes the change of H_{cp} with temperature (Sander, 2015).

2.9.5.1 O₂ Consumption

Using the measured alteration rate of O₂ concentration ($\frac{dc_{O_2}}{dt}$) the cellular respiration rate (also "O₂ consumption rate") could be estimated. First, the oxygen transfer rate (OTR) was calculated at every timepoint. The OTR describes the transition rate of oxygen from the air into the medium as:

$$OTR = k_L a \cdot (c_{O_2,max} - c_{O_2}) \quad (2.14)$$

(Atkinson and Mavituna, 1991) with the oxygen mass transfer coefficient $k_L a \approx 230 \text{ s}^{-1}$ at the given shaking speed (supplied by m2p-labs). Without cellular respiration, O₂ concentration in the medium would change with the rate given by the OTR. Thus, the difference between the measured alteration rate and this theoretical alteration rate of oxygen concentration gave the cell caused ("cc") oxygen alteration rate. Normalizing this rate to the weight of biomass m_{BM} and taking the negative of the result yielded the (specific) oxygen consumption rate ($\widehat{(\frac{dc_{O_2}}{dt})}_{resp}$ or "q_{O₂}":

$$\left(\frac{dc_{O_2}}{dt}\right)_{cc} = \frac{dc_{O_2}}{dt} - OTR \quad (2.15)$$

$$q_{O_2} = \widehat{\left(\frac{dc_{O_2}}{dt}\right)}_{resp} = -\left(\frac{dc_{O_2}}{dt}\right)_{cc} \cdot \frac{1}{m_{BM}} \quad (2.16)$$

2.9.5.2 Growth Rates

The exponential growth rates μ of scatter, riboflavin, and predicted biomass were calculated using the function *platexpress::dpseg_plate* with setting *log = TRUE*. For this, the respective data was smoothed by *sm.spline* and fed into the function. The result was time ranges with constant growth rates.

2.9.6 Modeling

A Monod model for glucose growth was calculated. The ODE model consisted of eqn. 1.1, as well as

$$\frac{dc_{BM}}{dt} = \mu \cdot c_{BM} (-D \cdot c_{BM}) \quad (2.17)$$

$$\frac{dc_S}{dt} = (D \cdot (c_{S,in} - c_S)) - \frac{\mu}{Y} \cdot c_{BM} \quad (2.18)$$

These differential equations were proposed for continuous cultures by Monod (Herbert,

Elsworth, and Telling, 1956). No dilution through added medium (concentration $c_{S,in}$) takes place in batch culture. Thus, the dilution rate D equals zero. Furthermore, no decrease of estimated biomass was observed for any experiment conducted with glucose. Therefore, including a separate term of cell death by subtracting biomass with a constant death rate instead of the omitted dilution term did not seem sensible, as well.

The yield Y was determined on glucose and acetate. This was done by fitting a linear model to the final predicted biomass of glucose samples from Exs. HighGA, HighG, and LowG against the used substrate concentration. The yield on acetate was only predicted from Ex. HighGA, where the estimated biomass of acetate samples at their respective scatter-drops was used. The slopes of these linear models were considered the yields (eqn. 1.2 & section 3.5.1).

Additionally, the maximum growth rate $\mu_{BM,local}$ of each well in glucose samples of Exs. HighGA, HighG, and LowG was extracted. These growth rates were then plotted against the respective substrate concentration. To avoid initial noisy variations of the growth rates, only time ranges after 2 h were considered. Then a curve according to eqn. 1.1 was fit to the data using the *nls* function with μ_{max} and K_S as fitting variables. Similarly, μ_{max} and K_S were determined for acetate. There, only acetate samples of Ex. HighGA were used, evaluating $\mu_{BM,local}$ for time ranges after 5 h.

The ODE model was then calculated for the initial glucose concentrations of Ex. HighGA. These models were fit to the biomass estimates from Ex. HighGA glucose samples. The mutual starting time of all models was varied, thus parallelly shifting them on the time-axis, until models and data showed the best overlap. Computationally, the modeled data was again smoothed using *pspline::sm.smooth* (*norder = 3*). Also, a *predict* function was set up for the prediction of the Monod models at the timepoints of Ex. HighGA minus a variable offset. *nls* then solved for this optimal offset.

Results

E. coli shows complex growth behavior on (M9) minimal medium for specific added carbon/ energy sources. Here, batch growth on glucose or acetate gradients was observed in real-time. The used BioLector Pro bioreactor allowed for parallel, optical measurements of different culture parameters (backscatter, O₂ saturation, pH, and riboflavin and NADH fluorescence). Seven experiments were conducted (for summary see Tab. 3.1). There, time series were measured with either variation of the initial substrate concentration or cell density or the measurement of dry mass. For the latter, the growth curves were divided according to drops in the scatter signal (example of scatter curves in Fig. 3.1, for details see section 3.2.2) and scatter or riboflavin data calibrated with the weighed dry mass. Afterward, the online measurements were evaluated by also calculating growth constants, such as yield and growth rates, and biomass-normalized (specific) metabolic rates. Then, the observed growth was divided into differently behaving points and phases and a Monod ODE model was fit to the data.

The samples of Ex. BMG were analyzed in a parallel study by Burmester (2020). Using flowcytometric measurements the samples were tested for measurable, phenotypic changes during the growth of *E. coli*.

3.1 Preculture Similarity

In the process of creating the inoculum of OD = 1 from the precultures for the BioLector experiments the OD of each experiment's preculture was measured (Tab. 3.1). The precultures of Exs. HighGA to HighG, which were all grown on glucose and used before the three months of laboratory downtime, collectively reached ODs between 3 and 4. In the second group of experiments three months later Exs. BMA and LowG were inoculated using precultures with OD just below 2. With the same growth conditions both precultures therefore only showed a cell density of 50–60 % compared to the previous experiments. Ex. InocG, which was conducted the following

day, then used a preculture reaching a more similar OD of 3.0 again. Even though the acetate-grown preculture of Ex. HighA was given two days of growth, it only reached an OD of 1.53.

3.2 Biomass Estimation

3.2.1 Filter Weights

To estimate biomass as dry cell weight, sterile filters (0.2 µm) were weighed repetitively before ("pre") and after("post") vacuum filtration of a constant culture volume (5 ml if not stated otherwise) and drying of the filters at 60 °C. These culture samples were taken as time series spanning the growth curves (vertical lines in Figs. 3.1a & 3.1b). However, the applied biomasses were very little, ranging from 2.66 % to 7.74 % of filter weights (pre, around 90 mg) in Ex. BMG, with a propagated standard deviation (eqn. 2.9) of up to 0.23 % of filter weights (values taken from 48 h of drying). Ex. BMA produced much lower biomass weights, ranging from only 0.46 % to 1.83 % of filter weights, and a much larger propagated standard deviation of up to 0.64 % of filter weights. Continued drying and re-measuring of the filters did not improve this and, unexpectedly, filter weights and variances between repetitive measurements even increased with time (Fig. S1a). Addition of CaCl₂ as a desiccant in the drying step only slightly improved the measurement errors. Followingly, the calibration to biomass by this method, as used in the following sections, can only be considered as preliminary.

3.2.2 Estimation Model

The 48 h dry mass weights obtained from glucose samples of Ex. BMG were chosen as the basis for biomass estimation. These weights showed a monotonic increase with their respective riboflavin values (points in the upper part of Fig. 3.3a). Due to the falling scatter values at the scatter drop, the dry-mass-scatter relation was distorted and could not easily be calibrated using a single function. Nonetheless,

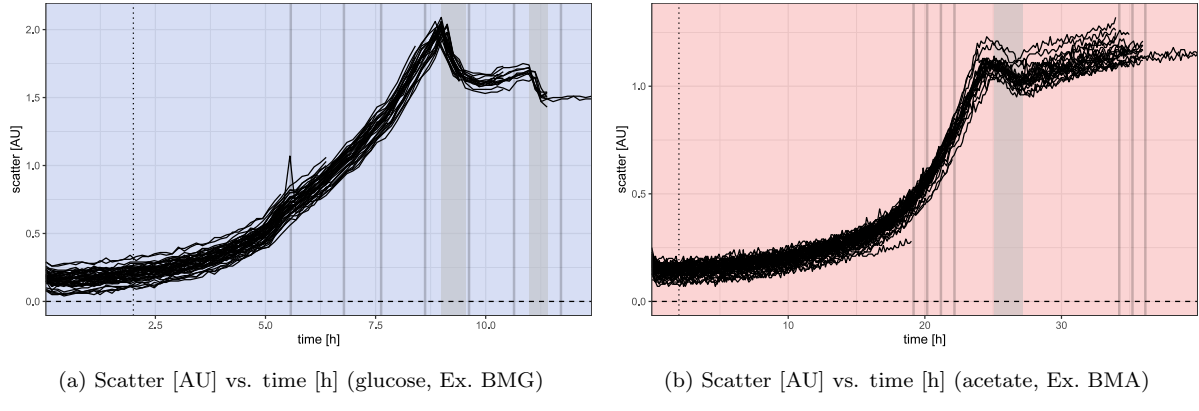


Figure 3.1: **Scatter [AU] vs. time [h] for *E. coli* batch growth on 119.88 C-mM glucose (Ex. BMG) or acetate (Ex. BMA).** Blue background coloring marks an experiment using glucose, red marks acetate. Grey shaded areas show time ranges of automatically determined scatter-drops. Grey vertical lines show approximate sampling times for biomass collection. All 45 inoculated wells are depicted. Lines representing sampled wells are discontinued at their sampling time.

Table 3.1: **Summary of conducted experiments.** Noted are varying conditions of experiments and precultures. Preculture "glucose" cultures grew for one day, "acetate" cultures for two days before the respective experiment. The preculture ODs were measured shortly before the start of each experiment. The division between Ex. HighG and Ex. BMA marks a gap of three months, after which new media and source cultures were used. Precultures grew at 37 °C with 250 rpm shaking. Experiment cultures grew at 37 °C with 900 rpm shaking and optical measurements each 8 min.

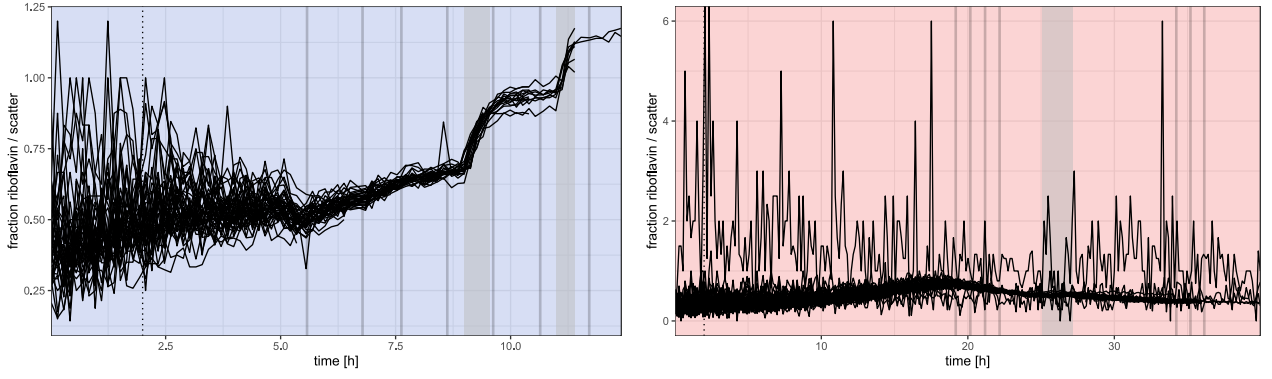
Ex.	Substrate	Experiment Description	Preculture	
			Substrate	OD
Ex. HighGA	glucose/acetate	substrate gradients	glucose	3.92
Ex. BMG	glucose	time-series biomass weighing	glucose	3.33
Ex. HighG	glucose	substrate gradient	glucose	3.52
Ex. BMA	acetate	time-series biomass weighing	glucose	1.96
Ex. LowG	glucose	low-concentration substrate gradient	glucose	1.80
Ex. InocG	glucose	gradient of initial cell density	glucose	3.00
Ex. HighA	acetate	substrate gradient	acetate	1.53

a conversion factor of 0.603 mg ml⁻¹ AU⁻¹ used by Britner fit data of the first growth phases reasonably well (Britner, 2019; green, big-dotted line in Fig. 3.3a).

Furthermore, the fraction of riboflavin to scatter values was observed (Figs. 3.2, S3f, S2d, S7d, S14b, S18b & S20d). This ratio was unsteady during all experiments and generally very noisy during the first 2 h of most glucose experiments, where both scatter and riboflavin signals were low (e.g. Figs. 3.5c & S3a). The mean of this ratio usually varied around 0.5 up to the scatter-drops, where the falling scatter values caused the ratio to rise rapidly (Fig. 3.2a). Increasing the inoculation OD led to strongly

reduced noise and a lowered initial ratio of riboflavin to scatter, which then rose to regular levels during the first two hours (Fig. S18b).

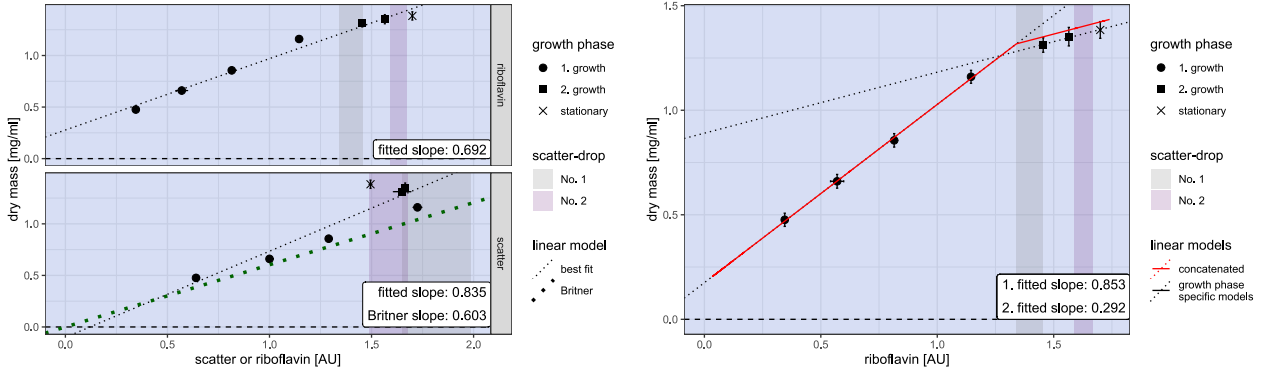
Importantly however, the experiment used for biomass estimation (Ex. BMG) appeared as notable exception to these general observations: There, the fraction of riboflavin and scatter began with strongly varying values between 0.25 and 1 and tended to 0.5 over the course of ca. 5 h (Fig. 3.2a). Notably, at the time of the first sampling the ratio quickly dropped by ca. 10 % and afterward began a linear increase until reaching a value of ca. 0.7 at the onset of the SD1. These strong variations in the relation of



(a) Ratio of riboflavin to scatter vs. time [h] on glucose (Ex. BMG)

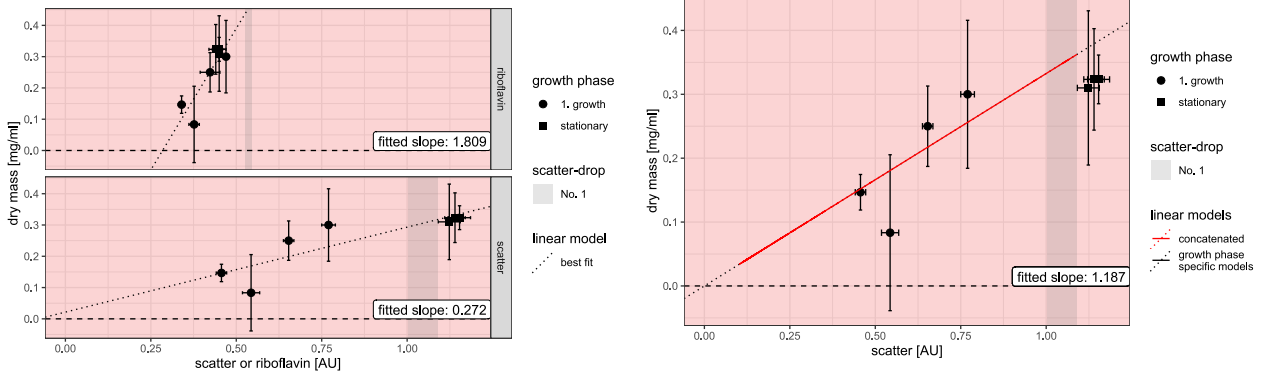
(b) Ratio of riboflavin to scatter vs. time [h] on acetate (Ex. BMA)

Figure 3.2: Fraction of riboflavin and scatter of Exs. BMG or BMA vs. time [h] for *E. coli* batch growth on glucose or acetate. Used experiment in parentheses. Samples of Ex. BMG grew with 119.88 C-mM glucose, samples of Ex. BMA with 119.88 C-mM acetate. Grey shaded areas mark time ranges of automatically determined scatter-drops. Grey vertical lines show approximate sampling times for biomass collection. All 45 inoculated wells are depicted. Lines representing sampled wells are discontinued at the sampling time.



(a) Linear models for dry mass [mg ml^{-1}] vs. scatter or riboflavin [AU] on glucose (black, dotted lines). Green line shows biomass-scatter conversion in Britner, 2019. (Ex. BMG)

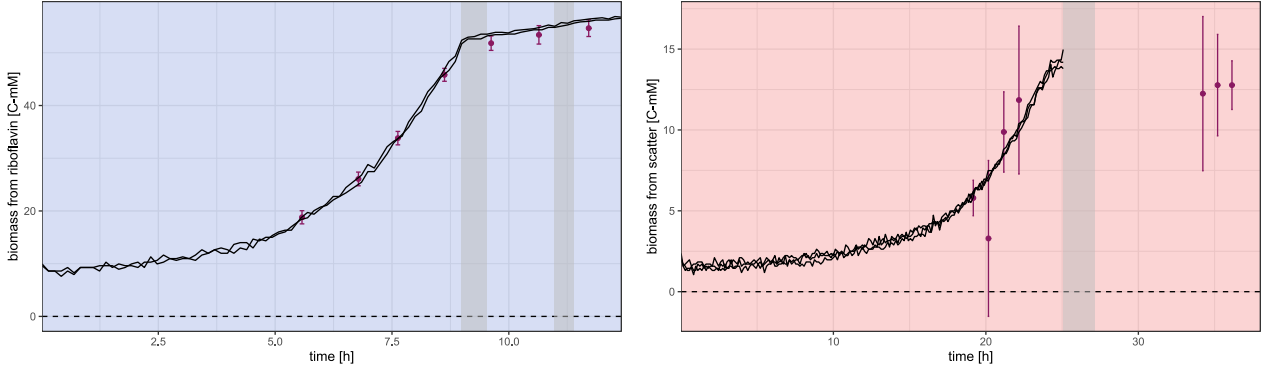
(b) Concatenated linear model for dry mass [mg ml^{-1}] vs. riboflavin [AU] on glucose (red line). Component linear models as black, dotted lines. (Ex. BMG)



(c) Linear models for dry mass [mg ml^{-1}] vs. scatter or riboflavin [AU] on acetate (black, dotted lines). (Ex. BMA)

(d) Linear model for dry mass [mg ml^{-1}] vs. scatter [AU] on acetate using only data before the SDA (black and red line). (Ex. BMA)

Figure 3.3: Dry mass concentration [mg ml^{-1}] of Exs. BMG or BMA vs. respective scatter or riboflavin measurements [AU] for *E. coli* batch growth on glucose or acetate. Used experiment in parentheses. Samples of Ex. BMG grew with 119.88 C-mM glucose, samples of Ex. BMA with 119.88 C-mM acetate. Point shape shows an approximate respective growth phase. Vertical error bars denote one standard deviation using propagation of uncertainty (eqn. 2.9). Horizontal error bars show one standard deviation of $n = 2$ (Ex. BMG) or $n = 3$ (Ex. BMA) representative wells. Purple or grey shaded areas mark scatter or riboflavin values during the respective scatter-drops.



(a) Estimated and measured biomass concentrations [C-mM] vs. time [h] on glucose (Ex. BMG)

(b) Estimated and measured biomass concentrations [C-mM] vs. time [h] on acetate (Ex. BMA)

Figure 3.4: Estimated biomass concentration [C-mM] (black lines) for Exs. BMG or BMA vs. time [h] for *E. coli* batch growth on glucose or acetate. Used experiment in parentheses. Samples of Ex. BMG grew with 119.88 C-mM glucose, samples of Ex. BMA with 119.88 C-mM acetate. Estimation using models in Figs. 3.3b and 3.3d. Purple points show biomass derived from dry mass measurements. Error bars denote one standard deviation using propagation of uncertainty (eqn. 2.9). Grey shaded areas mark the time ranges of the respective scatter-drops.

riboflavin and scatter showed that the sampling procedure most likely altered the measured scatter and riboflavin values. This observation was substantial as riboflavin values were used for the biomass estimation of all glucose experiments. Neither riboflavin nor scatter associations to dry mass could be well represented by simple linear models (see. black lines in Figs. 3.3a). That is because riboflavin data of samples preceding and following the SD1 showed linearity with notably different slopes (0.853 and 0.292 respectively). They could, thus, be fit better using separate linear models (respective black, dotted lines in Fig. 3.3b). Interestingly, the intercept of those separate models had a riboflavin value close to that at the SD1s starting point. The latter was already being determined computationally and therefore its time was further used as a switching point for the concatenated model (see. red line in Fig. 3.3b). This coupling point, however, laid at a slightly larger riboflavin value (1.34 AU) than the intercept (1.28 AU). Thus, the biomasses from points in the second phase were also slightly overestimated by a constant amount of ca. 0.036 mg ml⁻¹. Additionally, due to the first linear model having an ordinate of 0.175 mg ml⁻¹, this biomass concentration was estimated if no riboflavin was measured. Therefore, non-zero biomasses were even estimated for blanks and the starting values of all other wells

were affected as well (Fig. 3.4a).

For acetate neither riboflavin nor scatter values showed a clear relation to dry mass. First and foremost, the large variances in the estimated biomasses caused by the disagreeing repeated measurements often had the same order of magnitude as the estimated biomasses themselves (see error bars in Fig. 3.3c). Fitting a model to this data, therefore, was largely speculative. Furthermore, similarly to glucose samples the ratio of riboflavin and scatter signals varied over time (Fig. 3.2b) and even between some experiments: In Ex. HighGA acetate samples, the ratio started off around 0.5 and then repeatedly rose and fell between different POIs and phases by a factor up to two (Fig. S2d). The ratios of Exs. BMA and HighA were qualitatively similar to those of Ex. HighGA, but included generally more noise (Figs. 3.2b, S20d & 3.2b). In contrast to Ex. HighGA the riboflavin-scatter-ratio of Ex. HighA stayed relatively close to 0.5 over the whole experiment (Fig. S20d). Furthermore, other than in Ex. BMG the sampling points did not seem to exert a strong influence on the ratio of Ex. BMA (Fig. 3.2b). Due to their fraction changing with the time and between experiments, the choice of riboflavin or scatter as basis for the biomass estimation

would quantitatively affect the estimates and could also lead to discrepancies between the experiments' biomass estimates.

To gain an approximate understanding of the growth on acetate, linear models were fitted to the data nonetheless (Fig. 3.3c). Due to the riboflavin values decreasing after the scatter-drop, data points of dry mass plotted against respective riboflavin values bulked up for all but the first two timepoints. The linear model fit to the riboflavin data did not produce a visually good fit and was not useful in the context of biomass because of its strongly negative ordinate of -0.51 mg ml^{-1} . On the other hand, plotting dry mass against scatter resulted in the data points being more drawn out and separated into groups measured before and after the SDA (Fig. 3.3c). All samples collected after the SDA possessed very similar scatter and dry mass values, as they were collected relatively far into the stationary phase. Interestingly, their measured dry mass was also similar to that of the last sample taken before the SDA. The linear model for the scatter data which considered all data points showed a y-axis intercept of nearly 0 mg ml^{-1} and passed through all one-sd error bars. This made it more fitting as a basis for the biomass estimate than the model using riboflavin data. However, the plot of dry mass against scatter showed certain qualitative traits, that the linear model did not replicate: Similar to glucose samples, the data points preceding the SDA visually laid on a line with a higher slope than the overall linear model. A linear model fit through only those data points in the beginning, though, would produce a negative ordinate, as well as large residuals to the data points following onto the SDA. This model was therefore also not pursued. It was decided to exclude the data points following the SDA as no satisfactory explanation for their low dry masses could be found. Instead, a different linear model with forced zero-ordinate was fit through the remaining points (red line in Fig. 3.3d). As the data following the SDA was excluded from the modeling function, the biomass estimation and all normalized variables were also only defined up to this point. For each well the SDA found for the respective acetate concentration was chosen

as the cut-off. If no SDA was determined, the experiments' smallest starting time of an SDA was chosen instead.

3.3 Points and Phases

To characterize the recorded growth curves, first, the online or derived measurements were searched for points-of-interest (POI). Here, this term denotes short time ranges mostly between 30 min and a few hours in which distinctive changes in one or more measured variables took place. POIs present in only one experiment were noted if identifiable in multiple samples. The time ranges between two POIs or a POI and the beginning or end of the experiment were then called a phase and characterized as well. Glucose samples showed up to four POIs separating five phases which differed most notably in their respective scatter signals, (biomass) growth rates, respiration rates, NADH production, or development of pH. Similarly, up to five POIs and five phases with differences in the previously mentioned variables were suspected for acetate grown samples.

3.3.1 Glucose

The glucose experiments Ex. HighGA and Ex. HighG agreed in most qualitative and quantitative traits of the measured variables (compare Figs. 3.5, S3, S6 & S7). However, some measurements especially the estimated growth rates showed a higher level of noise between replicate wells of Ex. HighG. The NADH curves of Exs. BMG and HighG were parallel between replicate wells but shifted on the y-axis (Figs. S5e & S7e). This shifting led to high variability of the normalized NADH data between technical replicates and a qualitative behavior differing from all other experiments (Figs. S5a & 3.5g). During the timepoints of sampling, many measurements of Ex. BMG showed abnormal behavior, and especially the O₂ saturation decreased strongly at those points (Figs. S4 & S5). Because of this irregularity, Ex. BMG was not fully comparable to other experiments and did not

allow for the determination of the often subtle changes produced by POIs. The measurements of Ex. LowG did mostly comply with those recorded for low concentrations in Exs. HighGA and HighG (compare Figs. S11 - S14, 3.5, S3, S6 & S7). However, the small concentration range of glucose prohibited making general characterizations of the POIs. Instead, it served to further characterize POIs at low concentrations. At the inoculation OD used for all other experiments (0.1) Ex. InocG also showed similar results to previous experiments (compare Figs. 3.6, S16 - S18, 3.5, S3, S6 & S7). An exception to those similarities, however, was the second scatter-drop (section 3.3.2) which strongly changed: Instead of a sudden and strong decrease of scatter signal, the scatter growth rate μ_{scat} was only lowered slightly below 0 (Fig. 3.6b). However, μ_{scat} remained negative roughly three to four times longer than recorded for the other experiments.

Thus, for evaluation of growth on glucose mainly Exs. HighGA and HighG were used. Exs. LowG and InocG served to further characterize found POIs or phases if present there. Ex. BMG was rarely considered in the search for POIs.

3.3.1.1 Lag Phase

During ca. the first 30 min of each run the data points of many online measurements were highly noisy and strongly increasing while the temperature and humidity rose to their specified values (Fig. 3.5, temperature and humidity not shown). This effect was especially present in pH and O₂ saturation but scatter values were also effected.

After this initial period of noisiness most measurements settled on relatively static mean values (see data before annotation "1" in Fig. 3.5). Both scatter and riboflavin remained at low values with often small or noisy growth rates (Fig. 3.5d, S3b). μ_{ribof} varied especially strongly around its half-maximal values. Because of the positive ordinate of the biomass estimation function, the biomass started at ca. 9–10 C-mM. The biomass growth rate (μ_{BM}) also stayed at a low (< 0.1 h⁻¹), sometimes noisy level. Between low- and high-glucose

samples q_{O_2} remained at a basal level of approximately 7.5 to 10 mmol g⁻¹ h⁻¹ respectively. In samples inoculated to low or medium ODs, the normalized NADH ("NADH") decreased from initial, noisy values around 5000–10000 AU g⁻¹ to static levels below 5000 AU g⁻¹ (Fig. 3.6c). This descent was caused by a negative normalized alteration rate of NADH (" $\frac{d\widehat{NADH}}{dt}$ ") (Fig. 3.6d). With low inoculation OD $\frac{d\widehat{NADH}}{dt}$ slowly rose but did not exceed 0 AU g⁻¹ by far in the lag phase. At high initial cell densities (OD > 0.1), however, the normalized alteration rate increased much more quickly and surpassed 0 AU g⁻¹ after one to two hours. Thus, following the initial descent \widehat{NADH} increased already during the lag phase (Fig. 3.6c). After the noisiness in the first 2 h the pH slightly decreased, i.e. the predicted proton export rate (" $\frac{d\widehat{H^+}}{dt}$ ") became slightly positive and then continued to rise in a slow, linear fashion (Fig. S17d).

3.3.1.2 End-of-Lag

The End-of-lag point ("EOL"), hence, marked the end of the lag phase. It was primarily identified from the first strong and coordinated increase of μ_{BM} between wells (Fig. 3.5b). Until ca. 20 C-mM glucose the value to which μ_{BM} rose was positively correlated with the glucose content (Fig. S11b). This value laid between 0 and 0.2 h⁻¹ and was the maximum reached in that sample. However, for higher levels of glucose μ_{BM} did not increase further than 0.2 h⁻¹ during the EOL. Compared to the new maximum provided by the five-hour-point ("FHP", below) this value was then ca. half-maximal (Fig. 3.5b). Notably, the estimated biomass for all but high-inoculation samples laid at ca. 10 C-mM, only slightly above the starting value (e.g. Figs. 3.5a & S16a). A common scatter value between 0.2 and 0.25 AU was also met (Fig. 3.5c).

The timing of this point was relatively constant between varying substrate concentrations (Fig. 3.7a). However, due to noisiness in the starting values of μ_{BM} the exact timing of this POI was not always apparent (Fig. 3.5b). Especially for low inoculation OD the increase of μ_{BM} could be gradual or split into two steps (Fig. 3.6a).

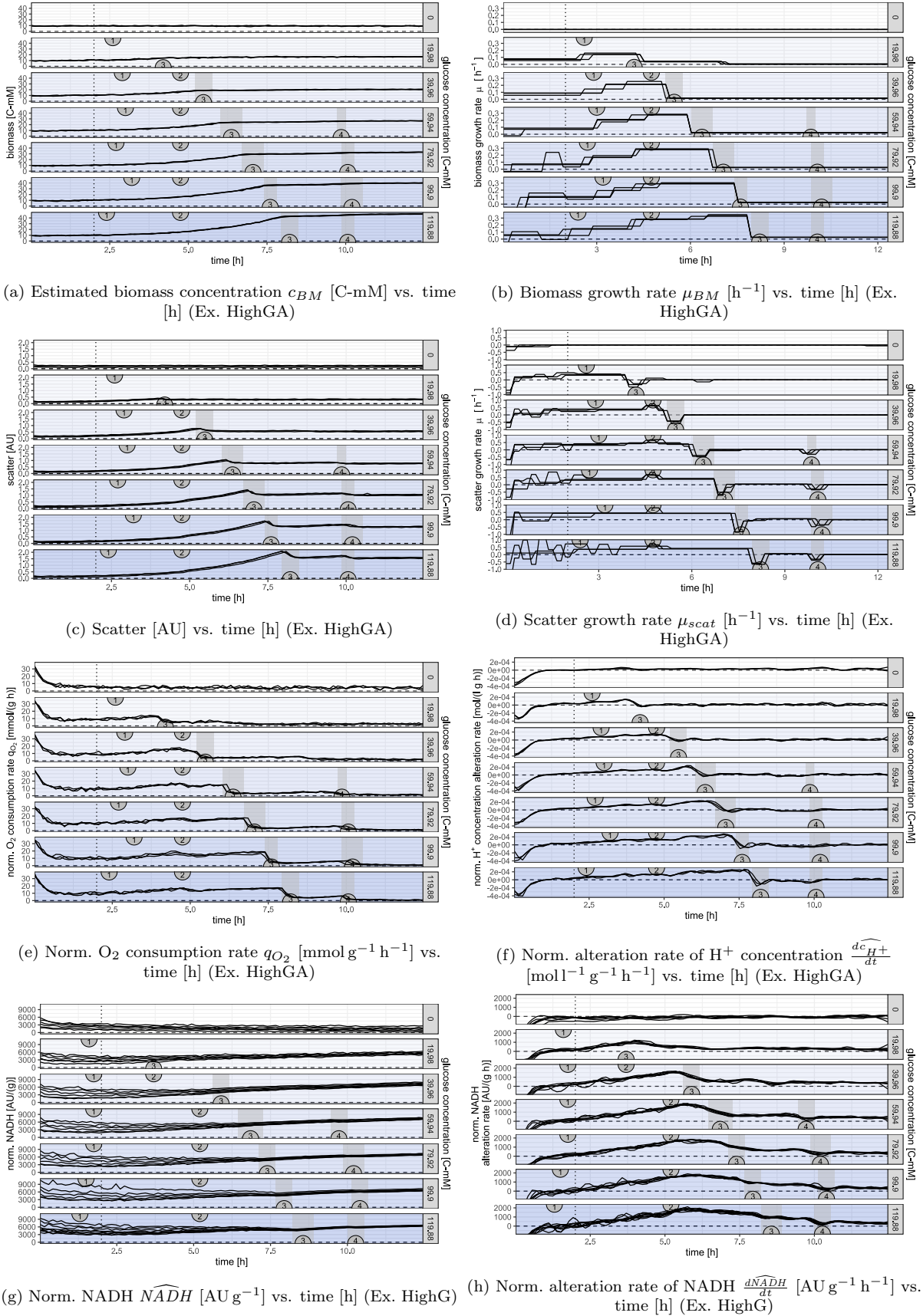


Figure 3.5: **Selected online or derived measurements vs. time [h] for *E. coli* batch growth on glucose.** Used experiment in parentheses. Plots vertically separated by the used glucose concentration (linear gradient: 0 C-mM - 119.88 C-mM), also represented by strength of blue background. Each concentration is represented by $n = 3$ (Ex. HighGA) or $n = 6$ (Ex. HighG) technical replicates. Grey shaded areas mark time ranges of automatically determined scatter-drops. Numbers in semicircles show the manually annotated mid points of POIs: 1) End-of-lag, 2) 5 h point, 3) Scatter-drop 1, 4) Scatter-drop 2.

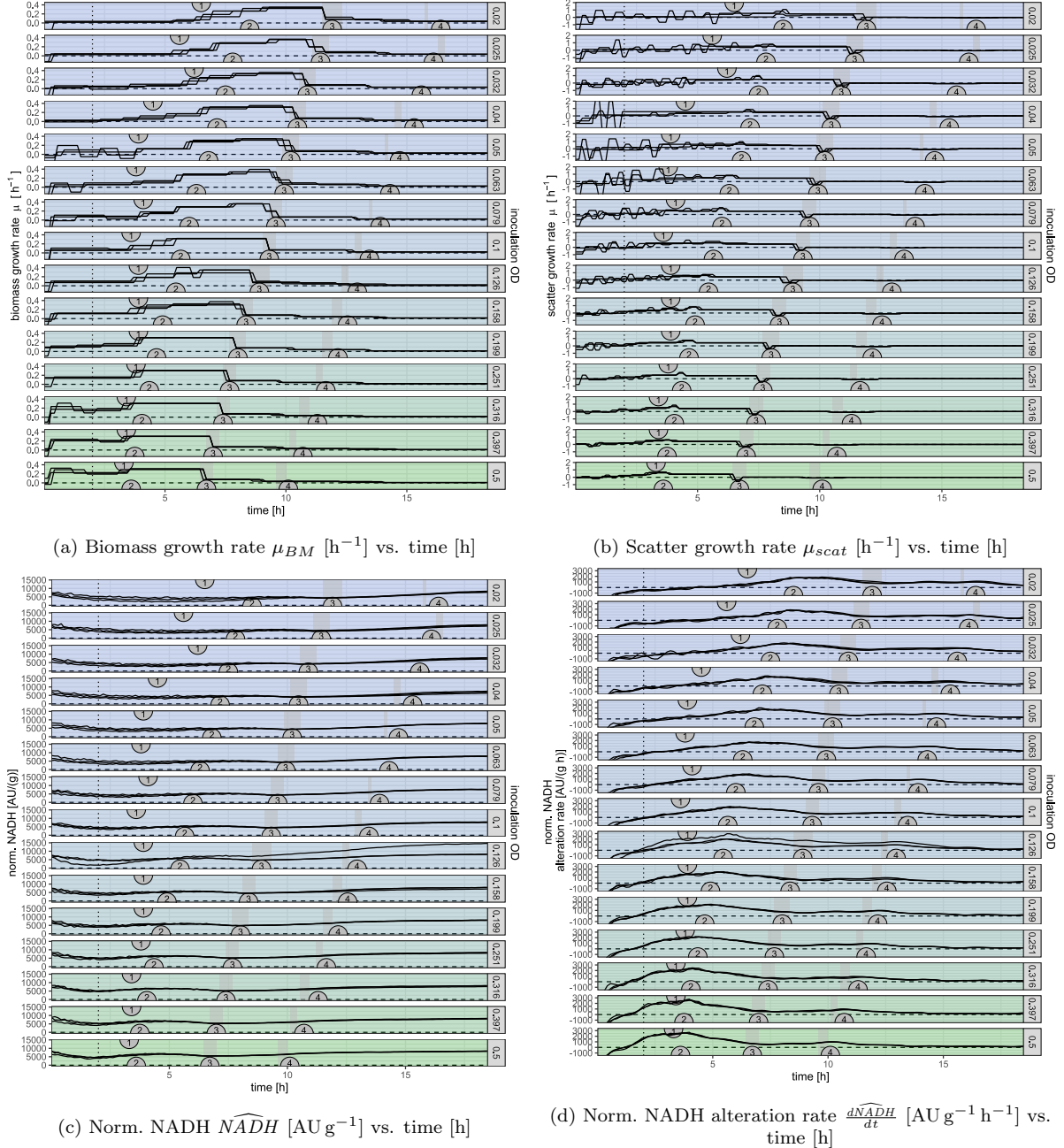


Figure 3.6: Selected online or derived measurements of Ex. InocG vs. time [h] for *E. coli* batch growth on 119.88 C-mM glucose with variation of the inoculation OD. Plots vertically separated by the wells OD after inoculation (logarithmic gradient: 0.02–0.5), visualized by the amount of green in the background. The constant blue tint shows the constant glucose concentration. Each OD-grouping is represented by $n = 3$ technical replicates. Grey shaded areas mark time ranges of automatically determined scatter-drops. Numbers in semicircles show the manually annotated mid points of POIs: 1) End-of-lag, 2) 5 h point, 3) Scatter-drop 1, 4) Scatter-drop 2.

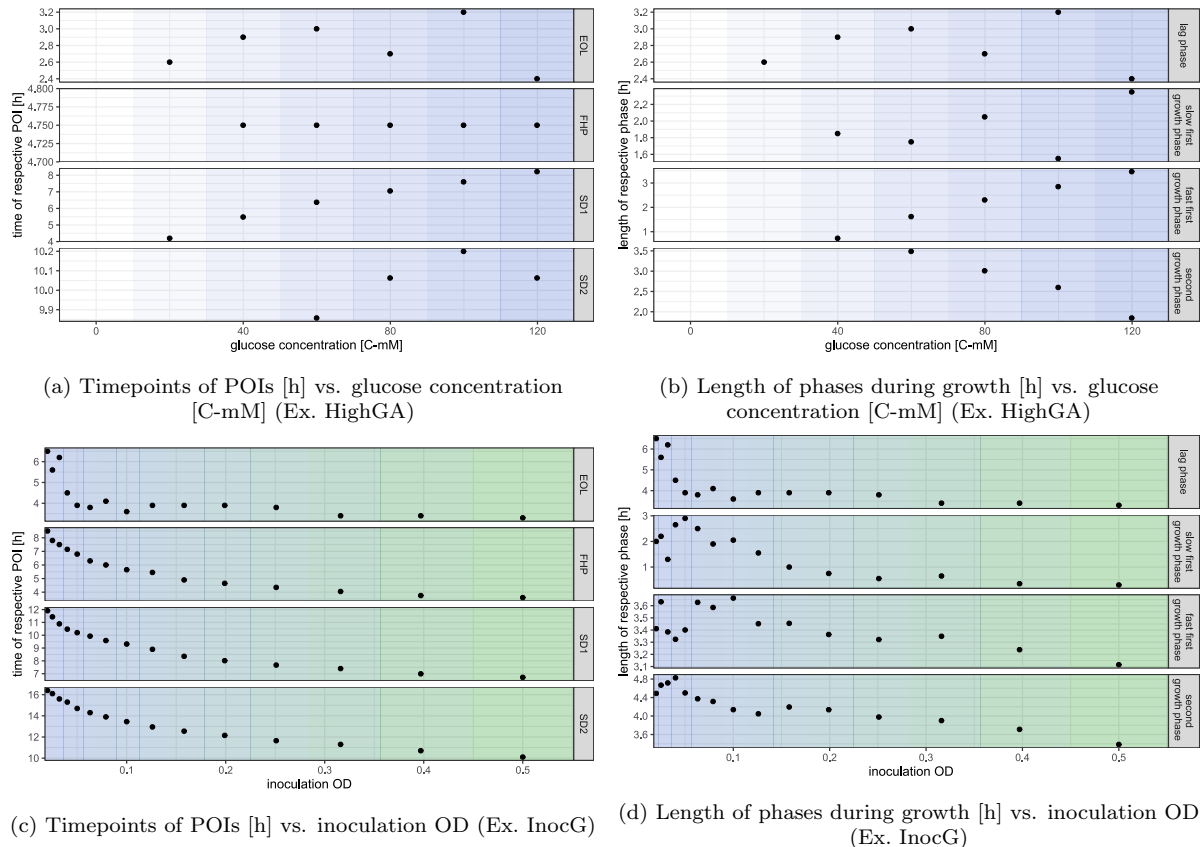


Figure 3.7: Timings or lengths of POIs and Phases vs. varied glucose concentration or inoculation OD.
The underlying timepoints were extracted from manually annotated points-of-interest and their time differences.
Background color visualizes glucose concentration (strength of blue) or inoculation OD (strength of green).

Nonetheless, the timing seemed to be positively correlated with low inoculation ODs (Fig. 3.7c). For increasing initial cell densities the EOLs time saturated at around 3 h. The experiments with medium inoculation OD (Exs. HighGA and HighG), on the other hand, showed this point between 2 and 3 h (Figs. 3.7a & S8a). In Ex. LowG it only took place after ca. 4–6 h (Fig. S15a).

The EOL also seemed to mark $\frac{dNADH}{dt}$ surpassing 0 AU g⁻¹ h⁻¹ in experiments with medium to low inoculation OD (Fig. 3.6d). Ex. LowG, though, already showed elevated rates of $\frac{dNADH}{dt}$ at this point. It is, thus, unclear if the EOL had an influence on the alteration of NADH levels.

A different characteristic of the EOL was the linear increase of qO_2 starting shortly after μ_{BM} had risen. In wells of Ex. HighGA $\frac{dc_{H^+}}{dt}$ either continued its linear increase or plateaued for a short time (Fig. 3.5f). Another possible effect of the EOL was an increase of the riboflavin growth rate (" μ_{ribof} ") to its maximal value. This observation, though, was only made in some wells due to the strong noise (Fig. 3.8f).

3.3.1.3 Slow First Growth Phase

During the beginning of the following phase *E. coli* mostly grew with a relatively constant, maximal or half-maximal growth rate. At high glucose concentrations μ_{BM} would already rise to its maximal value during the slow first growth phase, ca. an hour before the next recorded POI (Fig. 3.5b). The value of this maximum, $\mu_{BM,local}$, was highly dependent on the samples' glucose content. This relation roughly followed the prediction of the nutrient law (eqn. 1.1 & Fig. 3.11a). Meanwhile, for the low-glucose samples of Ex. LowG an increase of μ_{BM} to its maximum was also seen less than an hour after the EOL (Fig. S11b).

With rising inoculation OD the length of this phase decreased until it was almost immeasurable at an initial OD of 0.5 (Fig. 3.7d). This decrease in phase-length appeared to be approximately exponential for medium or high inoculation.

The O₂ consumption increased linearly throughout this phase and had approximately doubled to around 20 mmol g⁻¹ h⁻¹ at the end (Fig.

3.8g). Both $\frac{dNADH}{dt}$ and $\frac{dc_{H^+}}{dt}$ also continued to rise. While the former showed a continuation of its previous linear increase, the latter slightly peaked with 0.1 - 0.15 μmol l⁻¹ g⁻¹ h⁻¹ in all glucose concentrations of Ex. HighGA (Fig. 3.5h & ca. 4 h in Fig. 3.5f). Other experiments did not consistently show this peak of $\frac{dc_{H^+}}{dt}$. A slow increase of NADH might also be possible (Fig. 3.5g, 3.6c & S13a). Also, with rising initial cell densities the strong increase of $\frac{dNADH}{dt}$ seemed to be initiated during the lag phase already and continued over the EOL point (Fig. 3.6d).

3.3.1.4 Five-Hour-Point

The five-hour-point occurred in both Exs. HighGA and HighG around the 5 h mark (Fig. 3.7a). It was only present in samples with medium to high glucose concentrations. There, the most noticeable effect was a temporary 50 % increase in the scatter growth rate for ca. 30 min (Fig. 3.5d). In the same time range the O₂ consumption first peaked with its global maximum of consistently 15–20 mmol g⁻¹ h⁻¹ and afterward decreased by about 25 % in the course of 30 min to 1 h (Fig. 3.5e). Glucose concentration did not seem to affect the timing except for the 36.96 C-mM samples of Ex. HighG (Fig. 3.7a). There, the characteristic increase of μ_{scat} appeared earlier but without the accompanying decrease of O₂ consumption (Figs. S6d & S6h). However, this effect was not repeatable in any other experiment. The POI was no longer detectable at glucose contents below ca. 20 C-mM (value estimated from Ex. LowG, Fig. S15a) where the concentration-dependent first scatter-drop (see below) and the FHP would fall into the same time range. Furthermore, an inoculation-dependency of the FHP was measurable. Both the point's time of appearance and the time difference to the EOL decreased with rising inoculation OD (Figs. 3.7c & 3.7d). The former relation appeared as a logarithmic dependency where the time of appearance declined linearly with the logarithmically rising OD. At the highest initial inoculation both EOL and FHP were in very close proximity and, again, almost indistinguishable (Fig. 3.6).

Another characteristic feature of the FHP laid in $\frac{d\widehat{NADH}}{dt}$ rising over the points time range and reaching its maximum at ca. $2000 \text{ AU g}^{-1} \text{ h}^{-1}$ shortly after. \widehat{NADH} , on the other hand, interestingly showed very similar values of ca. 5000 AU g^{-1} in all samples of Ex. LowG and medium to low OD samples of Ex. InocG (Figs. S13a & 3.6c). The irregular \widehat{NADH} measurements of Ex. BMG laid in the vicinity of this value, between ca. 3100 and 6750 AU g^{-1} with a median of 4250 AU g^{-1} (Fig. 3.5g). Furthermore, a similar biomass of ca. 20 C-mM was met by most samples (Fig. 3.5a). In many cases, $\frac{dc_{H^+}}{dt}$ was also effected such that it either plateaued at a static value or slightly decreased (Fig. 3.5f).

3.3.1.5 Fast First Growth Phase

Similar to the preceding FHP the fast first growth phase was only present in samples with medium or high glucose concentrations where the following scatter-drop had not yet replaced the FHP (Fig. 3.7b). At contents higher than these 20 C-mM the length of the phase was linearly dependent on the concentration. Inoculation, though, seemed to not affect the timing (Fig. 3.7d).

O_2 consumption increased linearly with similar slopes between glucose concentrations (Fig. 3.5e). Thus, samples with long phases, i.e. high glucose concentrations, reached their maximum q_{O_2} again in the end. As mentioned for the FHP $\frac{d\widehat{NADH}}{dt}$ reached its maximum after ca. $1-2 \text{ h}$ into the phase (Fig. 3.5h). Afterward, the rate decreased slowly and linearly. About 25 min before the start of the following scatter drop $\frac{d\widehat{NADH}}{dt}$ started to decrease faster such that at the end of the phase the rate had in most cases reached the half-maximum around $1000 \text{ AU g}^{-1} \text{ h}^{-1}$. Likewise, in Ex. InocG \widehat{NADH} also decreased linearly by 20 to 30 % (Fig. 3.6c). Exs. HighG and LowG, on the other hand, showed slightly rising or curving behaviors (Figs. 3.5g & 3.6c). After the slight decrease during the FHP $\frac{dc_{H^+}}{dt}$ quickly rose to its global maximum of ca. $0.2 \mu\text{mol l}^{-1} \text{ g}^{-1} \text{ h}^{-1}$ (Fig. 3.5f). There, it remained until steeply decreasing again around 30 min before the scatter-drop. The time frame of this descent matched with

the one observed for $\frac{d\widehat{NADH}}{dt}$ (compare Figs. S7b & 3.5h). In the same period all μ_{BM} , μ_{ribof} , and μ_{scat} dropped to or below 0 h^{-1} (Figs. 3.5b, S3b & 3.5d).

3.3.1.6 Scatter Drop 1

The most remarkable POIs were the scatter-drops (here "scatter-drop 1", "SD1"). In a span of 30 min to 1 h the blanked scatter signal dropped by 20–30 % (Fig. 3.5c). The negative μ_{scat} during this time reached values around -0.5 to -1 h^{-1} (Fig. 3.5d). These values' absolutes often surpassed the μ_{scat} during the previous maximum. Furthermore, the O_2 consumption quickly decreased to ca. $5 \text{ mmol g}^{-1} \text{ h}^{-1}$, about half the value measured for the lag phase (Fig. 3.5e). Meanwhile, $\frac{d\widehat{NADH}}{dt}$ fell to or stayed at its half-maximal value ($1000 \text{ AU g}^{-1} \text{ h}^{-1}$) (Fig. 3.5h). $\frac{dc_{H^+}}{dt}$ also quickly dropped to $0 \text{ mol l}^{-1} \text{ g}^{-1} \text{ h}^{-1}$ or even below $-0.1 \mu\text{mol l}^{-1} \text{ g}^{-1} \text{ h}^{-1}$ for the highest glucose concentrations (Fig. 3.5f). Together with the growth rates of biomass and riboflavin being at nearly zero this POI, therefore, effected all variables measured online. Especially the drop in scatter signal could be seen already in the raw data. The timing of this POI seemed to be linearly dependent on the glucose concentration but exponentially on the inoculation OD (Figs. 3.7a & 3.7c).

3.3.1.7 Second Growth Phase

The second growth phase was only present in samples, which experienced a second scatter drop, i.e. with medium to high glucose concentrations (e.g. Fig. 3.5b). All others directly entered a form of stationary phase (see below). The length of this phase showed a negative, linear dependence on the samples' glucose concentration (Fig. 3.7b). Interestingly though, the timings of both the FHP and the following scatter-drop were very constant between glucose concentrations (Fig. 3.7a). This also meant the lengths of the growth phases to both sides of the SD1 in- or decreased with similar slopes. Inoculation OD seemed to cause a very slight, possibly exponential decrease of the phase length (Fig. 3.7d). During the phase the growth rates μ_{BM} and μ_{ribof} mostly

stayed at their previous values slightly above zero (Figs. 3.5b & S3b). Meanwhile, μ_{scat} also rose to such a static value (Fig. 3.5d). This resulted in very slowly increasing riboflavin and scatter signals and nearly no biomass gain during the whole phase (Figs. S3a, 3.5c & 3.5a). The initial biomass growth rate of this phase was observed to be slightly higher for samples with high glucose concentrations (Fig. 3.6a). In these samples μ_{BM} then decreased again during the phase. In other cases μ_{ribof} rose slightly before the end of the second growth phase (Fig. S3b). $\widehat{\frac{dc}{dt}}$ varied between slightly positive and slightly negative for different samples but always ended up negative before the start of the next POI (Fig. 3.5f). The O₂ consumption stayed at its low value around 5 mmol g⁻¹ h⁻¹ or very slightly increased over the course of the phase (Fig. 3.5e). As for the first fast growth phase $\widehat{\frac{dNADH}{dt}}$, $\widehat{\frac{dc}{dt}}$, and μ_{scat} started to strongly decrease ca. 30 min before the next scatter drop (Figs. 3.5h, 3.5f & 3.5d).

3.3.1.8 Scatter Drop 2

Like the first drop the second scatter-drop ("SD2") lasted for around 30 min to 1 h and was characterized by a sharply dropping scatter signal (Fig. 3.5c). The corresponding μ_{scat} reached -0.25 - -0.5 h⁻¹ (Fig. 3.5d). Comparatively this was ca. half the absolute value of μ_{scat} during the SD1. Again, the O₂ consumption decreased strongly, as did $\widehat{\frac{dNADH}{dt}}$ (Figs. 3.5e & 3.5h). SD2 also showed a negative $\widehat{\frac{dc}{dt}}$ at ca. -0.05 μmol l⁻¹ g⁻¹ h⁻¹, the half-minimal level (Fig. 3.5f). All of these rates in- or decreased back to zero throughout the SD2. An exception to this was seen in Ex. InocG, where the described changes were stretched out over the course of ca. 2 h and of much lower intensity (Fig. 3.6). Also, during the SD2 or in the following hour μ_{ribof} decreased to 0 h⁻¹ in all glucose experiments (e.g. Fig. S3b). The timing of this POI was very stable between glucose concentrations at ca. 10 h in Exs. HighGA and HighG (Fig. 3.7a & S8a). With the varying inoculation OD, however, the timing showed an exponential relation very similar to that of the SD1 (Fig. 3.7c). A notable observation was, that an SD2 was only found in samples, that also showed sep-

arated FHP and SD1 points (Fig. 3.5c).

3.3.1.9 Stationary Phase

The stationary phase was reached in two ways. Either by samples with low glucose concentrations after passing the SD1 and not entering a second growth phase, or by high-glucose samples after showing the second scatter-drop (e.g. Fig. 3.5b). In this phase all growth rates decreased to 0, likewise did the the q_{O_2} and $\widehat{\frac{dc}{dt}}$ (Figs. 3.5e & 3.5f). The norm. NADH alteration rate stayed at slightly positive values for most experiments (Fig. 3.5h). After entering this phase all measurements approached static values and no notable changes were observed further (Fig. 3.5).

3.3.2 Acetate

For the growth on acetate only Exs. HighGA and HighA could be used as references for finding POIs. Like in Ex. BMG the measurements of Ex. BMA were distorted through the sampling procedure and often noisy (e.g. S4f). Furthermore, both Exs. BMA and HighA showed massive discrepancies to the data from Ex. HighGA. While the first increase of growth rate could be seen in the latter after between 2 and 4 h, Ex. HighA showed no growth for around 20 h (compare Figs. 3.8b & S19b). Multiple POIs found in Ex. HighGA did also not appear in Ex. HighA or differed in specific measurements' behaviors (see following sections). Additionally, the data obtained from Ex. HighA was particularly noisy and contained a large number of outliers (section 3.4.3). Ex. BMA on the other hand showed qualitatively similar growth to the high-acetate samples of Ex. HighGA but took about 10 h longer than expected from Ex. HighGA to reach the target scatter value for sampling. During the evaluation of growth on acetate, therefore, mostly Ex. HighGA was used. This made the definitions of POIs more ambiguous as they were not backed by multiple experiments.

3.3.2.1 Lag Phase

During the the first 30 min to 1 h of the growth on acetate, again, a period of strong noisiness with increasing pH and O₂ saturation was observed (Figs. S2c & S2a). At the same

time, Exs. HighA and BMA also showed $\widehat{\frac{dNADH}{dt}}$ starting at massively negative values and quickly rising (Fig. 3.9b). After ca. 2 h the rate had risen close to 0 AU g⁻¹ h⁻¹ and passed into a more gentle increase. It was, however, questionable if these negative values were caused by *E. coli* were also present in samples without added acetate (section 3.4.3). The norm. O₂ consumption similarly decreased to a static value between 25 and 50 mmol g⁻¹ h⁻¹ (Fig. 3.8g). $\widehat{\frac{dc_{H^+}}{dt}}$ rose to a slightly positive, static value (Fig. 3.8h). The oscillations appearing in said rate were found to be artifacts (section 3.4.3). Although often noisy all experiments also showed a slow and linear increase of normalized riboflavin signal (e.g. Fig. S2b).

3.3.2.2 End-of-Lag

Similar to glucose the EOL primarily presented itself as the first, strong increase of μ_{BM} (Fig. 3.8b). This increase, however, was not always sharp but was sometimes divided into two steps. Nonetheless, in most cases μ_{BM} eventually reached 0.05–0.1 h⁻¹, about 30–50 % of its maximum in that sample. During the EOL $\widehat{\frac{dc_{H^+}}{dt}}$ began to slowly decrease again and became negative for medium to high acetate concentrations before the next POI was reached (Fig. 3.8h). In contrast to the lag phase, $\widehat{\frac{dNADH}{dt}}$ began to differ between *E. coli* with and without supplemented acetate. In samples with an added acetate content the rate slowly rose while for the latter it remained static at 0 AU g⁻¹ h⁻¹ (Fig. 3.9b). At the same time the NADH signal began to slowly descent (Fig. 3.9a). As mentioned before, the timing of the EOL on acetate differed strongly between experiments but varied less between acetate concentrations (Fig. 3.10a). Since μ_{BM} was noisy at the beginning of the measurements, the timepoints might not be annotated exactly. However, it appeared as if the EOL showed up earlier for medium acetate concentrations in comparison to high or low ones (Figs. 3.8b & 3.10b).

3.3.2.3 Slow Growth Phase

During the slow growth phase the *E. coli* cells continued to grow with the previous, ca. half maximal growth rate of 0.05–0.1 h⁻¹

(Fig. 3.8b). q_{O_2} also either stayed at the value adopted during the EOL or slightly decreased throughout the phase (Fig. 3.8g). The pH slightly increased and $\widehat{\frac{dc_{H^+}}{dt}}$ sank below 0 mol l⁻¹ g⁻¹ h⁻¹ (Figs. S2c & 3.8h). This increase seemed to be stronger for higher acetate concentrations. \widehat{ribof} was seen to slowly increase until the next POI while $\widehat{\frac{dNADH}{dt}}$ continued its linear decrease (Figs. S2b & 3.5h).

3.3.2.4 Growth Increase

The growth increase point ("GRI") was only observed in Ex. HighGA. There, the growth rates μ_{BM} and μ_{scat} increased for a second time, reaching their respective maxima of 0.15–0.2 h⁻¹ (Figs. 3.8b & 3.8d). This increase could take place in two steps. Similar to glucose the value of this local maximum $\mu_{BM,local}$ was highly dependent on the used acetate concentration (Fig. 3.11b). However, it only showed a Monod-like increase at low concentrations. Raising the acetate content over 60 C-mM caused $\mu_{BM,local}$ to plateau first and then strongly decrease with rising acetate supplementation (Fig. 3.11b). In Ex. HighGA μ_{ribof} also decreased by ca. 50 % in parallel to the increase in μ_{BM} (Fig. 3.8f). This relation was stronger for higher acetate concentrations. Growth rates behaved differently in Ex. HighA. There, μ_{BM} increased to the maximum in multiple small steps over a longer period and μ_{ribof} did not decline (Figs. S19b & S19f). Exs. HighGA and BMA also possibly showed \widehat{ribof} reaching its maximum of 2000–2500 AU g⁻¹ and declining afterward (Figs. S2b & S10c). In Ex. BMA a decrease of both $\widehat{\frac{dNADH}{dt}}$ and NADH might also be visible at the respective time (Figs. S10b & S10a). The timing of the GRI was relatively constant in Ex. HighGA with varying acetate content (Fig. 3.10a).

3.3.2.5 Fast Growth Phase

During the fast growth phase growth took place with the now maximal growth rates $\mu_{BM,local}$ between 0.1 and 0.2 h⁻¹ (Fig. 3.8b). Like in the slow growth phase the pH continued to slowly increase while \widehat{ribof} linearly decreased (Figs. 3.8h & S2b). The latter however was only observed if the following O₂-dip was

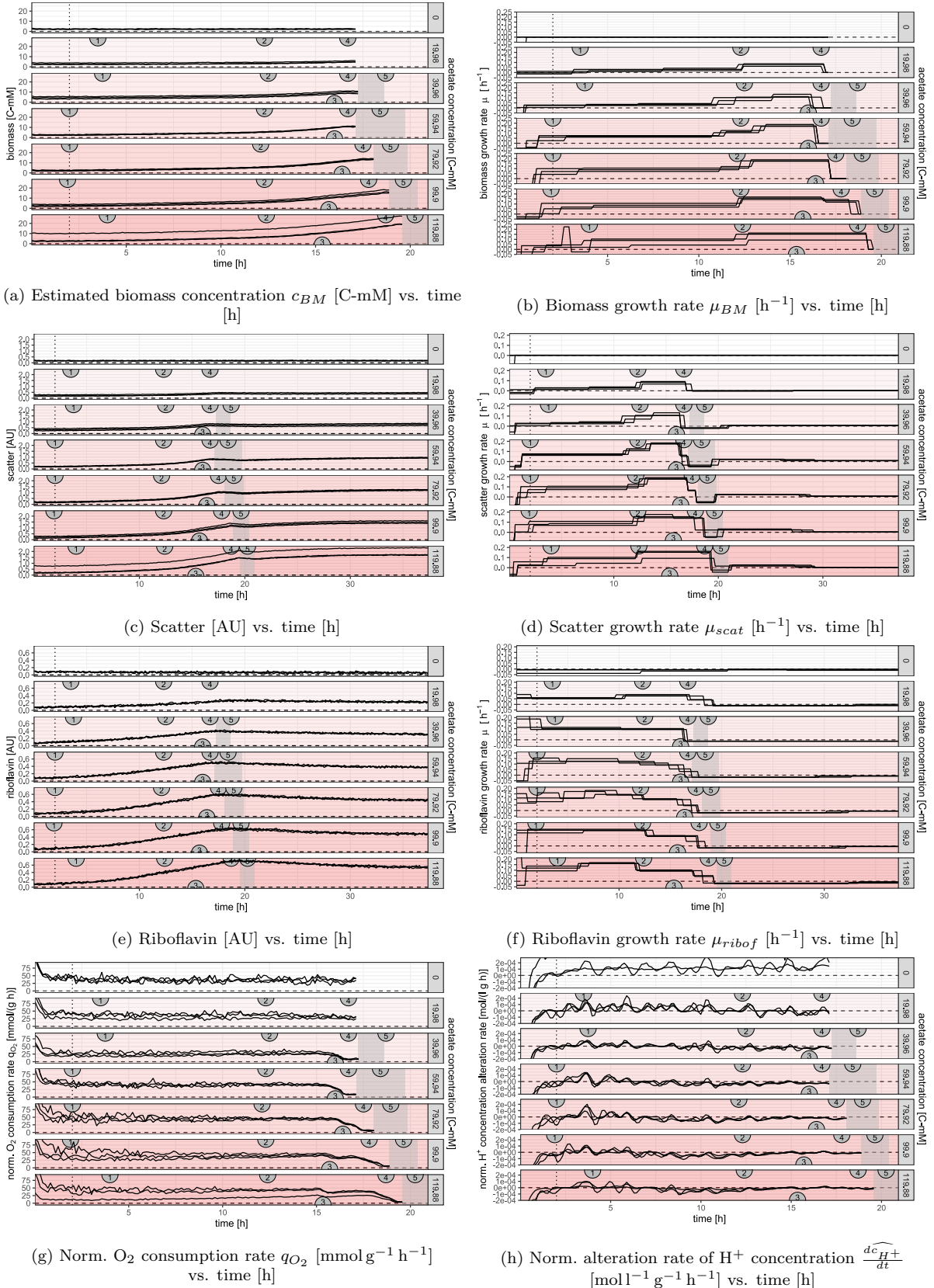


Figure 3.8: **Selected online or derived measurements of Ex. HighGA acetate samples vs. time [h] for *E. coli* batch growth on acetate.** Plots vertically separated by the used acetate concentration (linear gradient: 0 C-mM - 119.88 C-mM), also represented by strength of red background. Each concentration is represented by $n = 3$ technical replicates. Grey shaded areas mark the time range of an automatically determined scatter drop. Since biomass was only determined until the scatter drop, all normalized variables are also only defined up to that point. Numbers in semicircles show the manually annotated mid points of POIs: 1) end-of-lag, 2) growth increase, 3) O_2 -dip, 4) growth decrease, 5) acetate scatter drop.

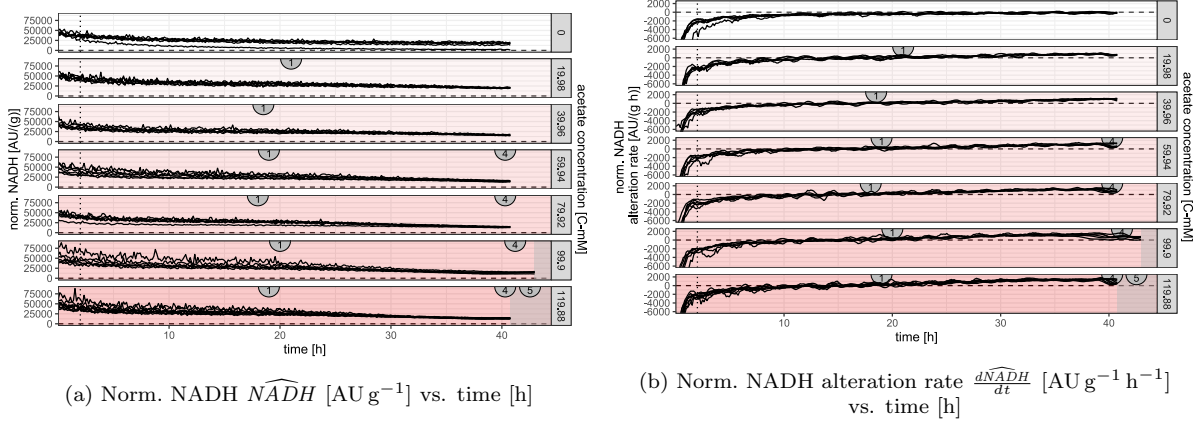


Figure 3.9: **Measurements of normalized NADH and normalized NADH alteration rate of Ex. HighA vs. time [h] for *E. coli* batch growth on acetate.** Plots vertically separated for by the used acetate concentration (linear gradient: 0 C-mM - 119.88 C-mM), also represented by strength of red background. Each concentration is represented by $n = 7$ technical replicates. Grey shaded areas mark the time range of a automatically determined scatter drop. Since biomass was only determined until the scatter drop, the normalized variables are also only defined up to that point. Numbers in semicircles show the manually annotated mid points of POIs: 1) end-of-lag, 2) growth increase, 3) O₂-dip, 4) growth decrease, 5) acetate scatter drop.

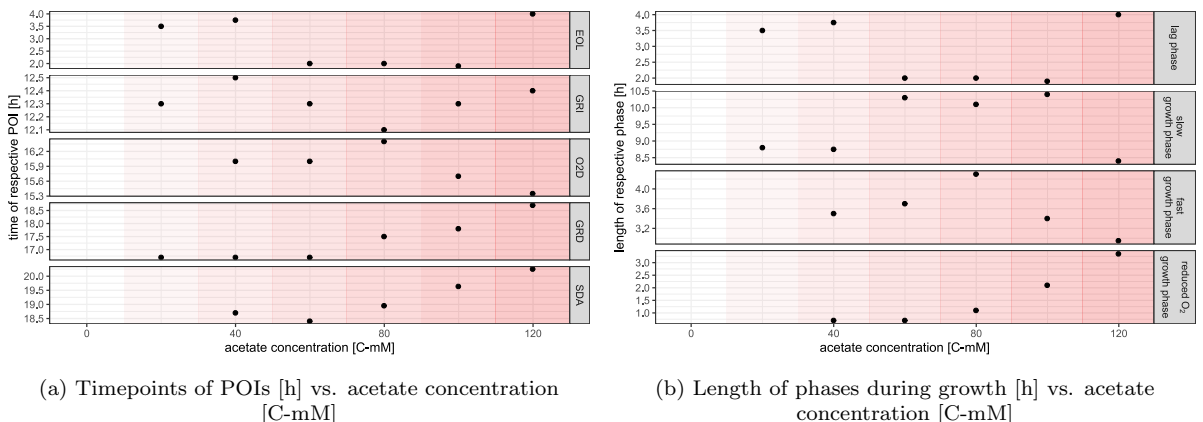


Figure 3.10: **Timings or lengths of POIs and Phases [h] vs. used acetate concentration [C-mM].** The underlying timepoints were extracted from manually annotated points-of-interest and their time differences in acetate samples of Ex. HighGA. Background color visualizes acetate concentration (strength of red).

also present (Fig. S2b). Furthermore, after being negative during the previous phase $\widehat{\frac{dc_{H^+}}{dt}}$ returned close to 0 $\text{mol l}^{-1} \text{g}^{-1} \text{h}^{-1}$. This caused the pH to reduce its ascent or begin to plateau in some cases (Fig. 3.8h).

3.3.2.6 O₂-Dip

The O₂-dip ("O2D") was only present in samples of Ex. HighGA with medium to high acetate concentrations and a few strong outliers of Ex. HighA (e.g. Figs. S2a & S19g). For decreasing acetate concentrations an effect similar to the FHP took place. There, the distance to both the following growth decrease point ("GRD", see below) and SDA continuously dwindled until the GRD masked or fully replaced the O₂-dip (Fig. 3.10a). The O2D primarily appeared as a sudden decrease in O₂ consumption to between 25 and 40 $\text{mmol g}^{-1} \text{h}^{-1}$, i.e. by ca. 25 to 50 %, in about 30 min (Fig. 3.8g). This also caused a temporary increase in O₂ saturation that was visible from the raw data (Fig. S2a). Samples without an O2D showed a static O₂ consumption rate and steadily increasing pH (Figs. 3.8g & S2c).

3.3.2.7 Reduced O₂ Growth Phase

Samples experiencing the O2D continued growth with maximal μ_{BM} , μ_{scat} and ca. half-maximal μ_{ribof} (Figs. 3.8b, 3.8d & 3.8f). q_{O_2} remained stationary at its lowered value (Fig. 3.8g). At medium acetate levels the following GRD followed directly onto the O2D and no reduced O₂ growth phase was visible (Fig. 3.10b). The length of this phase thus depended on the used acetate concentration which seemed to happen in an approximately exponential manner.

3.3.2.8 Growth Decrease

The effect of the GRD point was determined to be similar to the ending of the fast first growth phase for growth on glucose. Starting ca. 2 h before the following scatter-drop μ_{BM} quickly dropped to 0 h^{-1} in one steep decrease (Fig. 3.8b). It was accompanied by μ_{ribof} , which descended to slightly below 0 h^{-1} in multiple smaller steps (Fig. 3.8f). This caused the riboflavin signal to peak and begin a slight

exponential decrease afterward (Fig. 3.8e). A decrease of μ_{scat} to below 0 h^{-1} was often slightly delayed behind the other two growth rates or happened in two steps (Fig. 3.8d). This delay, however, was likely to be a computational artifact as the biomass was directly estimated from scatter signal. Furthermore, q_{O_2} linearly decreased starting with the dropping of μ_{BM} and arriving at 0 $\text{mmol g}^{-1} \text{h}^{-1}$ shortly before the SDA (Fig. 3.8g). In samples where the GRD followed directly onto the O2D, the decreases of q_{O_2} caused by both phases combined into one strong decline (Fig. 3.8g). Additionally, $\widehat{\frac{dc_{H^+}}{dt}}$ often became slightly negative because of a slow increase of pH (Figs. 3.8h & S2c). Exs. BMA and HighA also showed a GRD point. There, \widehat{NADH} became stationary at its lowest measured value around 15000 AU g^{-1} while $\widehat{\frac{dNADH}{dt}}$ decreased to 0 AU $\text{g}^{-1} \text{h}^{-1}$ (Figs. 3.9a & 3.9b). Because of the long time range of these processes the GRD was considered a separate POI which directly preceded the SDA, instead of being part of the previous phase.

3.3.2.9 Acetate Scatter Drop

The scatter-drop on acetate had a weaker effect on the scatter signal than was recorded for glucose. The negative value of μ_{scat} measured around -0.01–0.1 h^{-1} (Fig. 3.8d). This corresponded to only ca. 5 % when compared to the μ_{scat} that were measured during SD1 and 10 % compared to those found for SD2 (Fig. 3.5d). The shape of the SDA also seemed to be dependent on acetate concentration. Samples with low concentrations showed a much wider phase of negative μ_{scat} with lower absolute values (Fig. 3.8d). At medium to low acetate concentrations no negative μ_{scat} was detected. Furthermore, μ_{ribof} remained at its negative value while the pH still increased linearly throughout the SDA (Figs. 3.8f & S2c). This point was present in all experiments conducted with acetate, although drop in scatter appeared a lot weaker in Ex. HighA (Fig. S19d).

3.3.2.10 Unknown Phase

The phase following the SDA showed an unexpected behavior. In samples with medium to high acetate concentrations μ_{scat} rose from

its negative values during the SDA to slightly above 0 h^{-1} . There it remained for almost 10 h before returning to 0 h^{-1} (Fig. 3.8d). The Riboflavin signal on the other hand continued decreasing exponentially, as its growth rate stayed constantly negative (Figs. 3.8e & 3.8f). This decrease persisted for over 10 h in high-acetate samples. However, the riboflavin signal of those samples with the lowest added acetate concentrations still decreased at the end of the evaluated time frame, corresponding to over 17 h. O_2 saturation seemed to be stably at its maximum of 100 % (Fig. S2a). The pH also plateaued shortly after the SDA (Fig. S2c). A slow decrease in pH, that was noticed for medium to low acetate samples, was most likely an artifact (section 3.4.3). Lastly, both Exs. BMA and HighA showed the NADH signal continuously rising throughout the evaluated time range of the unknown phase (Figs. S10e & S20e). The slope of this increase seemed to also be dependent on the underlying acetate concentration (Figs. S10b & 3.9b).

3.4 Various

Some additional observations were made when comparing different POIs and phases of growth or when looking at the recorded growth as a whole.

3.4.1 Glucose

The whole of *E. coli* growth in between the EOL and SD1 was characterized by high cellular activity in form of elevated growth rates (ca. $0.1\text{--}0.4 \text{ h}^{-1}$), O_2 consumption ($10\text{--}20 \text{ mmol g}^{-1} \text{ h}^{-1}$) and the acidification of the medium (Figs. 3.5b, 3.5e & S3e). The basal level of q_{O_2} , as a sign of cellular activity, was even reached during lag-phase. Furthermore, higher values of μ_{BM} seemed to be generally accompanied by higher levels of O_2 consumption. The second growth phase appeared differently with growth at maximal $\mu_{\text{BM},\text{local}}$ and reduced O_2 consumption (Figs. 3.5b & 3.5e). However, q_{O_2} was still elevated above the level present for the lag phase. In comparison, growth rates and O_2 consumption following the SD1 were of

generally low level and accompanied by only slight changes in pH (Figs. 3.5b, 3.5e & S3e). With increasing inoculation OD the rise of $\frac{d\widehat{\text{NADH}}}{dt}$ until the FHP also became progressively steeper (Fig. 3.6d).

In Ex. InocG the maxima of μ_{BM} reached up to 0.4 h^{-1} while samples of Ex. HighGA with equivalent glucose content only reached 0.3 h^{-1} (Figs. 3.6a & 3.5b). Furthermore, the base level of q_{O_2} during the lag phase was elevated to $> 20 \text{ mmol g}^{-1} \text{ h}^{-1}$ in Ex. InocG (Fig. S17b). Neither $\mu_{\text{BM},\text{local}}$ nor the level of q_{O_2} proved to be responsive to the inoculation OD varying by a factor of up to 25 (Figs. 3.6a & S17b).

The normalized riboflavin signal monotonically rose until the stationary phase (Fig. S3c). Since biomass was estimated from riboflavin by a linear model, this change was an effect of the positive ordinate of the estimation model. The normalized scatter (not shown) similarly rose by up to a factor of 4.

Both Exs. BMG and HighG showed massive variations in $\widehat{\text{NADH}}$ in the beginning of their measurements (Figs. S5a & 3.5g). These curves then mostly focused until reaching the FHP (not annotated for Ex. BMG). From there on they showed mostly parallel curve progression. In contrast, the $\widehat{\text{NADH}}$ graphs of Exs. LowG and InocG showed a low noise level and parallel curves from the start (Figs. S13a & 3.6c).

3.4.2 Acetate

In comparison to glucose samples, μ_{BM} and q_{O_2} seemed to behave independently from each other in acetate experiments. O_2 consumption stayed constant for most of the growth leading up to the SDA and only for the GRD did both variables change at the same time (Figs. 3.8b & 3.8g). However, in measurements of Ex. HighGA the value of this basal q_{O_2} was seen to vary between 25 and $50 \text{ mmol g}^{-1} \text{ h}^{-1}$ dependent on acetate concentration (Fig. 3.8g). Ex. HighA did not show this behavior (Fig. S19h).

3.4.3 Outliers

Several outlier wells were detected for all experiments. These outliers, though, did usually only show one or two online measurements that

differed from those of their technical replicate wells. That is why these outlier-wells were not excluded from the data set per se and their differing measurements are still visible in the plots. In those cases, however, the scaling of the plots was often set to best represent the wells not perceived as outliers. Therefore, some outlier signals were cut off to allow for better visibility. Instead of excluding the wells from the data sets, outliers were ignored during data analysis. Notable here was Ex. HighA which amassed the most outliers among the experiments. In one of these outliers even an intermediate O₂ saturation of 0 % was recorded (Fig. S19g).

Besides these outliers, that were specific for each experiment, some systematic anomalies were also identified:

Firstly, as noted for both lag phases, pH and O₂ saturation started with strongly lowered values which increased quickly over the course of ca. 1 h (e.g. Figs. S3e & S3d). In comparison to their levels after 2 h, the beginning values of O₂ saturation were lowered as much as 30 % of the total range of measured values. For pH this deviation was around 20 %. The same effect was also present in NADH measurements where measurements were initially increased by ca. 1 % of the measured values' range (e.g. Fig. S7e).

While shaking and humidity control reached their target values relatively quickly, temperature control took far longer to heat the media to 37 °C. Especially so, as most well plates were cooled before inoculation to prevent cells from growing during the pipetting. The raw data (not shown) displayed water temperature first reaching 36 °C after ca. 2 h. It seemed possible, that the lowered temperature of the medium at the beginning was the main reason for the initially extreme measurements.

Another prominent technical artifact appeared in blanks or wells with low cellular activity, i.e. during the stationary phase in wells with low substrate concentrations. There, a constant, linear decrease of pH signal was observed (e.g. Fig. S3e). The reason for this pH drift is not yet known at the time of this writing and contact

was made to the manufacturer of the BioLector. Furthermore, a specific well showed up as an outlier in all experiments measured. Well "F1" generated a characteristic shape of the pH curve with strongly dropping values after ca. 1–2 h (e.g. outlier of "0" in Fig. S3e). This behavior differed from all its technical replicates. NADH values of this well could be affected similarly by a constant increase (e.g. "0.126" in Fig. 3.6c). These effects added to the regular measurements seen in the replicate wells, such that some impacts of POIs and phases were still visible. For the experiments newly packaged well plates, different plate layouts, and media were used. Therefore, the reason for this phenomenon likely was within the BioLector itself. The manufacturer was also informed of this observation. Well F1 appeared in group "0" of Exs. HighGA, HighG, and HighA; in group "119.88" of Exs. BMG and BMA; in group "22.834" of Ex. LowG, and in group "0.126" of Ex. InocG.

Oscillations appeared in the $\frac{dc_{H^+}}{dt}$ of acetate experiments that were produced by the *sm.spline* smoothing used for rate determination. The low resolution of pH values (0.1 step size) coupled with their amplification upon calculating the H⁺ concentration (10^{-pH}) resulted in large jumps between data points and, thus, strong rate changes.

3.5 Modeling

Next, a Monod model was fit to the biomass measurements using parameters estimated from the data.

3.5.1 Growth Constants

The local maxima of μ_{BM} ($\mu_{BM,local}$) were plotted for each well against the used concentrations of either glucose or acetate (Figs. 3.11a & 3.11b). Exs. HighGA, HighG and LowG were used as representatives of growth on glucose. In the case of acetate, only Ex. HighGA was used for this analysis.

A curve following the nutrient growth law by Monod (eqn. 1.1) posed a visually good fit for most of the glucose data with non-

linear-least-squares estimated parameters of $\mu_{max} = 0.418 \text{ h}^{-1}$ and $K = 31.706 \text{ C-mM}$ (Fig. 3.11a). Data points with high glucose concentrations of Exs. HighGA and HighG showed an almost linear increase of $\mu_{BM,local}$ which was well captured by the saturating nutrient law curve. The low end of the curve exhibited stronger divergence. On one hand, the increasing values of Exs. HighGA and HighG with glucose concentration were still fit well (Fig. 3.11a). On the other hand, the data of Ex. LowG increased with a comparatively much steeper slope and, thus, diverged stronger from the model for increasing glucose concentrations. The latter experiment even showed growth rates around 0.3 h^{-1} . This corresponded to the highest values recorded for Exs. HighGA and HighG at a third of their used glucose content. Ex. LowG would, therefore, imply a higher μ_{max} estimate. Nonetheless, since both Ex. HighGA and Ex. HighG generally agreed with the fitted nutrient law model it was used for parameter estimation.

As mentioned before, in Ex. HighGA values from the low range of acetate supplementation also showed an almost linear increase of $\mu_{BM,local}$ with the substrate (Fig. 3.11b). However, for acetate added to $> 60 \text{ C-mM}$ the recorded local growth rate maxima suddenly plateaued and began to decrease when further raising the acetate content. Since the nutrient law predicts a monotonically increasing and saturating relation of growth rate and substrate, a fit to the data did not produce satisfying results.

Furthermore, the final estimated biomass concentrations ($c_{BM,local}$) of each well were plotted against the respective substrate concentrations (Figs. 3.11c & 3.11d).

A linear model fit to the $c_{BM,local}$ of glucose used a slope of 0.292 and a y-intercept of 10.28 C-mM (Fig. 3.11c). The non-zero ordinate represented the ca. 9–10 C-mM which were predicted by the biomass model for no present riboflavin. Thus, the slope of the model was taken as the glucose yield Y of *E. coli*. Again, the data sets of Exs. HighGA and HighG were fit better by the model, than that of Ex. LowG (Fig. 3.11c). The data points of the latter seemed to form

a slightly steeper linear increase, i.e. imply a slightly higher yield coefficient. Nonetheless, the model was accepted as Exs. HighGA and HighG provided a better resolution of biomass yield at high glucose concentrations.

For acetate a yield of 0.132 with a linear intercept of 2.85 C-mM was predicted (Fig. 3.11d). As opposed to the fit for $\mu_{BM,local}$, the yield seemed well represented by the fit. However, for the highest acetate concentrations, a slight deviation towards a lower biomass yield might be present.

3.5.2 Monod Model

The core assumption of the nutrient law, i.e. the monotonic increase of $\mu_{BM,local}$ with substrate concentration, was not met for acetate data. Therefore, a Monod model was only fit for glucose samples (Fig. 3.12a). There, Ex. HighGA was chosen as a representative. To fit the model, an ODE was set up with equations 1.1, 2.17 and 2.18. The parameter values were filled using the previously estimated growth constants μ_{max} , K , and Y . Then, the ODE was calculated for the initial glucose concentrations (" $c_{S,0}$ ") used in Ex. HighGA. All measured samples showed an initial biomass content. Thus, wells with the same amount of added glucose were grouped, and the mean of their initial estimated biomasses was calculated. Subsequently, this value was added to the calculated biomasses of the respective Monod model using the same initial glucose concentration. Afterward, all of these biomass curves were shifted parallelly on the time-axis until achieving the best fit to the Ex. HighGA c_{BM} data. The utilized *nls* function assigned a value of 2.81 h to this time offset (Fig. 3.12a).

The residuals of this model (Fig. 3.12d) were a partial reflection of the POIs and phases which affected the biomass data. For 0 C-mM glucose, which showed no growth during the experiments, the Model also predicted a stationary c_{BM} . Thus, the residuals varied around 0 C-mM. For all higher concentrations, the mutual starting point of the model curves, 2.81 h, coincided well with the EOL points of Ex. HighGA (ca. 3 h, Fig. 3.7a). In the

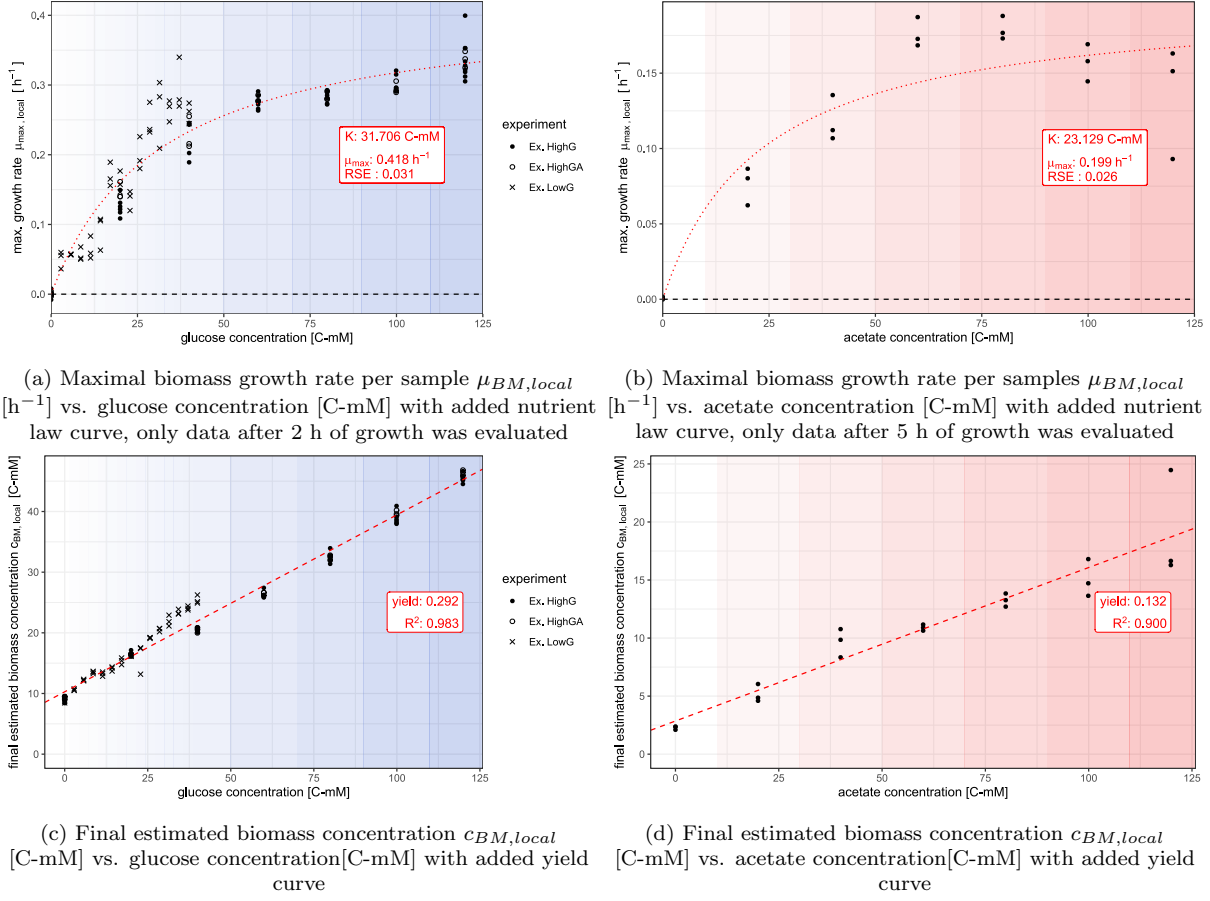


Figure 3.11: **Maximal biomass growth rate per sample $\mu_{BM,local}$ or final estimated biomass concentration $c_{BM,local}$ vs. used substrate concentration c_s [C-mM].** a, c) Data of Exs. HighGA, HighG & LowG with glucose as substrate, point shape shows used experiment, $\mu_{BM,local}$ appearing after 2 h were considered; b, d) Data of Ex. HighGA with acetate as substrate, $\mu_{BM,local}$ appearing after 5 h were considered. The red, dotted line in a) and b) shows a *nls* fit for eqn. 1.1. The final parameters K and μ_{max} , as well as the residual-standard error "RSE" for the fits are given in the red box. A linear model was added to graphs c) and d). In the red box, the slope is given as "yield" together with the model R^2 .

beginning, all residuals of these curves were negative at around -2 C-mM (Fig. 3.12d). This showed that the *E. coli* samples had already grown slightly during the lag phase. During the growth the residuals varied between -4 and 4 C-mM and appeared as two hill-like, concave curves connected at the first scatter drop. At medium substrate concentration the residuals reached 0 C-mM and became static at ca. the SD2s timepoint. Differently, the residuals of samples with high glucose content became largely negative there and stabilized at values between -1 and -3 mM. In these cases, the final biomass yield was therefore generally underestimated.

The mean-squared-error (MSE) of the models for 19.98 and 119.88 C-mM glucose showed them being especially deviant (Fig. 3.12e). The residuals were largely negative for both of these models meaning that the samples' biomasses were underestimated over the whole time frame (Fig. 3.12d). On the other hand, the non-growing samples, without added glucose, were estimated best (Fig. 3.12e). All other models showed an MSE between $1.5\text{--}2$ (C-mM) 2 . As the final c_{BM} varied between 10 and 45 C-mM, the MSE was in most cases at least one order of magnitude smaller.

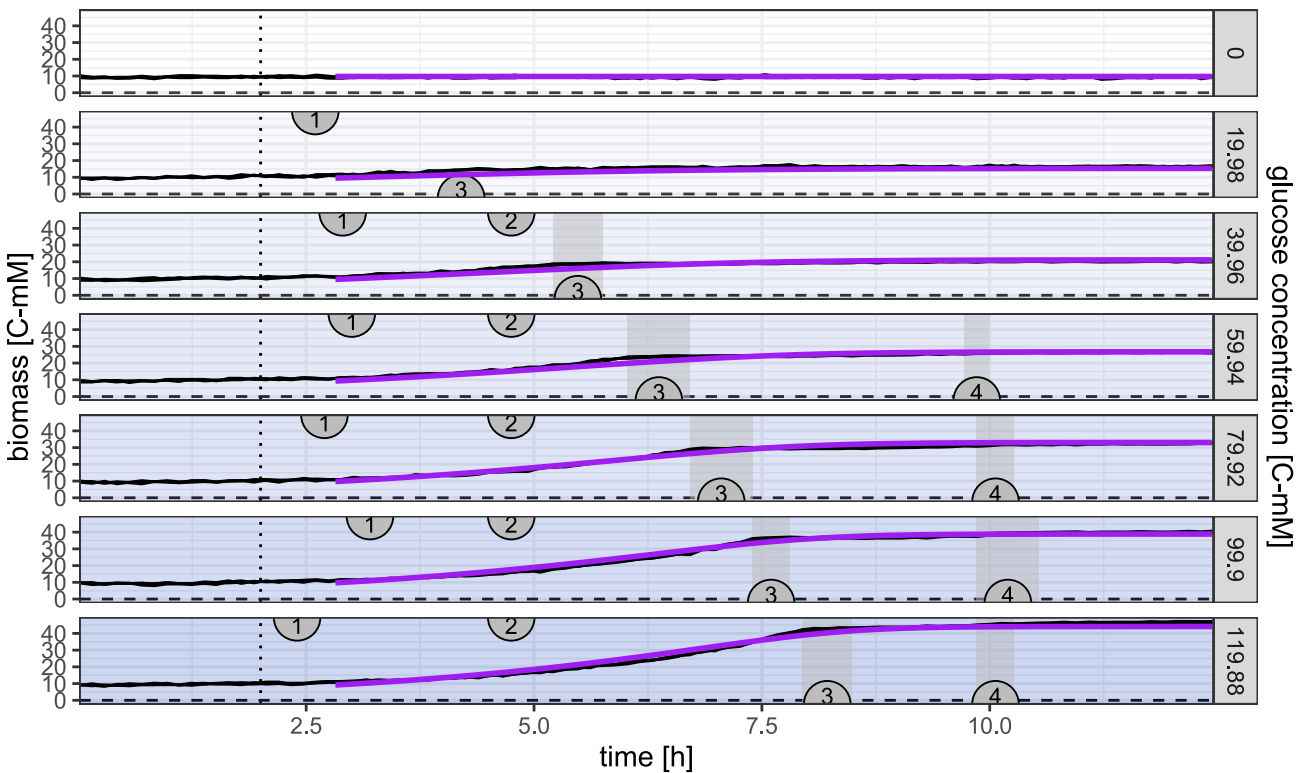
The initial modeled μ_{BM} values were given by the nutrient growth law curve which was fit to the same data (Fig. 3.11a). Therefore, they corresponded well to the $\mu_{BM,local}$ of the respective glucose concentrations.

The Monod model also predicted an almost linear decrease of the substrate and a related, monotonic decrease of μ_{BM} from its initial value (Figs. 3.12c & 3.12b). Furthermore, all models with medium to high glucose concentrations arrived at the growth rate's pivot point at around 8 h. They subsequently reached substrate exhaustion and stagnating growth after 10 h.

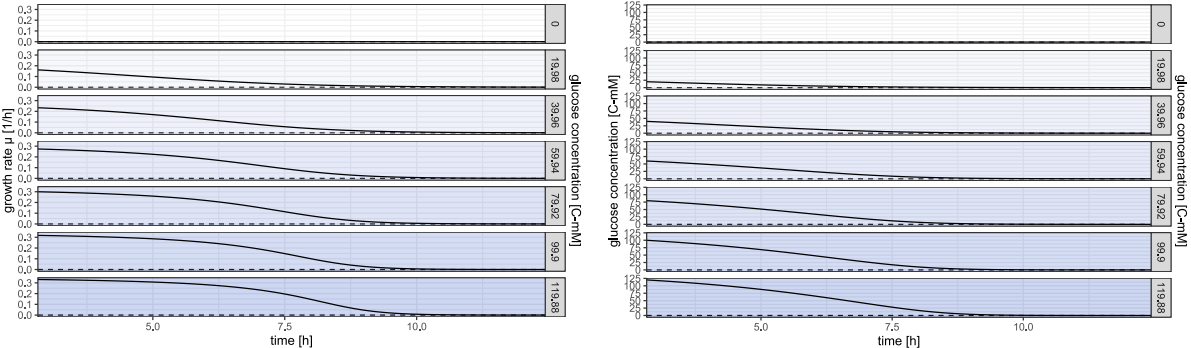
This development of μ_{BM} , however, did not reflect the observed behavior in glucose samples. The starting point of the models (2.81 h) was set approximately at the EOL (ca. 3 h, Fig. 3.7a). There, the measured growth rates started at a ca. half-maximal values and remained there

stably for the first growth phase (Fig. 3.5b). The growth rates of the Monod models, on the other hand, started with their local maxima and directly began to decrease (Fig. 3.12b). The following measured increase in growth rate at the FHP and subsequent growth with stable $\mu_{BM,local}$ (Fig. 3.5b) was therefore also not captured by the model. This increase at already lowered substrate concentrations would indeed object to the nutrient growth law. The same would be true for μ_{BM} remaining at static levels, i.e. not reacting to changing amounts of substrate. Also, since the growth rates of the Monod models gradually changed together with the substrate contents (Figs. 3.12b & 3.12c; eqn. 1.1), no sudden changes would be expected for either variable. However, especially during the scatter-drops rapid changes in μ_{BM} were measured (Fig. 3.5b).

Interestingly, both the measured onset of the stationary phase and the point at which the modeled μ_{BM} approached 0 h $^{-1}$ fell into the time range around 10 h (Figs. 1.1 & 3.7a).

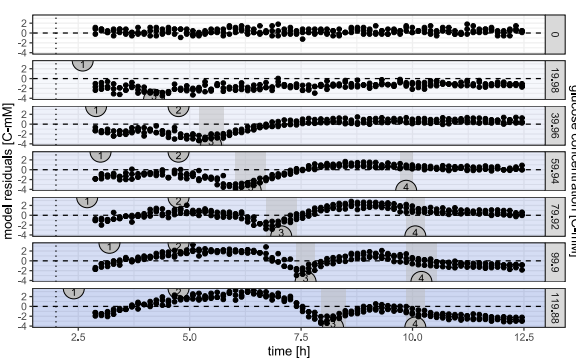


(a) Fit of Monod-ODE growth curves (purple lines) to estimated biomass concentrations c_{BM} [C-mM] of Ex. HighGA (black lines) vs. time [h]

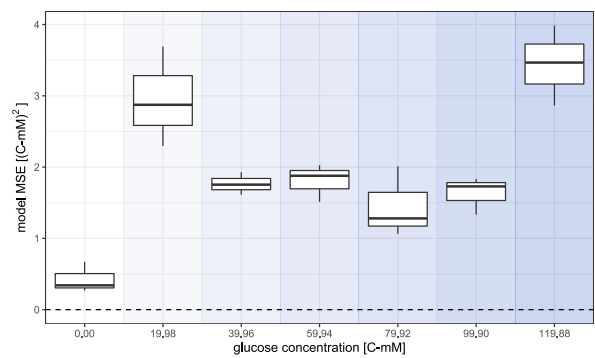


(b) Modeled values of μ_{BM} [h^{-1}] vs. time [h]

(c) Modeled glucose concentrations c_S [C-mM] vs. time [h]



(d) Residuals of the fit Monod-ODE growth curves [C-mM] vs. time [h]



(e) Mean-squared-error ("MSE") of each Monod-ODE growth curve fit to Ex. HighGA data $[(C-mM)^2]$ vs. glucose concentration [C-mM]

Figure 3.12: Variables of a Monod-ODE model fit to Ex. HighGA glucose samples vs. time [h] with goodness-of-fit measures. Plots a) - e) are vertically/ horizontally separated by the used glucose concentration (linear gradient: 0 C-mM - 119.88 C-mM), also represented by strength of blue background. In measured data each concentration is represented by $n = 3$ technical replicates. Grey shaded areas mark time ranges of a automatically determined scatter drop. Numbers in semicircles show the manually annotated mid points of POIs: 1) End-of-lag, 2) 5 h point, 3) Scatter-drop 1, 4) Scatter-drop 2.

Discussion

4.1 Multiple Growth Phases

The POIs and phases found in glucose-grown *E. coli* W3110Z1 had high repeatability. They reliably appeared in experiments conducted at different time points and followed sensible patterns when varying both substrate concentration and initial cell density. Thus, it seems very likely that these subdivisions represent changes and routines in *E. coli* growth behavior that can be generalized. These results of the following discussion are summarized in Fig. 4.1.

4.1.1 The Lag Phase

The lag phase is a well-known phenomenon for bacterial growth. Unfavorable conditions such as low temperatures or previous starvation may result in a phase of non-replication when cells enter new growth-media (Bertranda, 2019). Both of these conditions were fulfilled since the precultures were 1 d old at the time of use and were transferred into cooled growth media. Followingly, the main characteristic of lag, a growth rate close to zero (Monod, 1949), was met in every experiment performed in this work. Ignoring the probable artifacts at the beginning, *E. coli* also exerted noticeably little changes to variables like NADH, riboflavin, and the pH. Only for high initial cell densities did *E. coli* also show a strong generation of NADH during the lag. This alone might give the impression of dormancy. Oxygen consumption, however, continuously showed half-maximal rates of $10 \text{ mmol g}^{-1} \text{ h}^{-1}$ and in some cases even around $20 \text{ mmol g}^{-1} \text{ h}^{-1}$. The latter corresponds to the maximal q_{O_2} measured for *E. coli* growing on glucose (Andersen and Von Meyenburg, 1980). Having such a high respiratory activity the *E. coli* cells appeared rather active despite the missing growth. It has been observed that bacterial cells entering lag drastically alter their proteome and transcriptome in preparation of growth (Bertranda, 2019). Thus, a large amount of energy is invested in internal restructuring. This energy was shown to be mainly taken from the digestion of glycogen

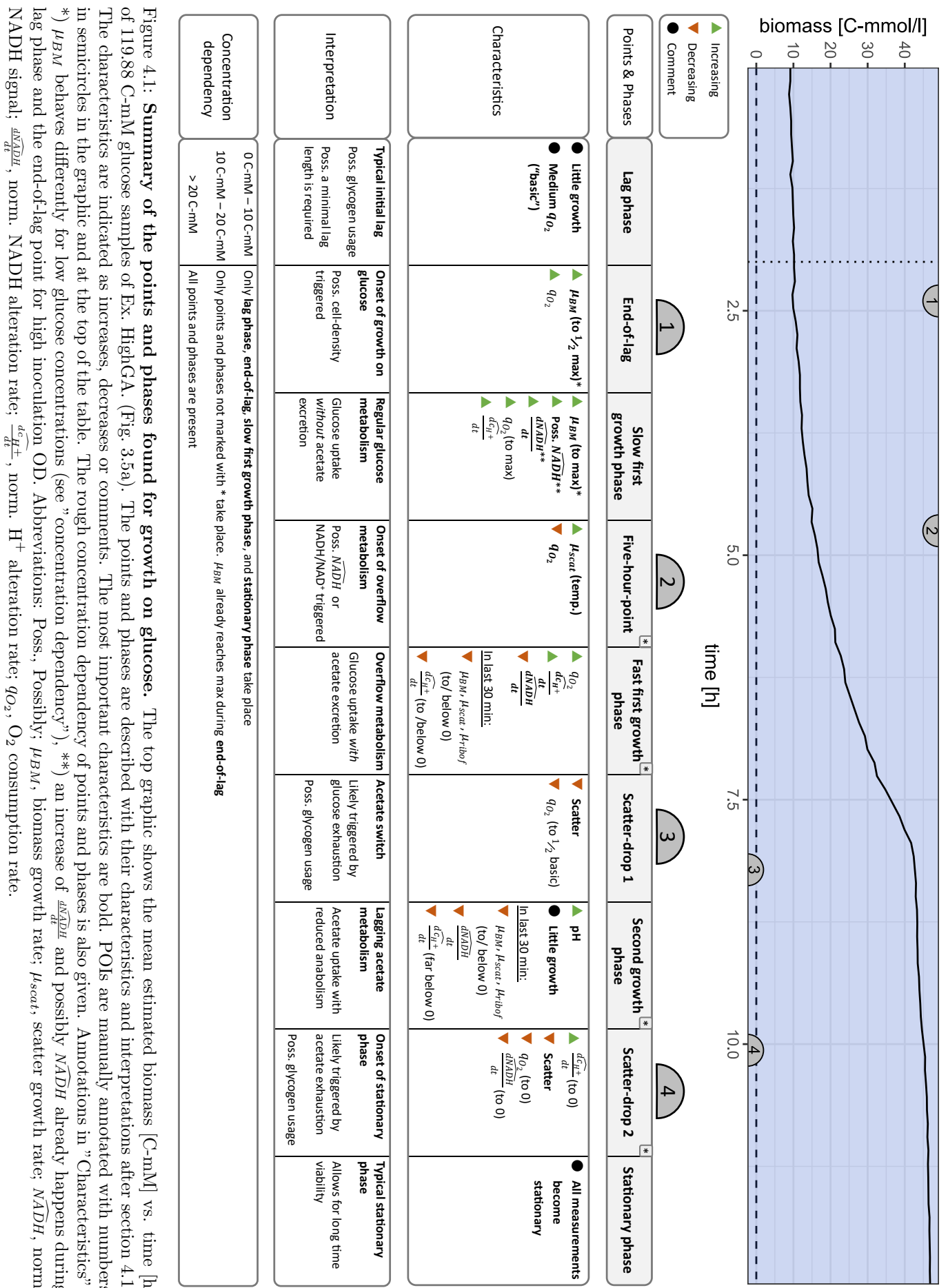
reserves (Bertranda, 2019; Yamamotoya et al., 2012). This state of preparation with strong respiration would sufficiently explain the observed trends. Samples without added glucose did not show an elevated respiration rate at the beginning. Therefore, the presence of extracellular nutrients might be required to induce a lag phase and metabolize the glycogen reserves (see also Bertranda, 2019).

4.1.2 The End of Lag

With the first increase of μ_{BM} at the end-of-lag point this lag phase ends in what is also called the acceleration phase (Monod, 1949). The matching times of the observed EOL point and the predicted time-offset of the Monod model reinforce that lag phase and EOL match with the growth phases laid out by Monod (Monod, 1949). As established previously, the cells are already highly active during the lag phase. Thus, it is not surprising that the sudden onset of growth was not accompanied by a likewise increase in respiration rate. Instead, a shift in activity from preparation to growth seemed to have taken place.

The length of the lag phase was shorter for higher initial cell densities (Fig. 3.7d), consistent with previous reports (Bertranda, 2019). The reason for this was theorized to be the random chance of *E. coli* cells to show abnormally low lag times as a trait (Bertranda, 2019). In large populations this event would, thus, be more likely. Between experiments, however, the estimated biomasses and scatter values at the EOL points were very similar (around 10 C-mM biomass and 0.2–0.25 AU scatter). This might imply, that a specific cell density is involved in triggering the end of the lag phase.

Nonetheless, *E. coli* seemed to approach a minimal lag period of 3 h for the highest inoculation ODs tested. This could mean that a minimum of 3 h of lag is required for the cells to induce mitosis in the tested environment even when the critical cell density is reached. Possibly, this is an effect of the cooled medium and the starving preculture cells. However, for samples



at this minimum lag the $\widehat{\frac{dNADH}{dt}}$ during the lag phase rose with an increasing initial cell density. At the same time the FHP, the assumed onset of overflow metabolism (section 4.1.4), which was characterized by a high $\widehat{\frac{dNADH}{dt}}$ followed up progressively closer to the end-of-lag point. Under these conditions, the above-mentioned production of NADH then seemed to be already initiated during lag. This might imply that the characteristic behavior of the following growth phase propagated back into the lag phase. A dependency of the lag-duration on the glucose concentration was not found. This further supports the view, that energy production during lag phase is fueled by internal glycogen reserves.

4.1.3 The Growth Phases

Experiments studying carbon-limited batch cultures of *E. coli* on glucose supplemented minimal medium generally showed the observed behavior of biomass development (Wolfe, 2005; Andersen and Von Meyenburg, 1980; O’Beirne and Hamer, 2000; Enjalbert et al., 2015). In these experiments, measured time series of glucose and acetate levels revealed the two separate growth phases produced by overflow metabolism. There, the first one possesses high growth rates while glucose is taken up and acetate is excreted. The second phase appears after exhaustion of glucose where the produced acetate is then taken up but very little biomass is produced. (Andersen and Von Meyenburg, 1980; Enjalbert et al., 2015; O’Beirne and Hamer, 2000). It was found that this second growth phase on acetate takes place during another lag period caused by overflow metabolism (Enjalbert et al., 2015). During this lag acetate is already being consumed while the q_{O_2} and the CO_2 production are strongly reduced (Enjalbert et al., 2015; Andersen and Von Meyenburg, 1980). Analysis of transcription revealed that central enzymes of acetate anabolism are also not induced during the lag. This causes the acetate to be metabolized without the production of biomass (Enjalbert et al., 2015). For larger quantities of acetate a phase of efficient growth is induced after the

lag period. However, due to the small amounts of acetate produced by overflow metabolism the substrate is exhausted during lag (Enjalbert et al., 2015). The description of this lag period matches the measured data of the first scatter-drop and the following growth. Around the scatter-drops μ_{BM} drastically dropped together with the q_{O_2} and both rates remained low afterward. The scatter-drops were also the only observed points where the growth rate consistently decreased between experiments. In this context, the falling $\widehat{\frac{dc_{H^+}}{dt}}$ during the first scatter-drop and the following alkalization of the medium also correspond well to the uptake of acetate and a lowered production of CO_2 and, thus, carbonic acid.

Therefore, it seems the logical to assume that the first scatter drop corresponds to the transition between acetate excretion and acetate consumption: The acetate switch. This would identify the preceding period of growth as the growth phase metabolizing glucose. The following period of growth would correspondingly represent the acetate-fueled growth.

4.1.4 The First Growth Phase

Following the lag, *E. coli* grew with a continuously elevated growth rate up until the first scatter-drop. This time range was hence deemed the first growth phase, i.e. the phase of glucose metabolism. However, for glucose concentrations exceeding 20 C-mM (0.07 % w/v) this growth was reliably split into two sub-phases. Here, the hypothesis is established that these sub-phases represent the growth on glucose preceding and following the onset of overflow metabolism:

For every experiment conducted with glucose the maxima of μ_{BM} were reached during the first growth phase. These $\mu_{BM,local}$ were highly dependent on the used glucose concentration and governed by Monod’s nutrient growth law (Monod, 1949). The calculated μ_{max} of 0.418 h^{-1} is in the vicinity of the value found for *E. coli* W3110 growing with glucose (0.49 h^{-1} , O’Beirne and Hamer, 2000). This supports the assumption that the combination of both sub-phases makes up the phase usually

identified as the growth phase for glucose. Since almost no biomass was produced following the first scatter-drop, the biomass yield is also mainly a result of the preceding growth. The found yield of $Y = 0.292 \frac{\text{C-mM}}{\text{C-mM}}$ ($\approx 0.246 \frac{\text{g}^{1-1}}{\text{g}^{1-1}}$), however, laid far below the recorded values of $0.49 \frac{\text{g}^{1-1}}{\text{g}^{1-1}}$ for strain W3110 (O’Beirne and Hamer, 2000). No published yield measurements were found for strain W3110Z1. Nonetheless, it should be noted that the final estimated biomasses of most samples were consistent with a common yield function. The yield was, therefore, mostly independent from the first growth phase being split or not. Thus, it seems overall likely that together both sub-phases make up the primary growth on the added glucose.

The first sub-phase, deemed slow first growth phase, was characterized by initial growth rates up to 0.2 h^{-1} and gradually increasing values of q_{O_2} , $\frac{dc_{H^+}}{dt}$, and $\widehat{\frac{dNADH}{dt}}$. This was the only phase with elevated growth found for samples with low glucose content. In this group of samples, the observed behavior of all online measurements was very similar between samples. Notably, the first sub-phases of samples with higher levels of glucose were also very similar to the low-glucose group in almost all measured variables. This might imply that during these periods *E. coli* possesses the same mode of growth. Since for low-glucose cultures no growth was found following the presumed acetate switch, likely no acetate excretion had taken place. In this case, the glucose taken up by the cells would have been fully metabolized and likely respired without the production of acidic acetate. This conclusion is supported by the high respiration rate and the relatively low $\frac{dc_{H^+}}{dt}$ measured in this time frame.

The transition between both sub-phases, here called five-hour-point, was characterized by a preceding, sudden increase of μ_{BM} together with a decrease in q_{O_2} and a steadily rising $\frac{dc_{H^+}}{dt}$. Therefore, it overall doesn’t compare to the lag period observed before the acetate switch or to lag during diauxic growth in general (Monod, 1949). Because of this, it seems additionally

unlikely, that the two sub-phases are caused by different nutrients being metabolized. According to the hypothesis the FHP would mark the switching of *E. coli* from the full metabolism of glucose to overflow metabolism. It has been shown that this switch is initiated when *E. coli* cells exceed a threshold growth rate (Basan et al., 2015; Szenk, Dill, and Graff, 2017; Valgepea et al., 2010). The found threshold values of μ_{BM} differ strongly between sources and the respectively used strain of *E. coli*. For strain K12 WT a threshold of 0.7 h^{-1} was found (Basan et al., 2015). On the other hand, strain K-12 MG1655 which is genetically close to W3110 (Hayashi et al., 2006) showed thresholds of 0.27 or 0.3 h^{-1} (Szenk, Dill, and Graff, 2017; Valgepea et al., 2010). In this work a similar μ_{BM} of ca. 0.2 h^{-1} was reached before the onset of a five-hour-point in most cases. Therefore, this growth rate could pose the relevant threshold. A different interpretation could be that 0.2 h^{-1} is the highest growth rate obtainable for *E. coli* W3110Z1 without inducing overflow metabolism.

It was furthermore hypothesized that the underlying cause for the overflow metabolism is a restriction of space or protein available for respiration (Basan et al., 2015; Szenk, Dill, and Graff, 2017; Andersen and Von Meyenburg, 1980). The reduction of NAD^+ during glucose metabolism could then exceed the limited capacity of the respiration. A rising NADH/NAD^+ ratio would be the result (Szenk, Dill, and Graff, 2017). This, in turn, could be a trigger for the initiation of the overflow metabolism (Szenk, Dill, and Graff, 2017; Vemuri et al., 2006). The q_{O_2} reaching its proposed maximum of $20 \text{ mmol g}^{-1} \text{ h}^{-1}$ (Andersen and Von Meyenburg, 1980) could represent this limited respiration. In this case, the rising $\widehat{\frac{dNADH}{dt}}$ could also show an increasing NADH/NAD^+ ratio. The common $\widehat{\frac{dNADH}{dt}}$ value of ca. 5000 AU g^{-1} prior to the FHP could then depict the threshold after which overflow metabolism is initiated. The down regulation of the TCA cycle during overflow metabolism could explain the following decrease of $\widehat{\frac{dNADH}{dt}}$. The measured values are, thus, compliant with

this interpretation.

For the time dependency on the inoculation OD two possible explanations are presented. A critical biomass concentration could be in place again since a common biomass of ca. 20 mM was reached. On the other hand, the inoculation dependency could also be another effect of a metabolic trigger: For increasing initial cell densities, *E. coli* seemed to also increase $\frac{dNADH}{dt}$, even crossing into the lag phase. Followingly, the critical NADH concentration would be reached progressively earlier.

The assumption that both respiration and glucose transporters are limited by the same membrane space (Szenk, Dill, and Graff, 2017) could also explain the existence of the first sub-phase despite high levels of glucose: For growth rates up to the threshold value the number of respiratory enzymes and glucose transporters would be adjusted to the requirements of growth. If at the threshold μ_{BM} the membrane space became limiting, a temporary compromise of the ratio of transporters to respiratory chain proteins might be found. If this ratio was independent of the extracellular glucose concentration, the glucose influx would reach a common limit and *E. coli* could show consistent behavior in the following growth phase. During this phase, the respiration would then also be limited by the amount of respiratory enzymes. Should the uptake of glucose exceed this capacity, the proposed increase in NADH/NAD⁺ ratio could result. This rising ratio could then trigger overflow metabolism. The initiated aerobic fermentation would lower the requirement for respiration and a reduction of respiratory chain proteins could proceed in favor of glucose transporters. After this point, acetate excretion would occur. If this protein ration were then dependent on the external glucose concentration again, a higher glucose influx and higher growth rates could be achieved for greater glucose concentrations. This would be then accompanied by higher acetate efflux.

The following second sub-phase, deemed fast first growth phase, was also in line with the hypothesis of induced overflow metabolism. The

growth of *E. coli* with maximal μ_{BM} despite the reduced respiration rate (O₂ consumption) points towards aerobic fermentation taking part in the metabolization of glucose (Szenk, Dill, and Graff, 2017). Furthermore, the excretion of acetate would also explain the intensified increase of $\frac{dcH^+}{dt}$. Since fermentation also generates fewer reducing equivalents (Szenk, Dill, and Graff, 2017), the lowered $\frac{dNADH}{dt}$ would result logically.

The observed, sudden decrease in growth and alteration rates near the following scatter-drop was also found in publicized data (Enjalbert et al., 2015). It seems possible, that this is caused by *E. coli* preparing for the following acetate switch (transcription in Fig. 3 of Enjalbert et al., 2015).

Low glucose concentrations would be exhausted earlier by *E. coli* growth. Therefore, the dependence of phase-length on glucose concentration is sensible. The independence from the initial cell density could, then, result from the comparable biomasses of ca. 20 C-mM at the acetate switch. With similar glucose and biomass concentrations in these cultures the exhaustion point would be reached after similar time ranges.

4.1.5 The First Scatter-Drop

As established previously, the first scatter-drop likely represents the acetate switch. There, the supplemented glucose is exhausted and a lag period is induced (Enjalbert et al., 2015). This lag marks a large reprogramming of the central metabolism to assimilate and metabolize acetate (Enjalbert et al., 2015). Strong repression of central enzymes in the TCA cycle and acetate anabolism (Enjalbert et al., 2015) explain well the observed reduction of growth. Since the TCA cycle produces NADH and CO₂, a weakened TCA cycle could also be the cause of the lowered reduction of NAD⁺ and decreases in the production of CO₂. With reduced production of carbonic acid from CO₂ and the beginning uptake of acetate the observed negative $\frac{dcH^+}{dt}$ is also plausible. The strongly reduced q_{O_2} was also found typical for this lag (Enjalbert et al., 2015). It can

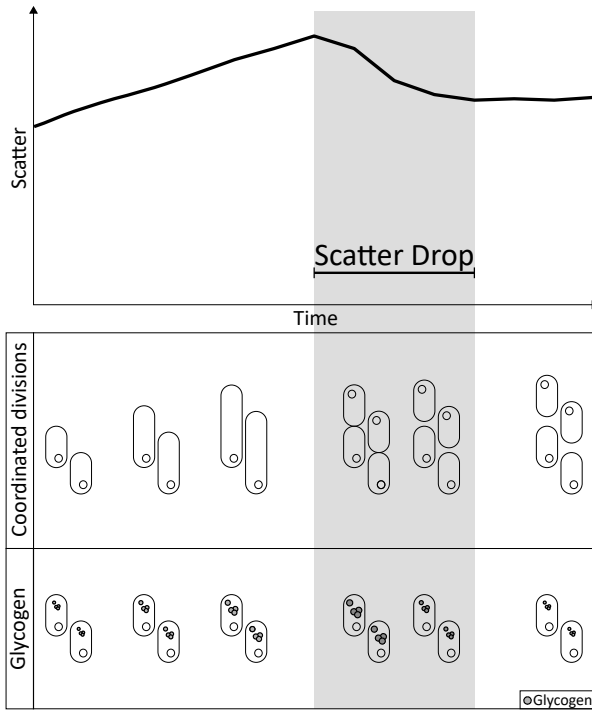


Figure 4.2: Hypotheses for the cause of scatter-drops. The top graph shows a schematic of scatter values vs. time around the scatter drop. The grey area marks the approximate time range of the scatter-drop. Bottom panels show the schematic behavior of *E. coli* cells. Coordinated divisions or changes in glycogen metabolism are given as hypotheses.

be assumed that the reason for this reduced respiration also lies in the cellular restructuring (changing transcription during acetate lag period) as increased O_2 consumption is seen for higher acetate concentrations after the lag period (Enjalbert et al., 2015).

However, the main characteristic of the scatter drop, the sudden decrease of scatter signal, remains unclear. Publicized data for *E. coli* growth on glucose does not show similar decreases in OD measurements. However, a slight decrease in biomass after glucose exhaustion was recorded (Fig. 2 in O’Beirne and Hamer, 2000). The dry weights measured in this work, however, suggest that no biomass was lost in the scale of dropped scatter signal (-20 - -30 %). Interestingly, upon exhaustion of ammonia in nitrogen-limited growth a drop of OD_{600} might be present (Fig. 1 in Yamamotoya, 2012). An imaginable cause for these alterations of scattering are for example coordinated cell divisions where a length increase during normal growth

and a sudden change from long to short cells at the scatter-drop could influence the scatter (Fig. 4.2). Otherwise, an internal restructuring of the cell might be possible. In the case of the OD-drop for the depletion of nitrogen an accompanying decrease of normalized glycogen content was measured (Fig. 2 in Yamamotoya, 2012). If the observed phenomena are comparable, this might make a sudden degradation of glycogen a suitable candidate for the cause of the scatter-drops (Fig. 4.2).

The flowcytometric and microscopic analysis of the biomass time-series samples conducted in a parallel study did not suggest a change in cell shape with progressing growth (Burmester, 2020). However, two subpopulations with differing cellular granularity were found. There, the ratio shifted toward the high-granularity group during exponential growth. Following the scatter-drops, however, the population’s mean granularity decreased and the ratio of low-granularity cells rose again (Burmester, 2020). Assuming that glycogen impacts this mentioned granularity, it might be a suitable candidate for explaining the scatter-drops and further research seems appropriate.

4.1.6 The Second Growth Phase

The observed growth following the acetate switch is likely the continuation of the begun lag period. The small μ_{BM} and continuously low q_{O_2} are in line with this interpretation. Importantly, the mostly negative $\frac{dc_{H^+}}{dt}$ also supports the uptake of acetate. The length of this phase would then reflect the amount of acetate produced and the overall acetate uptake rate by the grown biomass. Notably, none of the phases seen for growth on acetate were observed in this phase. The low yield of biomass further differed from the acetate experiments. This strongly supports the claim, that the metabolism of acetate alone is fundamentally different from that after the acetate switch (Enjalbert et al., 2015).

4.1.7 The Second Scatter Drop

Since both scatter-drops showed a very similar mode of changing measurements, it seems reasonable to assume that the exhaustion of the

substrate is their common cause. This is supported by experiments where the characteristically falling q_{O_2} followed directly on the depletion of acetate (Andersen and Von Meyenburg, 1980). In contrast to the acetate switch at first scatter-drop, the second scatter-drop likely marks the preparation for the stationary phase. Since the scatter decreases in the same manner for both of these phases, the processes could also be similar. It seems plausible, that the cellular changes that *E. coli* performs at both of these points are at least partially fueled by glycogen as the substrate concentrations are already low. As such, the break-down of glycogen remains a viable explanation for the drops in the scatter signal.

4.1.8 The Stationary Phase

Like the lag phase, this phase's primary feature is μ_{BM} being reduced to 0 h^{-1} (Monod, 1949). Furthermore, nearly all measured alteration rates also became stationary at zero, implying an almost fully halted metabolism. The cell state in this phase is sensibly allowing long time viability since source cultures survived the intervals of multiple days between transfers into new media. It has been shown that *E. coli* undergoes several cellular changes for this task ranging from the condensation of its chromosome to the packing of ribosomes and fortifications of the cell wall (Pletnev et al., 2015; Bertranda, 2019).

4.2 Growth on Acetate

For acetate fewer experiments were conducted and their results differed strongly. Thus, the found phases are much more ambiguous and only few interpretations can be made.

4.2.1 The Lag Phase

In most points the lag phase for acetate resembled the one described for glucose. When disregarding the initial temperature effects the phase of minimal growth was accompanied by mostly unchanging culture measurements. The slightly positive $\widehat{\frac{dc_{H^+}}{dt}}$ also indicates that no acetate was being consumed. This could mean

that the lag on acetate is also fueled by glycogen reserves. Because of the changing substrate, cells in acetate samples were transferred into an environment very different from the precultures and a much longer lag phase than seen on glucose would be expected (Bertranda, 2019). This is especially true since acetate is cytotoxic in higher concentrations (Wolfe, 2005; O'Beirne and Hamer, 2000). An increase in the lag duration, however, was only seen for part of the experiments. Already during lag a q_{O_2} of $25\text{--}50 \text{ mmol g}^{-1} \text{ h}^{-1}$ was measured, implying high activity. However, this value is unexpectedly high, as the O_2 consumption for growth on acetate was determined as ca. $18 \text{ mmol g}^{-1} \text{ h}^{-1}$ (Andersen and Von Meyenburg, 1980). Since the estimated q_{O_2} were sensible for glucose samples, errors in the O_2 measurements are unlikely. Underestimated biomass seems to be a more plausible cause for the high estimated q_{O_2} .

4.2.2 The End of Lag

The lag phase, again, ended with the first increase in growth rate to $0.05\text{--}0.1 \text{ h}^{-1}$. Changing rates of NADH alteration and H^+ production showed a complementary change in metabolic activity. Thereby, the beginning increase of the pH, that is seen when accounting for the pH drift, complies with the start of acetate consumption.

4.2.3 The Growth Phase

Following the end of the lag phase on acetate, *E. coli* also showed uninterrupted growth with increased μ_{BM} until the scatter-drop. Therefore, per the observations made for glucose this is likely a single growth phase in which acetate is used up.

This is backed by data from O'Beirne and Hamer where the exponential growth of *E. coli* strain W3110 was seen to last until the exhaustion of acetate (Fig. 2 in O'Beirne and Hamer, 2000). Due to the low time-resolution of this published data, possible POIs are hardly discernable. However, their measurements seem to point out changing growth behavior after 9–10 h. The stagnant acetate concentration and

CO_2 production at this point would correspond well to the stationary pH seen at the O_2 -dip. Therefore, the existence of sub-phases, as seen for glucose, also seems plausible:

The first of these sub-phases, deemed slow growth phase, showed the increase of μ_{BM} to ca. it's half-maximum. In the following fast growth phase the growth was then continued with the maximal growth rate. Of the conducted experiments one showed a clear separation of these sub-phases as the growth increase point. There, μ_{BM} rose in one to two steps. This was accompanied by declining values of μ_{ribof} and \widehat{ribof} . The riboflavin fluorescence likely includes FAD and FMN because of their similar excitation and fluorescence spectra (Drössler et al., 2003). All of these are essential for basic metabolism (Vitreschak et al., 2002) and, thus, the uncoupling of scatter and riboflavin signals likely indicates a change in metabolism or cell structure. The data collected during biomass measurements mostly agreed with this separation and additionally showed falling $\frac{d\widehat{NADH}}{dt}$ and \widehat{NADH} at the respective time point. This would promote the idea of a metabolic alteration.

However, the last experiment, which used a preculture grown on acetate instead of glucose, showed no differentiation of these two sub-phases. Instead, a continuous increase of μ_{BM} with no connected changes of riboflavin measurements was seen. This could mean that the formation of two separate phases is a consequence of the initial growth on glucose.

The value of $\mu_{BM,local}$ was strongly dependent on the acetate content. Until reaching 60 C-mM acetate the maximal growth rate increased with acetate content. For higher concentrations, however, this maximum dropped strongly. This behavior probably results from the toxicity of acetate (Wolfe, 2005; O'Beirne and Hamer, 2000) which was shown to also decrease maximal growth rates if added to cultures growing on glucose (O'Beirne and Hamer, 2000).

As mentioned previously, the following O_2 -dip might also be present in published data. There, the equivalent time range (9–10 h) shows almost no acetate uptake (Fig. 2 in O'Beirne

and Hamer, 2000). The stagnant pH and the reduced respiration found in this work would match that observation. Furthermore, only larger amounts of acetate were found to trigger this decrease in q_{O_2} . A beginning excretion of byproducts as seen with similar behavior at the five-hour-point on glucose seems unlikely, though. This is because no second growth phase and especially no second scatter-drop was recorded. For the following phase, deemed reduced O_2 growth, this means that the acetate-carbon might be used for glycogen production or other intracellular sinks of carbon besides the TCA cycle and respiration.

The growth decrease point preceding the scatter-drop had many similarities to the measurements taken before scatter-drops in glucose media. The growth and alteration rates tended to zero and, thus, most measurements became static. Similarly, this phase could also serve as preparation for the stationary phase. The most obvious difference, however, was this point's long duration. From the decrease of μ_{BM} to the scatter drop about 2 h elapsed. Therefore, the needed preparatory steps might be more time-consuming or initiated earlier in the presence of acetate.

Notably, the data of O'Beirne and Hamer (Fig. 2 in O'Beirne and Hamer, 2000) suggests a strongly reduced respiration following the exhaustion of acetate. However, in the collected data the measured q_{O_2} already decreased to almost 0 $\text{mmol g}^{-1} \text{h}^{-1}$ during growth decrease point. This suggests, that the growth decrease takes place after the acetate has already diminished. This would be surprising, as the scatter drops are hypothesized here to mark the timepoints of substrate exhaustion.

4.2.4 The Scatter-Drop

For acetate the scatter drop appeared slightly different than for glucose. First, the decrease of scatter happened much more slowly. Furthermore, most measurements had already plateaued beforehand and only the scatter signal seemed to be directly affected by the phenomenon. Especially the O_2 consumption, which began to decrease with the onset of the

scatter-drop in glucose, had already diminished. This could mean that growth decrease and scatter-drop are separate steps in preparation for the stationary phase. In this context, the former would be triggered by depletion of the substrate while the triggering point of the latter could be influenced by the kind of substrate. Then, primary growth on glucose would cause *E. coli* to induce the scatter drop already during its growth decrease point, leading to an overlap. For acetate, on the other hand, the cell would trigger GRD and SDA individually.

4.2.5 The Unknown Phase

In this work, the unknown phase is believed to represent the stationary phase. The static levels of O_2 and pH would suggest that respiration, the TCA cycle, and glycolysis are not active after the scatter-drop, since these pathway pathways consume O_2 or produce CO_2 . However, rising scatter and NADH values along with decreasing riboflavin show that the cell population was still changing over the course several hours.

Since the conducted biomass weighings several hours after the scatter-drop were very similar to those preceding it, a decrease of biomass during the unknown phase is also possible. However, the published data by O'Beirne and Hamer (Fig. 2 in O'Beirne and Hamer, 2000) shows a strong increase of biomass leading up to the point of substrate exhaustion. The large, equivalent decrease of biomass to those lower levels is unlikely.

Furthermore, ca. 2 h after depletion of acetate the biomass in the published data had reduced by ca. 10 % (Fig. 2 in O'Beirne and Hamer, 2000). In this case, the slow decrease of riboflavin, which was used for biomass estimation in glucose, might depict this event.

4.3 The Monod Model

It was seen, that the growth constants, μ_{max} , K , and Y were all accurately describable using the relations proposed by Monod. The growth constants were defined to summarize

the growth of bacteria in batch culture (Monod, 1949). Thus, it is sensible, that their general predictions would also hold for the observed cultures.

However, the Monod model which was fit to the data only inadequately depicted the observed growth. While the model did produce a fit describing the rough biomass development, due to its simplicity none of the previously described growth phases could be represented. That is because the substrate concentration is used as the only time-dependent input determining the modeled growth rate (eqn. 2.9.6). In the collected data, however, the growth rates during the recorded phases were constant in most cases. Changes to these static μ_{BM} usually marked transitions between phases and were also thought to be large alterations in the metabolism of *E. coli*. Furthermore, the depletion of substrate with time did not seem to have a continuous effect on the growth rate but was only clearly seen to affect the onset of growth-decrease and scatter-drops.

From this data it seems safe to say that the ODE is unable to predict the time-course of single batch-experiments. Especially the apparent preference of *E. coli* for constant growth rates can not be replicated. Furthermore, different triggers from critical cell densities to the NADH/ NAD^+ ratio were theorized for the onset of some phases. These could also not be included in the model.

Followingly, the observed agreement of the second scatter-drop and the substrate exhaustion in the model, i.e. the onsets of stationary phases in experiment and model, was likely a coincidence. Especially so since the depletion of glucose is thought to already happen around the first scatter-drop. This differs strongly from the model prediction.

The explanation for this discrepancy is that the Monod ODE model was developed to describe continuous cultures (Herbert, Elsworth, and Telling, 1956). In this type of cultivation the cell culture is continuously drained with a constant dilution rate D and supplied with fresh medium at the same rate. This way, a

constant influx of nutrients can be achieved. Culture parameters such as pH, O₂ saturation, and accumulation of by-products can also be controlled (Herbert, Elsworth, and Telling, 1956). In this environment *E. coli* has been shown to eventually grow exponentially with a μ_{BM} equal to the dilution rate and enter a steady-state (Monod, 1949; Herbert, Elsworth, and Telling, 1956). This means that substrate and biomass concentrations remain constant (Herbert, Elsworth, and Telling, 1956). In these static environmental conditions phase transitions triggered by bacterial densities or nutrient changes would therefore not occur. Overall, the Monod model was therefore not suited to be used in the given growth conditions. The changing environment resulting from the lack of dilution caused culture-effects differing from the continuous culture for which the model was defined.

4.4 Discussion of Errors

During the conduction of experiments some errors occurred that likely influenced data and conclusions:

The difference between experimental setups was increased by the large time differences between some experiments. Most importantly, the 3 months of COVID-19 lockdown separating Exs. HighG and BMA made the use of new source cultures necessary. This should be generally avoided. Moreover, small differences could have been introduced in the making of new media. The different preculture OD's of Exs. BMA and LowG when compared to all other experiments grown with glucose imply that these cultures were not sufficiently adapted to the growth conditions. The increased OD of the preculture of Ex. InocG might show this improved adaptation after longer growth in optimal conditions. The preculture conditions should therefore be more strongly defined and kept equal between experiments.

Two different methods were used for weighing.

All filters without biomass or up to 3 d of drying after biomass applications were weighed by placing the filter directly on the rim of

the scales weighting pan. This was done to simplify picking up the filters. Especially for the used, highly sensitive scales, however, this uneven weight distribution likely influenced the measurements. It was seen that differences in positioning of the filters could result in strong variations of the output weights. This is likely the reason for the large variations between repeated measurements seen in Ex. BMA. After this effect was noticed filters were instead placed in weighing boats and centered on the scale. However, it was later decided to not compare weighings with different measurement techniques which could result in including further variation. Furthermore, to keep Exs. BMG and BMA as similar as possible the 48 h measurements were chosen for biomass estimation. These represented the longest drying period present in both experiments. The biomass estimates were thus affected by a large sum of errors and should only be seen as a rough assessment. Additionally, it can't be ruled out that some moisture remained in the filters or that other samples stored in the same hybridization oven influenced the drying process. Therefore, it would be useful to redo Exs. BMG and BMA with optimized weighing and drying through e.g. a vacuum chamber. The time taken for sample collection should also be reduced to a minimum, since all wells are affected by the stopped shaking and temperature control.

The changing ratio of scatter and riboflavin levels in some samples also implies that both variables don't represent the biomass content equally well. This was seen especially during lag and the early growth phase. Further measurements determining the accuracy of each variable's predictions should be conducted.

4.5 Future Outlook

To test the generality of the identified phases of *E. coli* growth, further experiments seem advised:

First, time-series measurements of glucose or acetate concentrations, complementary to the online monitoring, could elucidate the timing of

growth decreases and scatter-drops. Similarly, extracting and measuring the time-dependent cellular contents of NADH and glycogen could help clarify if they take part in triggering phase transitions. For glycogen the role during the scatter drops could be examined, too.

The two experiments aimed at showing the behavior of *E. coli* on acetate differed strongly and, thus, few conclusions could be made for these samples. Therefore, additional experiments to confirm the phases should be conducted.

The behavior of *E. coli* at further increased concentrations of acetate or glucose could also be of interest. There, the predictions of phase lengths and maximal growth rates could be tested.

It might be useful to increase the time of growth and maximal cellular density through higher substrate contents and a different minimal medium. The increased density could then improve the signal strength and the signal-to-noise-ratio of the optical, online measurements. Since the Monod model was not suited for representing the observed batch growth, different models should be tested on the data. Therefore, in the making of this work a course-grained, metabolic ODE model was created. It remains to be seen if this model can better reflect the growth behavior of *E. coli*.

Lastly, the samples taken for biomass measurements were also analyzed by J. Burmester using microscopy and flow cytometry. Their final analysis of this data and further conclusion are highly anticipated.

References

- Andersen, K. B. and K. Von Meyenburg (1980). “Are growth rates of Escherichia coli in batch cultures limited by respiration?” In: *Journal of Bacteriology* 144.1, pp. 114–123. ISSN: 00219193. DOI: 10.1128/jb.144.1.114-123.1980.
- Aon, Juan C. and Sonia Cortassa (2001). “Involvement of nitrogen metabolism in the triggering of ethanol fermentation in aerobic chemostat cultures of *Saccharomyces cerevisiae*”. In: *Metabolic Engineering* 3.3, pp. 250–264. ISSN: 10967176. DOI: 10.1006/mbe.2001.0181.
- Atkinson, Bernard and Ferda Mavituna (1991). *Biochemical Engineering and Biotechnology Handbook*. 2nd ed. Stockton Press. ISBN: 9781561590124.
- Basan, Markus et al. (2015). “Overflow metabolism in Escherichia coli results from efficient proteome allocation”. In: *Nature* 528.7580, pp. 99–104. ISSN: 14764687. DOI: 10.1038/nature15765.
- Bertranda, Robert L. (2019). “Lag phase is a dynamic, organized, adaptive, and evolvable period that prepares bacteria for cell division”. In: *Journal of Bacteriology* 201.7, pp. 1–21. ISSN: 10985530. DOI: 10.1128/JB.00697-18.
- Borchers, Hans W. (2019). *pracma: Practical Numerical Math Functions*. R package version 2.2.9. URL: <https://CRAN.R-project.org/package=pracma>.
- Brauer, Matthew J. et al. (May 2005). “Homeostatic Adjustment and Metabolic Remodeling in Glucose-limited Yeast Cultures”. In: *Molecular Biology of the Cell* 16.5, pp. 2503–2517. ISSN: 1059-1524. DOI: 10.1091/mbc.e04-11-0968. URL: <https://www.molbiolcell.org/doi/10.1091/mbc.e04-11-0968>.
- Britner, Sergej (2019). “Energetics of Microbial Growth in Parallel Spectrometric Growth Platforms”. Bachelor’s thesis. Heinrich-Heine-University Düsseldorf.
- Burmester, Jonas (2020). “Cytometric Analysis of Escherichia coli Growth Phases”. Bachelor’s thesis. Heinrich-Heine-University Düsseldorf.
- Dowle, Matt and Arun Srinivasan (2019). *data.table: Extension of ‘data.frame’*. R package version 1.12.8. URL: <https://CRAN.R-project.org/package=data.table>.
- Drössler, P. et al. (Jan. 2003). “Fluorescence quenching of riboflavin in aqueous solution by methionin and cystein”. In: *Chemical Physics* 286.2-3, pp. 409–420. ISSN: 03010104. DOI: 10.1016/S0301-0104(02)00969-2. URL: <https://linkinghub.elsevier.com/retrieve/pii/S0301010402009692>.
- Enjalbert, Brice et al. (2015). “Acetate exposure determines the diauxic behavior of Escherichia coli during the glucose-acetate transition”. In: *Journal of Bacteriology* 197.19, pp. 3173–3181. ISSN: 10985530. DOI: 10.1128/JB.00128-15.
- Folsom, James Patrick and Ross P. Carlson (2015). “Physiological, biomass elemental composition and proteomic analyses of Escherichia coli ammoniumlimited chemostat growth, and comparison with iron- and glucose-limited chemostat growth”. In: *Microbiology (United Kingdom)* 161.8, pp. 1659–1670. ISSN: 14652080. DOI: 10.1099/mic.0.000118.
- Hadley Wickham (2016). *ggplot2: Elegant Graphics for Data Analysis*. Springer-Verlag New York. ISBN: 978-3-319-24277-4. URL: <https://ggplot2.tidyverse.org>.
- Hayashi, Koji et al. (2006). “Highly accurate genome sequences of Escherichia coli K-12 strains MG1655 and W3110”. In: *Molecular Systems Biology* 2. ISSN: 17444292. DOI: 10.1038/msb4100049.
- Herbert, D., R. Elsworth, and R. C. Telling (1956). “The Continuous Culture of Bacteria; a Theoretical and Experimental Study”. In: *Journal of General Microbiology* 14.3, pp. 601–622. ISSN: 0022-1287. DOI: 10.1099/00221287-14-3-601.

- Hobman, Jon L., Charles W. Penn, and Mark J. Pallen (2007). “Laboratory strains of Escherichia coli: Model citizens or deceitful delinquents growing old disgracefully?” In: *Molecular Microbiology* 64.4, pp. 881–885. ISSN: 0950382X. DOI: 10.1111/j.1365-2958.2007.05710.x.
- Kremling, Andreas et al. (Dec. 2018). “An ensemble of mathematical models showing diauxic growth behaviour”. In: *BMC Systems Biology* 12.1, p. 82. ISSN: 1752-0509. DOI: 10.1186/s12918-018-0604-8. URL: <https://bmcsystbiol.biomedcentral.com/articles/10.1186/s12918-018-0604-8>.
- Loomis, William F and Boris Magasanik (1967). “Glucose-Lactose Diauxie in Escherichia coli”. In: *Journal of Bacteriology* 93.4, pp. 1397–1401. ISSN: 0021-9193. DOI: 10.1128/JB.93.4.1397-1401.1967. URL: <https://jb.asm.org/content/93/4/1397>.
- m2p-labs GmbH (2011). *BioLection*. Baesweiler.
- (n.d.). *m2p-labs*. URL: <https://www.m2p-labs.com/>.
- Machne, Rainer (2020). *mugro: ODE Models of Microbial Growth*. R package version 0.0.1.
- (n.d.). *plateexpress: Inspection and Analysis of Microbial Growth and Gene Expression Data*. R package version 0.1.
- Monod, Jacques (Oct. 1949). “The Growth of Bacterial Cultures”. In: *Annual Review of Microbiology* 3.1, pp. 371–394. ISSN: 0066-4227. DOI: 10.1146/annurev.mi.03.100149.002103. URL: <http://www.annualreviews.org/doi/10.1146/annurev.mi.03.100149.002103>.
- O’Beirne, D. and G. Hamer (Oct. 2000). “The utilisation of glucose/acetate mixtures by Escherichia coli W3110 under aerobic growth conditions”. In: *Bioprocess Engineering* 23.4, pp. 375–380. ISSN: 16157591. DOI: 10.1007/s004499900176. URL: <http://link.springer.com/10.1007/s004499900176>.
- Orth, Jeffrey D., Bernhard Ø. Palsson, and R. M. T. Fleming (2010). “Reconstruction and Use of Microbial Metabolic Networks: the Core Escherichia coli Metabolic Model as an Educational Guide”. In: *EcoSal Plus* 4.1. ISSN: 2324-6200. DOI: 10.1128/ecosalplus.10.2.1. URL: <http://www.asmscience.org/content/journal/ecosalplus/10.1128/ecosalplus.10.2.1>.
- Petzoldt, Thomas (2020). *growthrates: Estimate Growth Rates from Experimental Data*. R package version 0.8.2. URL: <https://github.com/tpetzoldt/growthrates>.
- Pletnev, P. et al. (2015). “Survival guide: Escherichia coli in the stationary phase”. In: *Acta Naturae* 7.4, pp. 22–33. ISSN: 20758251. DOI: 10.32607/20758251-2015-7-4-22-33.
- Python Software Foundation (2020). *Python Language Reference*. URL: www.python.org.
- R Core Team (2020). *R: A Language and Environment for Statistical Computing*. R Foundation for Statistical Computing. Vienna, Austria. URL: <https://www.R-project.org/>.
- Raybaut, Pierre and Carlos Cordoba (2020). *The Scientific Python Development Environment*. URL: Spyder-IDE.org.
- Ripley, Jim Ramsey Brian (2017). *pspline: Penalized Smoothing Splines*. R package version 1.0-18, original by Jim Ramsey. R port by Brian Ripley at ripley@stats.ox.ac.uk. URL: <https://CRAN.R-project.org/package=pspline>.
- RStudio Team (2019). *RStudio: Integrated Development Environment for R*. RStudio, Inc. Boston, MA. URL: <http://www.rstudio.com/>.
- Sander, R. (2015). “Compilation of Henry’s law constants (version 4.0) for water as solvent”. In: *Atmospheric Chemistry and Physics* 15.8, pp. 4399–4981. ISSN: 16807324. DOI: 10.5194/acp-15-4399-2015.
- Sarkar, Deepayan (2008). *Lattice: Multivariate Data Visualization with R*. ISBN 978-0-387-75968-5. New York: Springer. URL: <http://lmdvr.r-forge.r-project.org>.
- Scott, Matthew and Terence Hwa (Aug. 2011). “Bacterial growth laws and their applications”. In: *Current Opinion in Biotechnology* 22.4, pp. 559–565. ISSN: 09581669. DOI: 10.1016/

- j . copbio . 2011 . 04 . 014. URL: <https://linkinghub.elsevier.com/retrieve/pii/S0958166911000772>.
- Soetaert, Karline, Thomas Petzoldt, and R. Woodrow Setzer (2010). “Solving Differential Equations in R: Package deSolve”. In: *Journal of Statistical Software* 33.9, pp. 1–25. ISSN: 1548-7660. DOI: 10.18637/jss.v033.i09. URL: <http://www.jstatsoft.org/v33/i09>.
- Swartz, James R. (2001). “Advances in Escherichia coli production of therapeutic proteins”. In: *Current Opinion in Biotechnology* 12.2, pp. 195–201. ISSN: 09581669. DOI: 10.1016/S0958-1669(00)00199-3.
- Szenk, Mariola, Ken A. Dill, and Adam M.R. de Graff (2017). *Why Do Fast-Growing Bacteria Enter Overflow Metabolism? Testing the Membrane Real Estate Hypothesis*. DOI: 10.1016/j.cels.2017.06.005.
- Valgepea, Kaspar et al. (2010). “Systems biology approach reveals that overflow metabolism of acetate in Escherichia coli is triggered by carbon catabolite repression of acetyl-CoA synthetase”. In: *BMC Systems Biology* 4.1, pp. 1–13. ISSN: 17520509. DOI: 10.1186/1752-0509-4-166.
- Vemuri, G N et al. (May 2006). “Overflow Metabolism in Escherichia coli during Steady-State Growth: Transcriptional Regulation and Effect of the Redox Ratio”. In: *Applied and Environmental Microbiology* 72.5, pp. 3653–3661. ISSN: 0099-2240. DOI: 10.1128/AEM.72.5.3653-3661.2006. URL: <https://aem.asm.org/content/72/5/3653>.
- Vitreschak, Alexey G. et al. (2002). “Regulation of riboflavin biosynthesis and transport genes in bacteria by transcriptional and translational attenuation”. In: *Nucleic Acids Research* 30.14, pp. 3141–3151. ISSN: 1362-4962. DOI: 10.1093/nar/gkf433.
- Wickham, Hadley (2007). “Reshaping Data with the reshape Package”. In: *Journal of Statistical Software* 21.12, pp. 1–20. URL: <http://www.jstatsoft.org/v21/i12/>.
- (2011). “The Split-Apply-Combine Strategy for Data Analysis”. In: *Journal of Statistical Software* 40.1, pp. 1–29. URL: <http://www.jstatsoft.org/v40/i01/>.
- (2019). *stringr: Simple, Consistent Wrappers for Common String Operations*. R package version 1.4.0. URL: <https://CRAN.R-project.org/package=stringr>.
- Wickham, Hadley and Lionel Henry (2020). *tidyverse: Tidy Messy Data*. R package version 1.0.3. URL: <https://CRAN.R-project.org/package=tidyr>.
- Wolfe, A. J. (2005). “The Acetate Switch”. In: *Microbiology and Molecular Biology Reviews* 69.1, pp. 12–50. ISSN: 1092-2172. DOI: 10.1128/mmbr.69.1.12-50.2005.
- Yamamotoya, Tomoaki et al. (2012). “Glycogen is the primary source of glucose during the lag phase of E. coli proliferation”. In: *Biochimica et Biophysica Acta - Proteins and Proteomics* 1824.12, pp. 1442–1448. ISSN: 15709639. DOI: 10.1016/j.bbapap.2012.06.010. URL: <http://dx.doi.org/10.1016/j.bbapap.2012.06.010>.

Appendix

Table S1: Recipes used for stock solutions.

Compound	End Concentration	Amount
Glucose Stock		
MilliQ		50 ml
α D-glucose	1 M	9.9 g
Filter through 0.2 μ m pore filter		
Acetate Stock		
MilliQ		50 ml
acetate	2 M	13.6 g
Filter through 0.2 μ m pore filter		
Trace 100x		
Na ₂ -EDTA	13.4 mM	5 g
FeCl ₃ · 6H ₂ O	3.1 mM	0.84 g
ZnCl ₂	0.62 mM	84 mg
CuCl ₂ · 2H ₂ O	76 μ M	13 mg
CoCl ₂ · 6H ₂ O	42 μ M	10 mg
H ₃ BO ₃	162 μ M	10 mg
MnCl ₂ · 4H ₂ O	8.1 μ M	1.6 mg
5x M9 Medium		
Na ₂ HPO ₄ · 2H ₂ O	238.7 mM	42.49 g
KH ₂ PO ₄	110.2 mM	15 g
NH ₄ Cl	93.5 mM	5 g
NaCl	42.7 mM	2.5 g
MilliQ		to 800 ml
NaOH (2.5 M)		to pH 7.2
MilliQ		to 1 l
autoclave		

Table S2: Recipes used for culture media (abbreviations in parentheses). Media were prepared as 250 ml 2x concentrate and diluted on use.

Compound	Stock Concentration	End Concentration	Amount for		
			"M9S"	"M9G"	"M9A"
MilliQ			141.95 ml	130.85 ml	125.3 ml
		autoclave			
5x M9 Medium	5x	2x	100 ml	100 ml	100 ml
Glucose Stock	1 M	44.4 mM		11.1 ml	
Acetate Stock	2 M	133.3 mM			16.65 ml
Trace 100x	100x	2x	5 ml	5 ml	5 ml
CaCl ₂	1 M	0.1 mM	50 µl	50 µl	50 µl
		mix thoroughly			
MgSO ₄	1 M	2 mM	1 ml	1 ml	1 ml
Thiamine	10 g l ⁻¹	30 µM	1 ml	1 ml	1 ml
Uracil	10 g l ⁻¹	178 µM	500 µl	500 µl	500 µl
Biotin	10 g l ⁻¹	40.9 µM	500 µl	500 µl	500 µl
		dilute 1:2 before use			

Table S3: Collection of all *R* packages used for data analysis

Package	Version	Citation
base	4.0.2	R Core Team, 2020
data.table	1.12.8	Dowle and Srinivasan, 2019
deSolve	1.28	Soetaert, Petzoldt, and Setzer, 2010
ggplot2	3.3.1	Hadley Wickham, 2016
growthrates	0.8.2	Petzoldt, 2020
lattice	0.20-41	Sarkar, 2008
mugro	0.0.1	Machne, 2020
plateexpress	0.1	Machne, n.d.
plyr	1.8.6	Wickham, 2011
pracma	2.2.9	Borchers, 2019
pspline	1.0-18	Ripley, 2017
reshape2	1.4.4	Wickham, 2007
stringr	1.4.0	Wickham, 2019
tidyR	1.0.3	Wickham and Henry, 2020

Table S4: Non-standard parameters for selected *R* functions (comments as < ... >)

Package	Function	Parameter	Value
platexpress	readExperiment	type	"BioLectorPro"
		blank.data	c("Biomass", "Riboflavin", "NADH - NADPH")
		skip.wells	<wells not currently analyzed>
	dpseg_plate	P	0.0001
pspline	sm.spline	addModel	TRUE
		norder	3 <regularly> 4 <for determining drops>
	predict	nderiv	1 <first derivative> 2 <second derivative>

Table S5: Parameters used in data analysis

Parameter	Value	Reference	Notes
$H_{cp}(T_{std} = 298.15 \text{ K})$	$1.3 \cdot 10^{-5} \text{ mol m}^{-3} \text{ Pa}^{-1}$	Sander, 2015	median of H_{cp} of "oxygen" in Tab. 6
$\frac{-\Delta_{sol}H}{R}$	1507.692 K	Sander, 2015	mean of $\frac{d \ln H}{d(1/T)}$ of "oxygen" in Tab. 6
k_{La}	230 h^{-1}	m2p-labs	supplied by producer
f_{BM}^C	0.474	Folsom and Carlson, 2015	mean % in Tab. 2: "Glucose-limited"
M_C	12 g mol^{-1}		per "mol" definition
p_{O_2}	21278.25 Pa		O_2 is ca. 21 % of air, which has 1 atm = 101,325 Pa at sea level

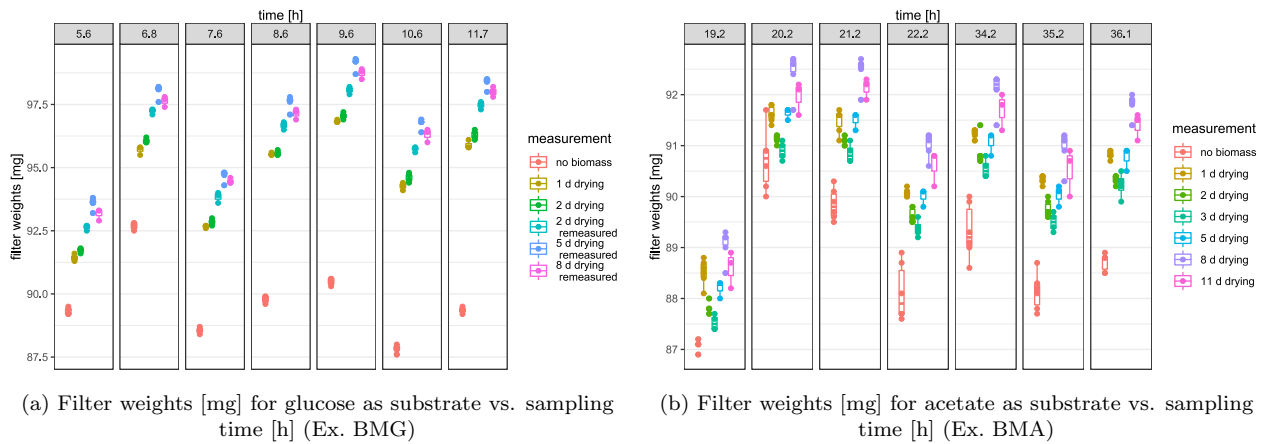


Figure S1: **Raw weights of filters for biomass weighing of Exs. BMG and BMA [mg] vs. sampling time [h]** as box-plots with added data points. Used experiment in parentheses. Separated columns show the extraction time [h]. Colors represent the status of the filter: either after 24 h of drying and before biomass filtering ("no biomass") or after biomass application and the given time of drying at 60 °C. "remeasured" filters were dried again after 3 months of storage to control their weights. An altered weighing protocol was used for "remeasured" weights, as well as for weighing after 3 d - 11 d in (b).

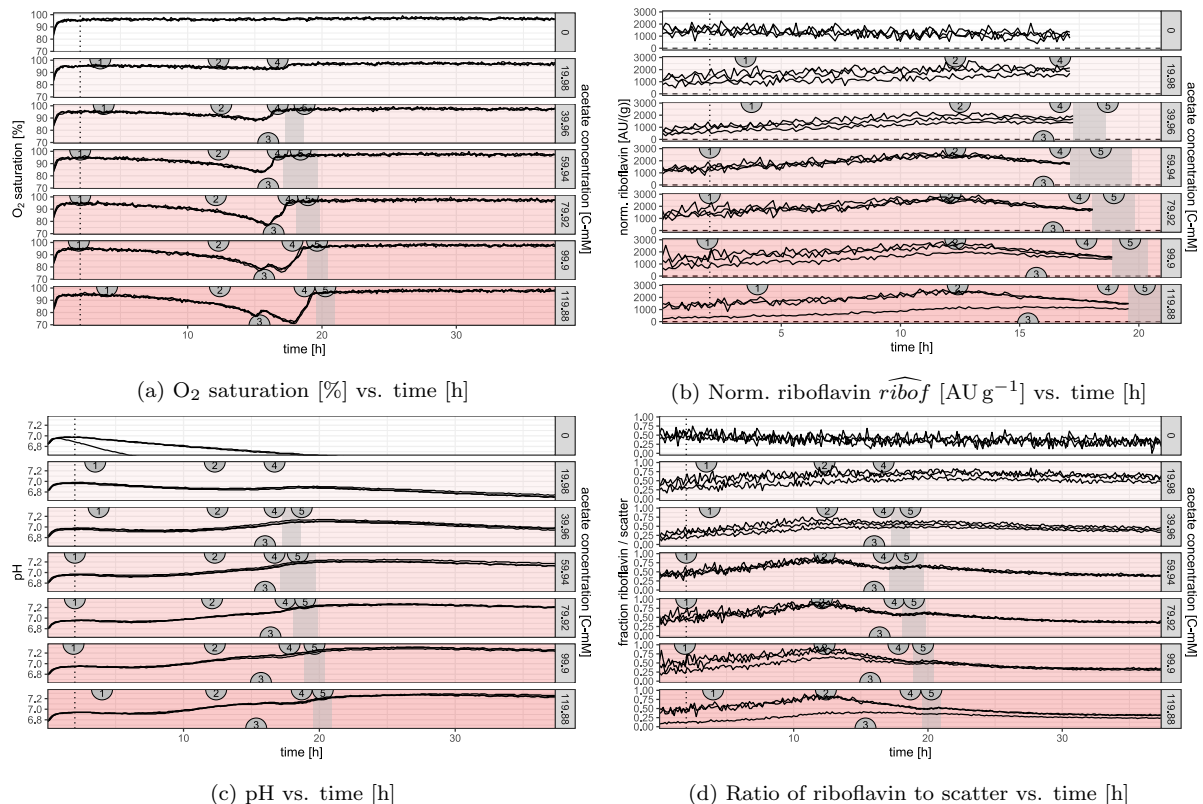


Figure S2: **Selected supplementary online or derived measurements of Ex. HighGA acetate samples vs. time [h] for *E. coli* batch growth on acetate.** Plots vertically separated by the used acetate concentration (linear gradient: 0 C-mM - 119.88 C-mM), also represented by strength of red background. Each concentration is represented by $n = 3$ technical replicates. Grey shaded areas mark time ranges of an automatically determined scatter drop. Numbers in semicircles show the manually annotated mid points of POIs: 1) end-of-lag, 2) growth increase, 3) O₂-dip, 4) growth decrease, 5) acetate scatter drop.

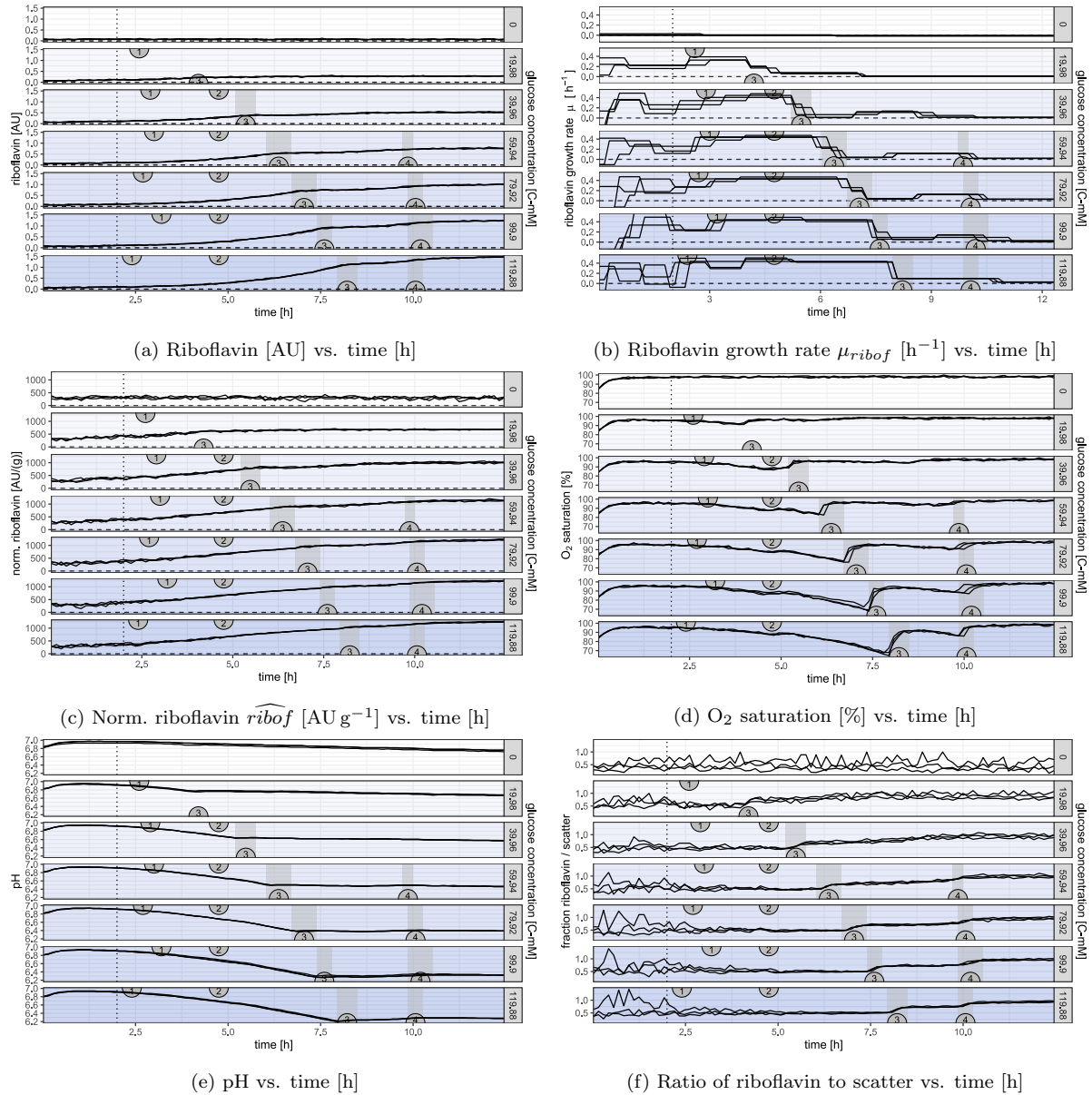


Figure S3: Selected supplementary online or derived measurements of Ex. HighGA glucose samples vs. time [h] for *E. coli* batch growth on glucose. Plots vertically separated by the used glucose concentration (linear gradient: 0 C-mM - 119.88 C-mM), also represented by strength of blue background. Each concentration is represented by $n = 3$ technical replicates. Grey shaded areas mark time ranges of automatically determined scatter-drops. Numbers in semicircles show the manually annotated mid points of POIs: 1) End-of-lag, 2) 5 h point, 3) Scatter-drop 1, 4) Scatter-drop 2.

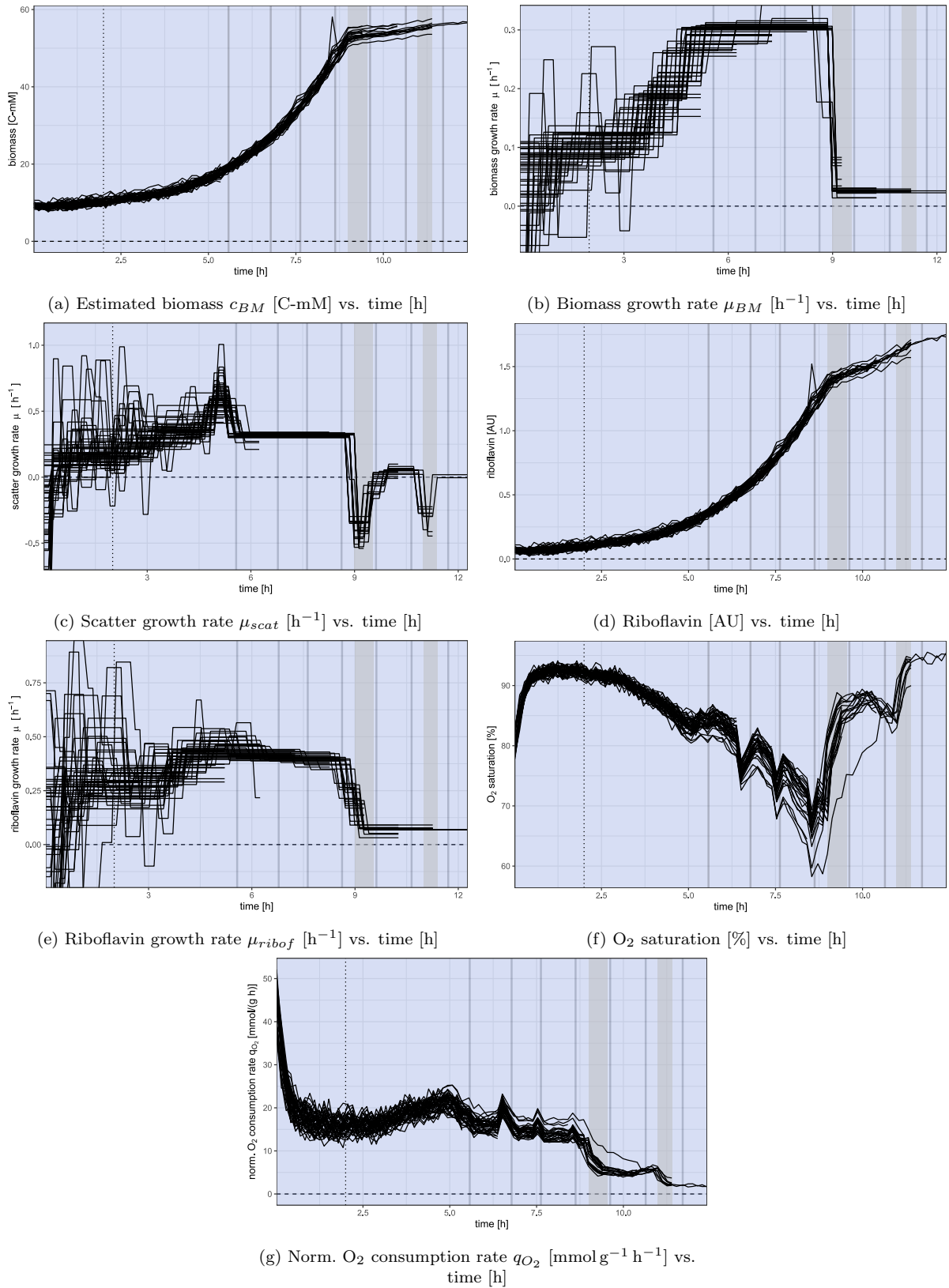


Figure S4: Selected supplementary online or derived measurements of Ex. BMG vs. time [h] for *E. coli* batch growth on 119.88 C-mM glucose. Grey shaded areas mark time ranges of automatically determined scatter-drops. Grey vertical lines show approximate sampling times for biomass collection. All 45 inoculated wells are depicted. Lines representing sampled wells are discontinued at their sampling time.

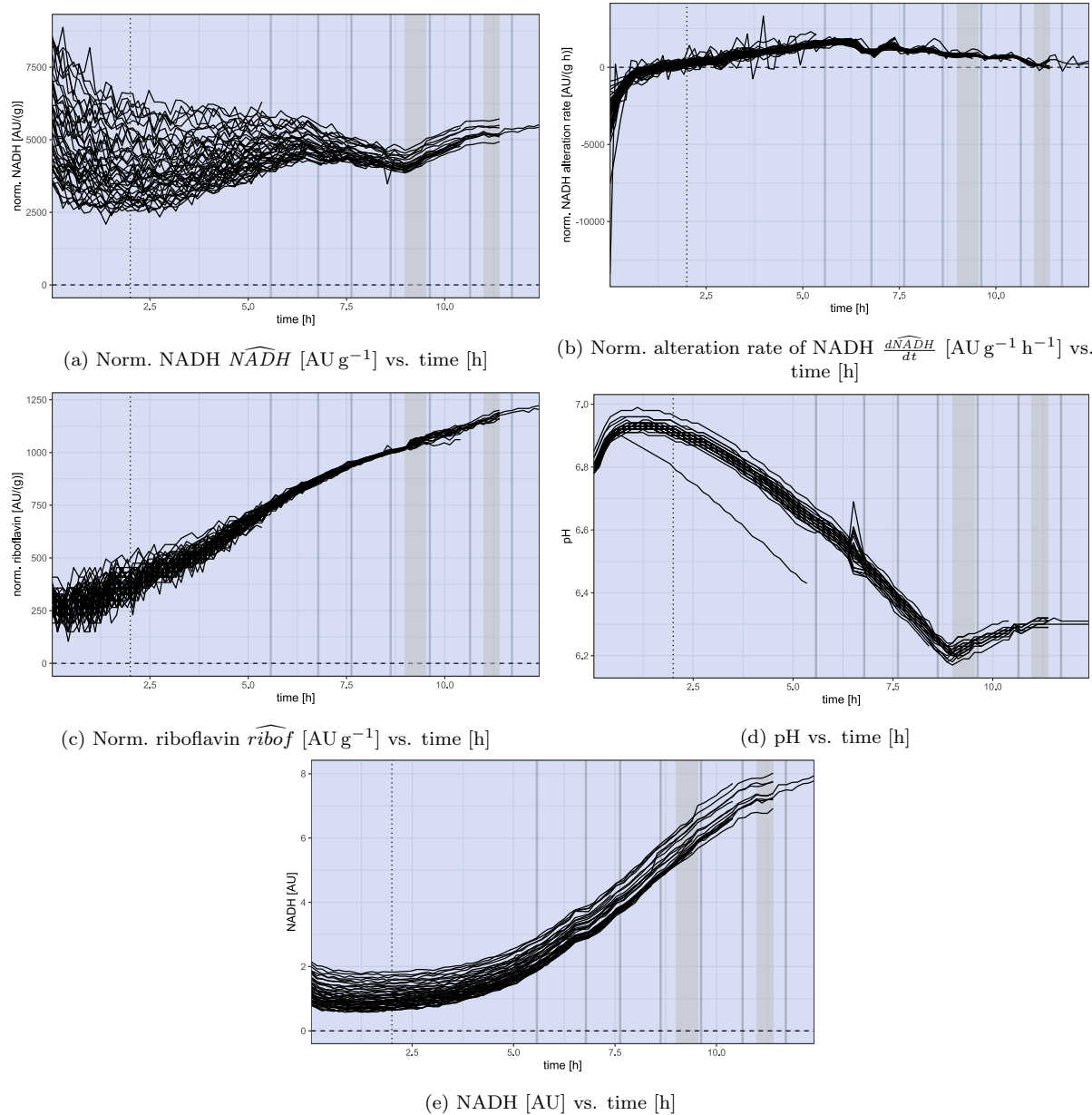


Figure S5: Selected supplementary online or derived measurements of Ex. BMG vs. time [h] for *E. coli* batch growth on 119.88 C-mM glucose. Grey shaded areas mark time ranges of automatically determined scatter-drops. Grey vertical lines show approximate sampling times for biomass collection. All 45 inoculated wells are depicted. Lines representing sampled wells are discontinued at their sampling time.

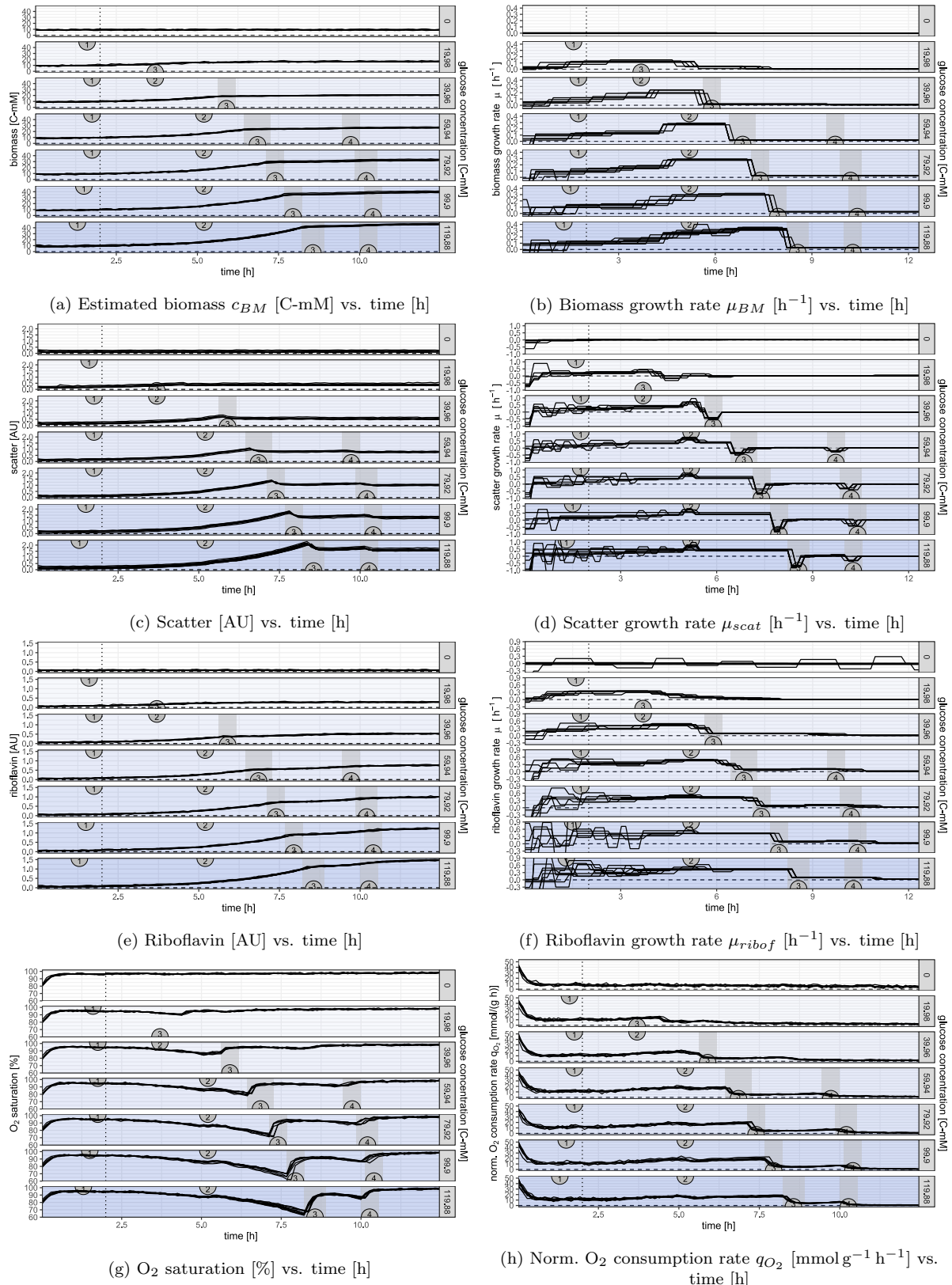


Figure S6: Selected supplementary online or derived measurements of Ex. HighG vs. time [h] for *E. coli* batch growth on glucose. Plots vertically separated by the used glucose concentration (linear gradient: 0 C-mM - 119.88 C-mM), also represented by strength of blue background. Each concentration is represented by $n = 6$ technical replicates. Grey shaded areas mark time ranges of automatically determined scatter-drops. Numbers in semicircles show the manually annotated mid points of POIs: 1) End-of-lag, 2) 5 h point, 3) Scatter-drop 1, 4) Scatter-drop 2.

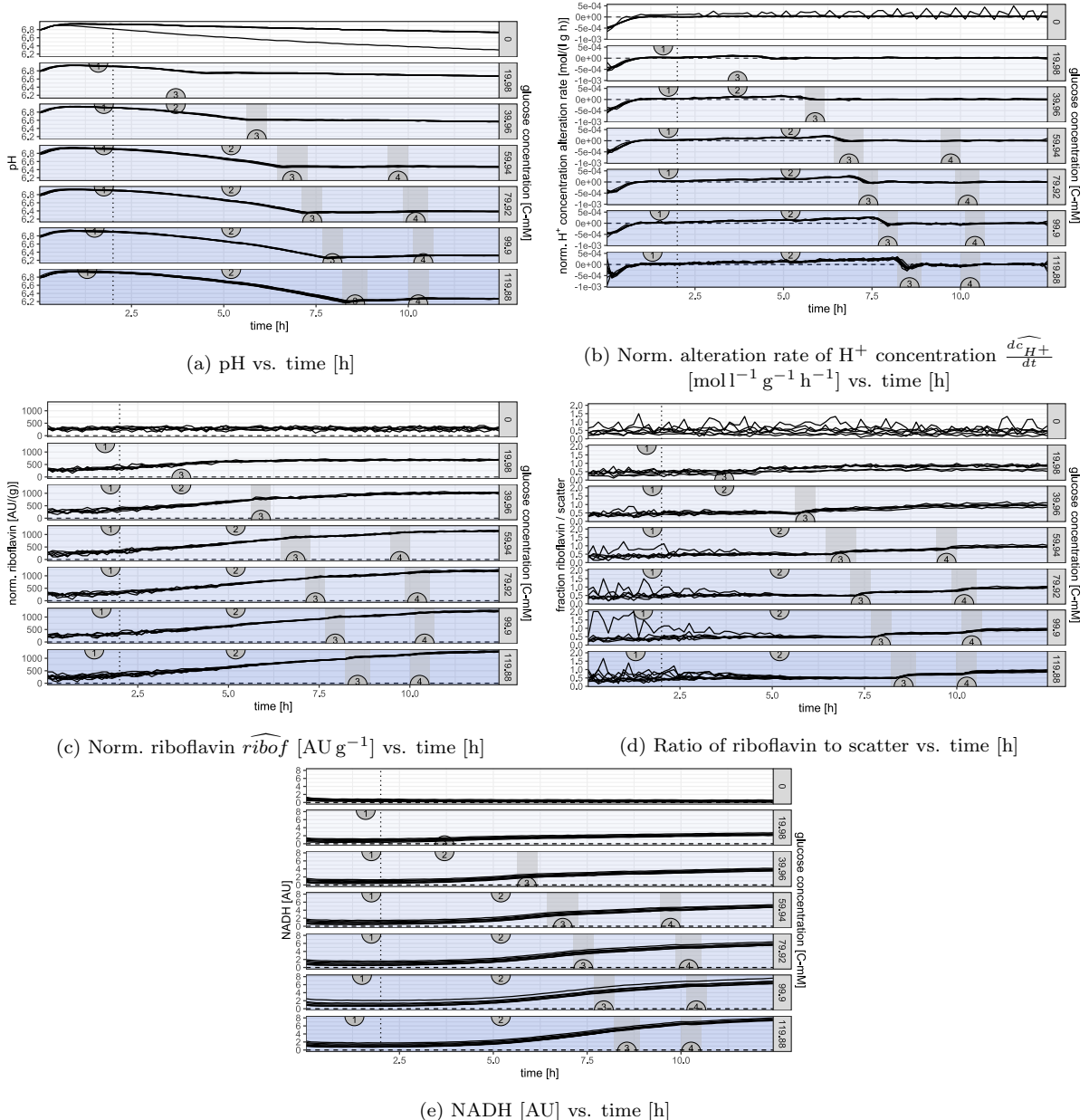


Figure S7: Selected supplementary online or derived measurements of Ex. HighG vs. time [h] for *E. coli* batch growth on glucose. Plots vertically separated by the used glucose concentration (linear gradient: 0 C-mM - 119.88 C-mM), also represented by strength of blue background. Each concentration is represented by $n = 6$ technical replicates. Grey shaded areas mark time ranges of automatically determined scatter-drops. Numbers in semicircles show the manually annotated mid points of POIs: 1) End-of-lag, 2) 5 h point, 3) Scatter-drop 1, 4) Scatter-drop 2.

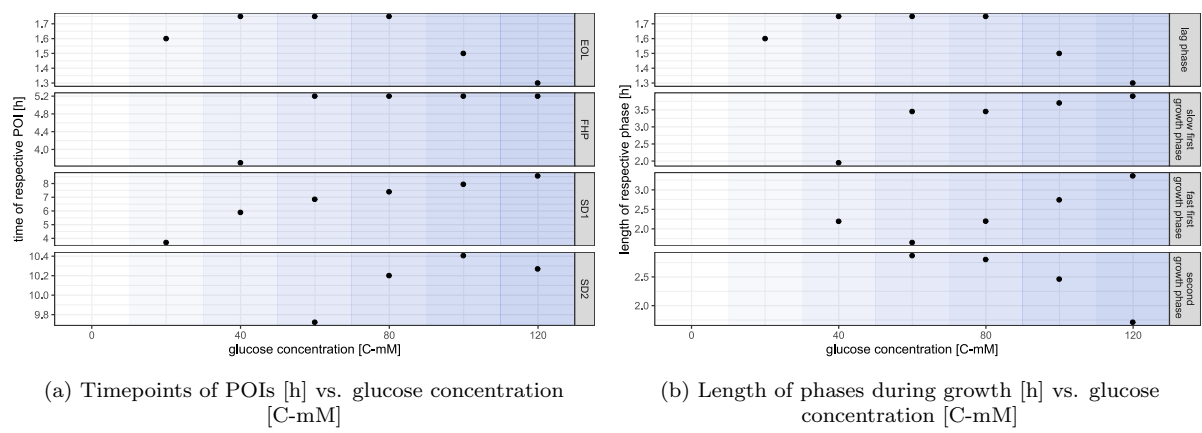


Figure S8: **Timings of POIs or lengths of phases of Ex. HighG vs. varied glucose concentration [C-mM] for *E. coli* batch growth on glucose.** The underlying timepoints were extracted from manually annotated points-of-interest and their time differences. Background color visualizes glucose concentration (strength of blue).

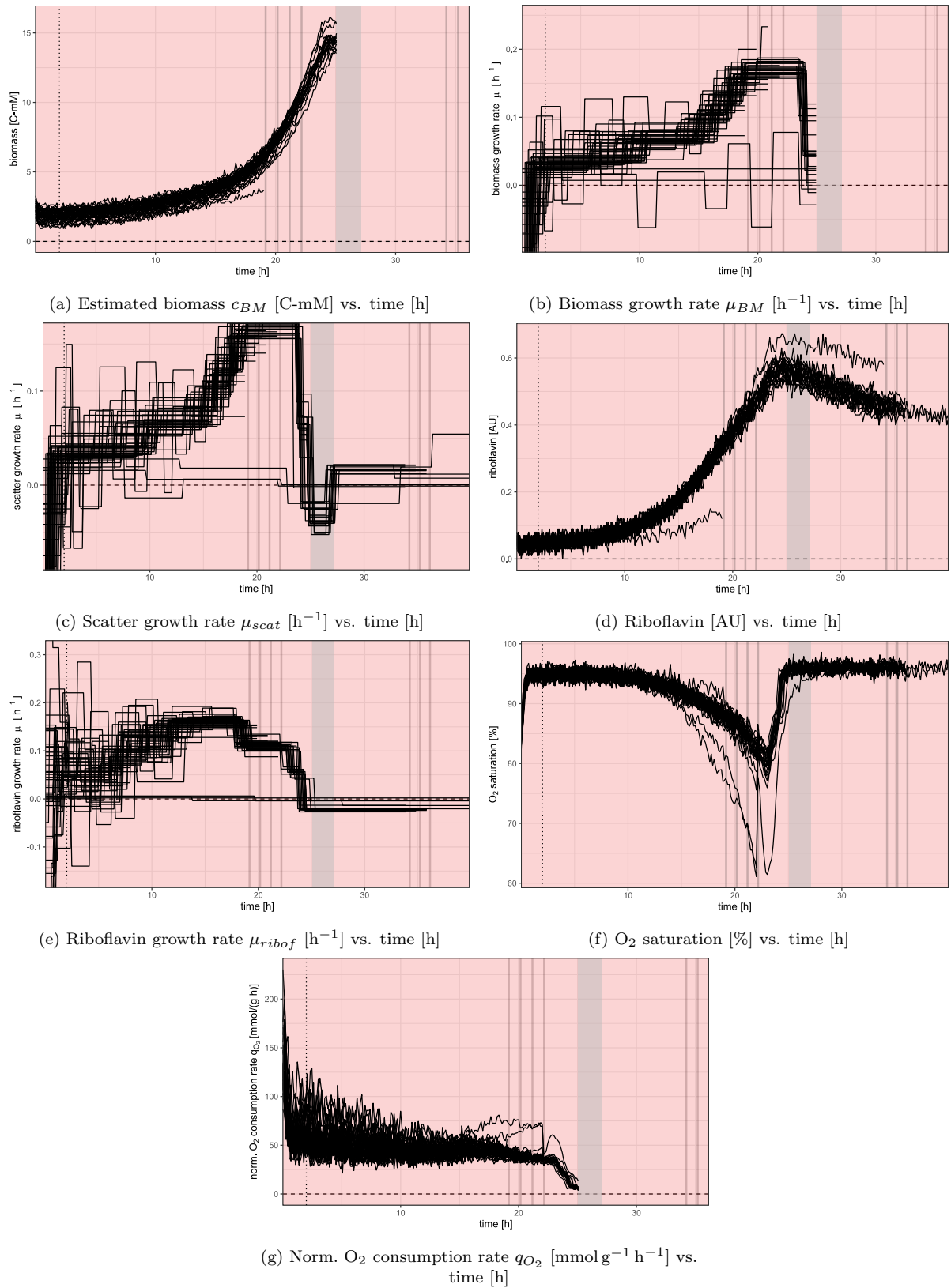


Figure S9: Selected supplementary online or derived measurements of Ex. BMA vs. time [h] for *E. coli* batch growth on 119.88 C-mM acetate. Grey shaded areas mark the time range of an automatically determined scatter-drop. Grey vertical lines show approximate sampling times for biomass collection. All 45 inoculated wells are depicted. Lines representing sampled wells are discontinued at their sampling time.

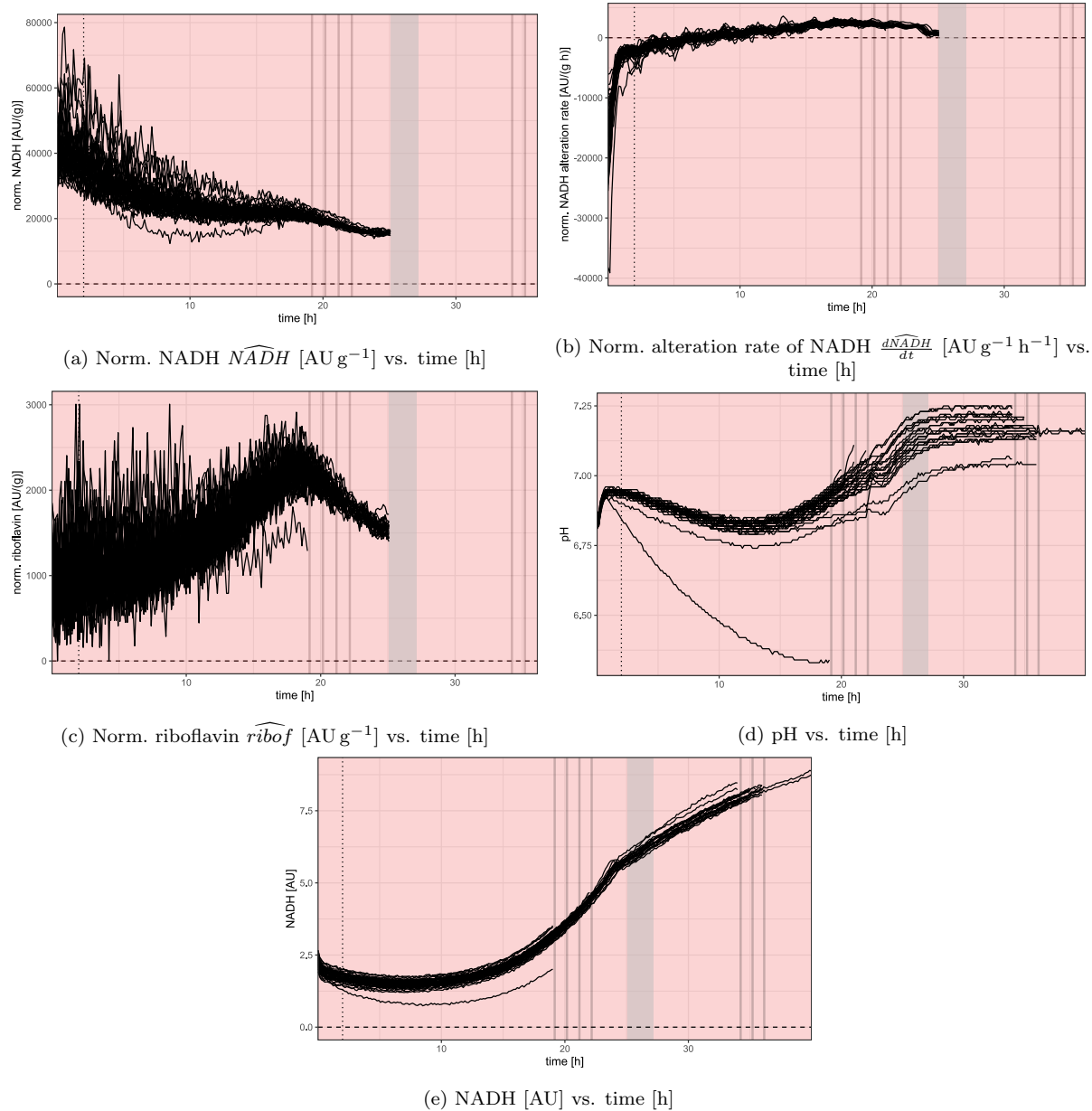


Figure S10: Selected supplementary online or derived measurements of Ex. BMA vs. time [h] for *E. coli* batch growth on 119.88 C-mM acetate. Grey shaded areas mark the time range of an automatically determined scatter-drop. Grey vertical lines show approximate sampling times for biomass collection. All 45 inoculated wells are depicted. Lines representing sampled wells are discontinued at their sampling time.

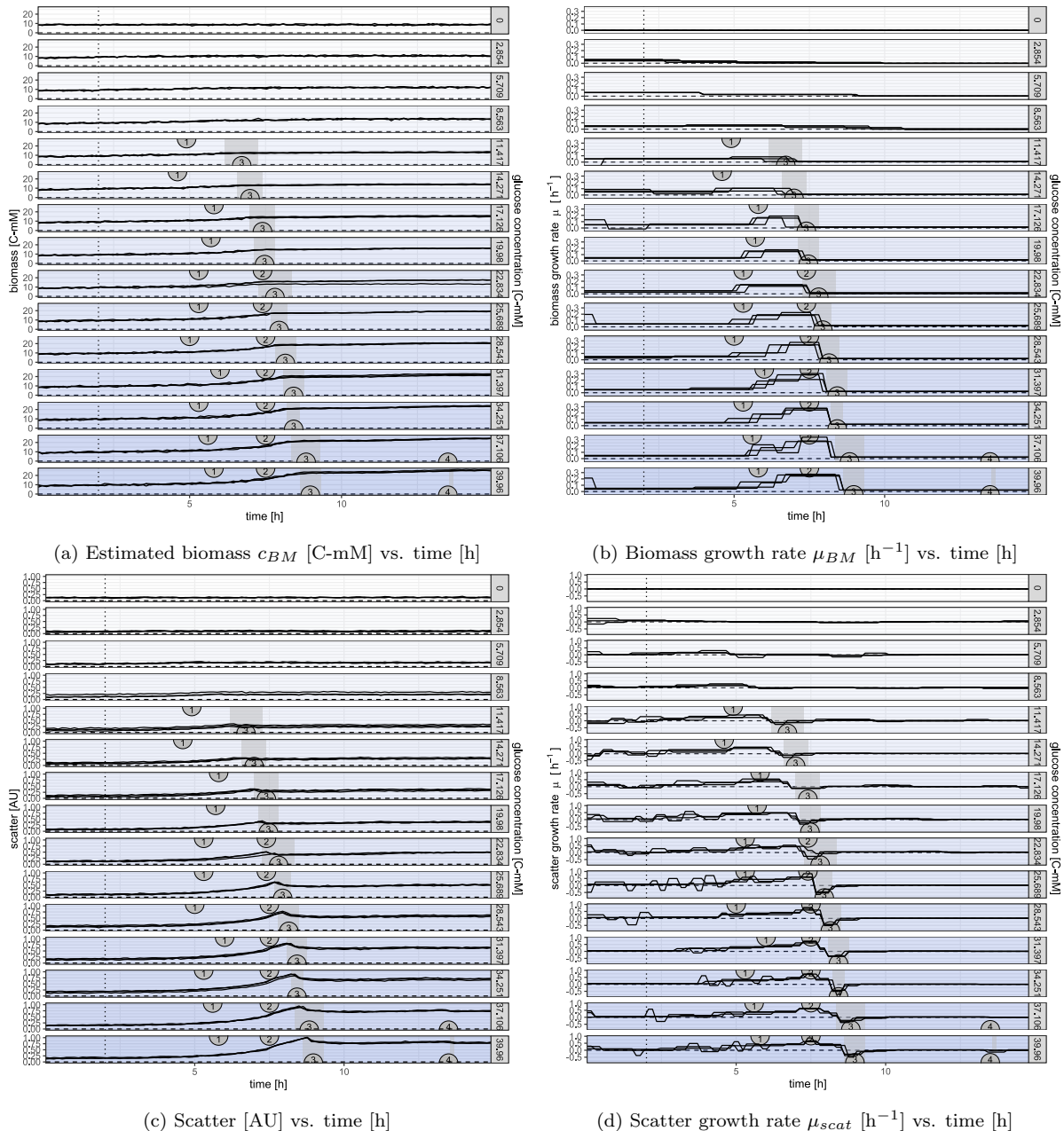


Figure S11: Selected supplementary online or derived measurements of Ex. LowG vs. time [h] for *E. coli* batch growth on glucose. Plots vertically separated by the used glucose concentration (linear gradient: 0 C-mM - 39.96 C-mM), also represented by strength of blue background. Each concentration is represented by $n = 3$ technical replicates. Grey shaded areas mark time ranges of automatically determined scatter-drops. Numbers in semicircles show the manually annotated mid points of POIs: 1) End-of-lag, 2) 5 h point, 3) Scatter-drop 1, 4) Scatter-drop 2.

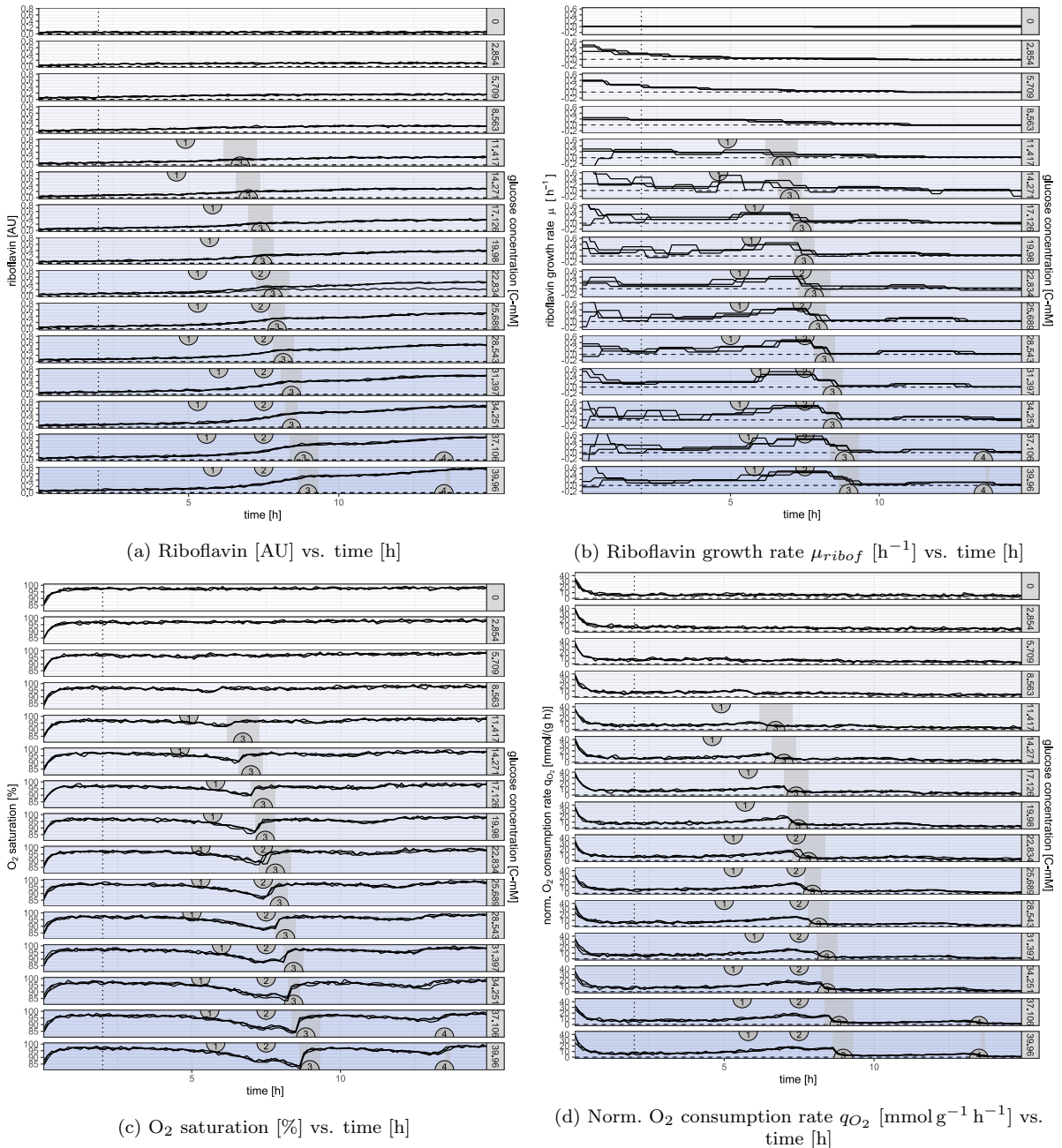


Figure S12: Selected supplementary online or derived measurements of Ex. LowG vs. time [h] for *E. coli* batch growth on glucose. Plots vertically separated by the used glucose concentration (linear gradient: 0 C-mM - 39.96 C-mM), also represented by strength of blue background. Each concentration is represented by $n = 3$ technical replicates. Grey shaded areas mark time ranges of automatically determined scatter-drops. Numbers in semicircles show the manually annotated mid points of POIs: 1) End-of-lag, 2) 5 h point, 3) Scatter-drop 1, 4) Scatter-drop 2.

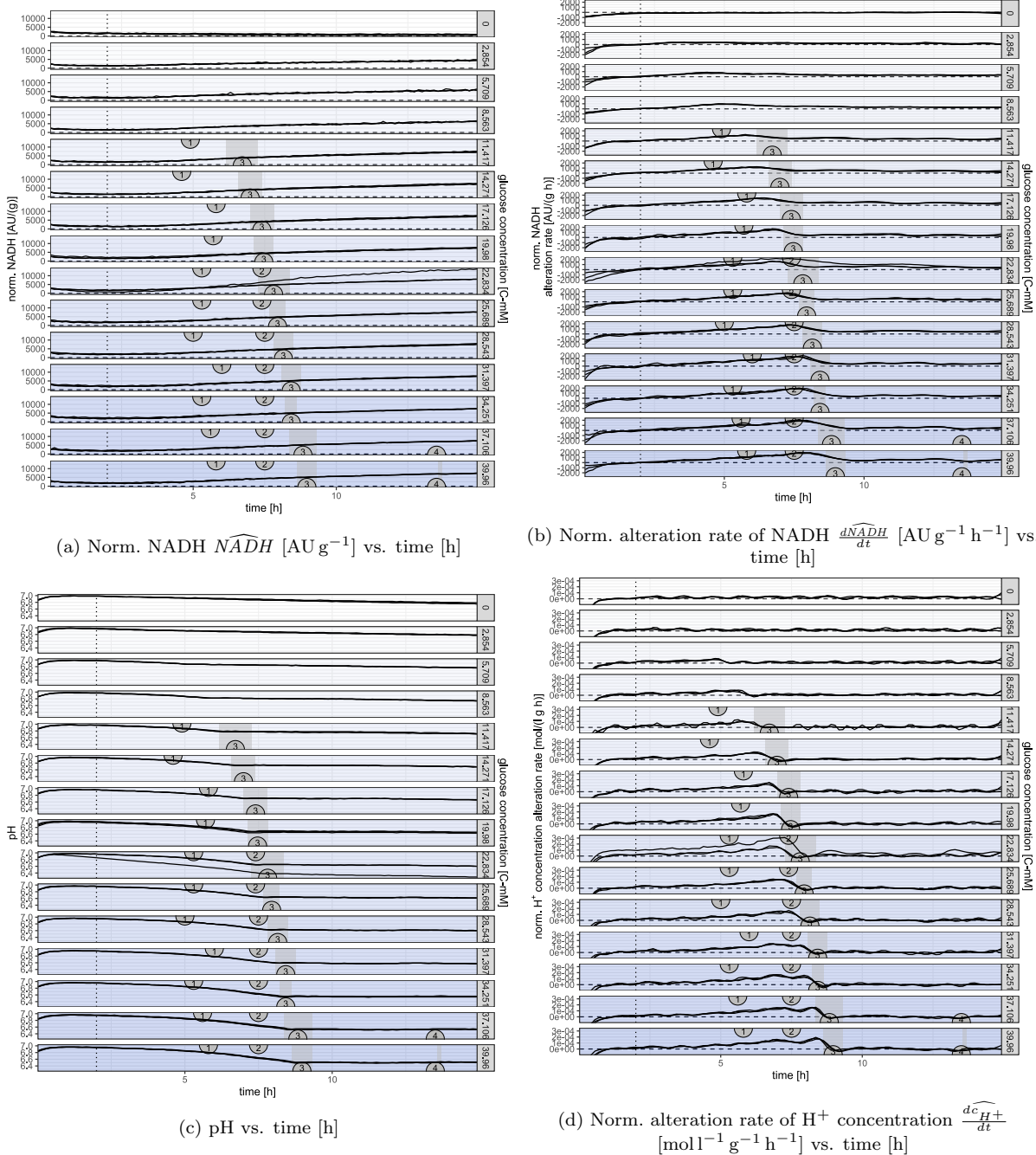


Figure S13: Selected supplementary online or derived measurements of Ex. LowG vs. time [h] for *E. coli* batch growth on glucose. Plots vertically separated by the used glucose concentration (linear gradient: 0 C-mM - 39.96 C-mM), also represented by strength of blue background. Each concentration is represented by $n = 3$ technical replicates. Grey shaded areas mark time ranges of automatically determined scatter-drops. Numbers in semicircles show the manually annotated mid points of POIs: 1) End-of-lag, 2) 5 h point, 3) Scatter-drop 1, 4) Scatter-drop 2.

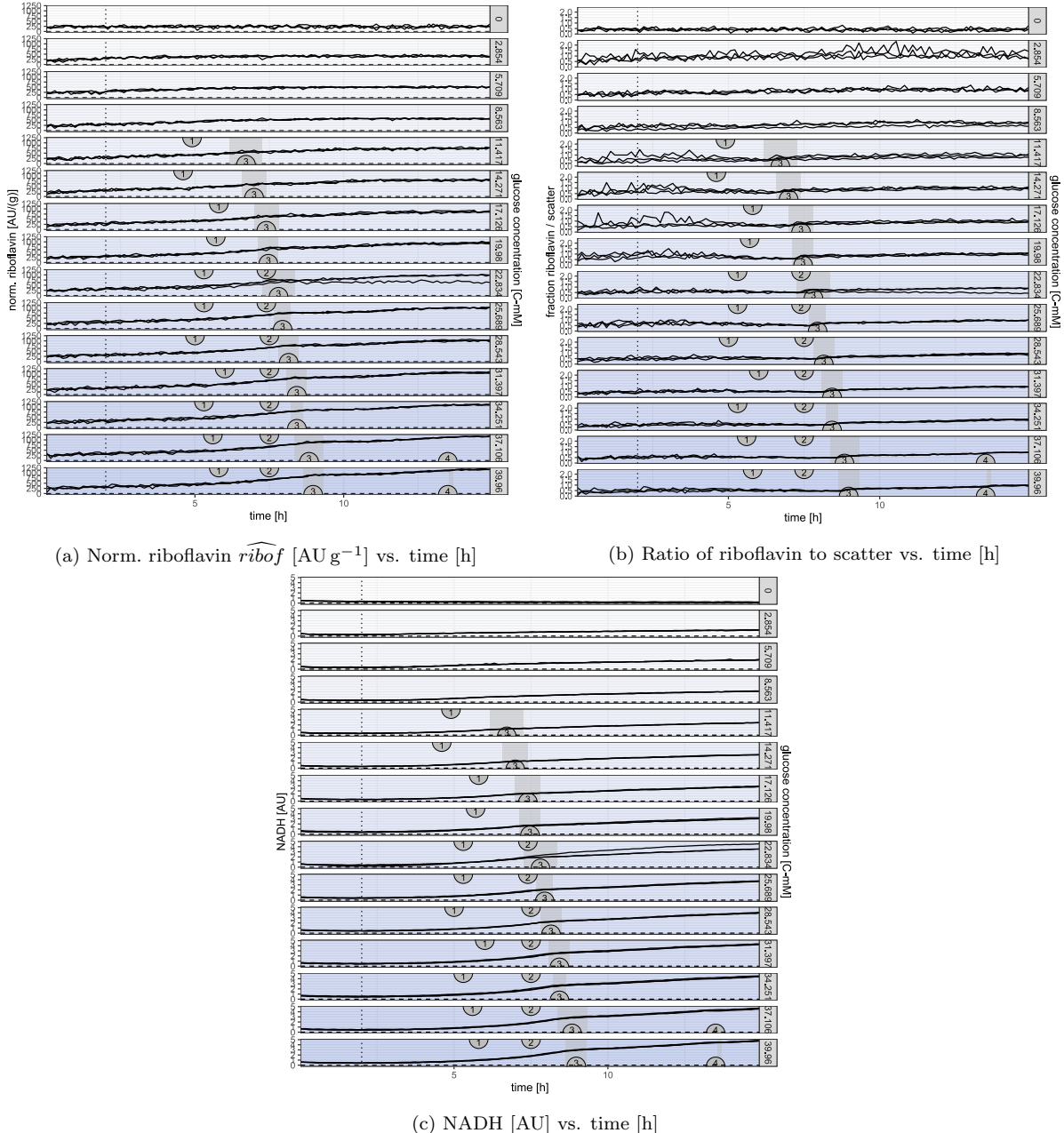


Figure S14: Selected supplementary online or derived measurements of Ex. LowG vs. time [h] for *E. coli* batch growth on glucose. Plots vertically separated by the used glucose concentration (linear gradient: 0 C-mM - 39.96 C-mM), also represented by strength of blue background. Each concentration is represented by $n = 3$ technical replicates. Grey shaded areas mark time ranges of automatically determined scatter-drops. Numbers in semicircles show the manually annotated mid points of POIs: 1) End-of-lag, 2) 5 h point, 3) Scatter-drop 1, 4) Scatter-drop 2.

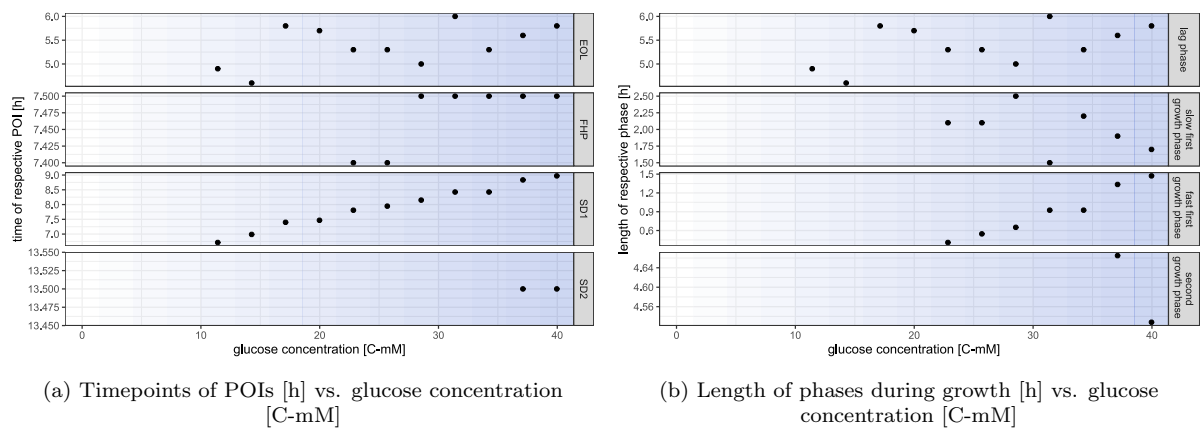


Figure S15: **Timings of POIs or lengths of phases of Ex. LowG vs. varied glucose concentration [C-mM] for *E. coli* batch growth on glucose.** The underlying timepoints were extracted from manually annotated points-of-interest and their time differences. Background color visualizes glucose concentration (strength of blue).

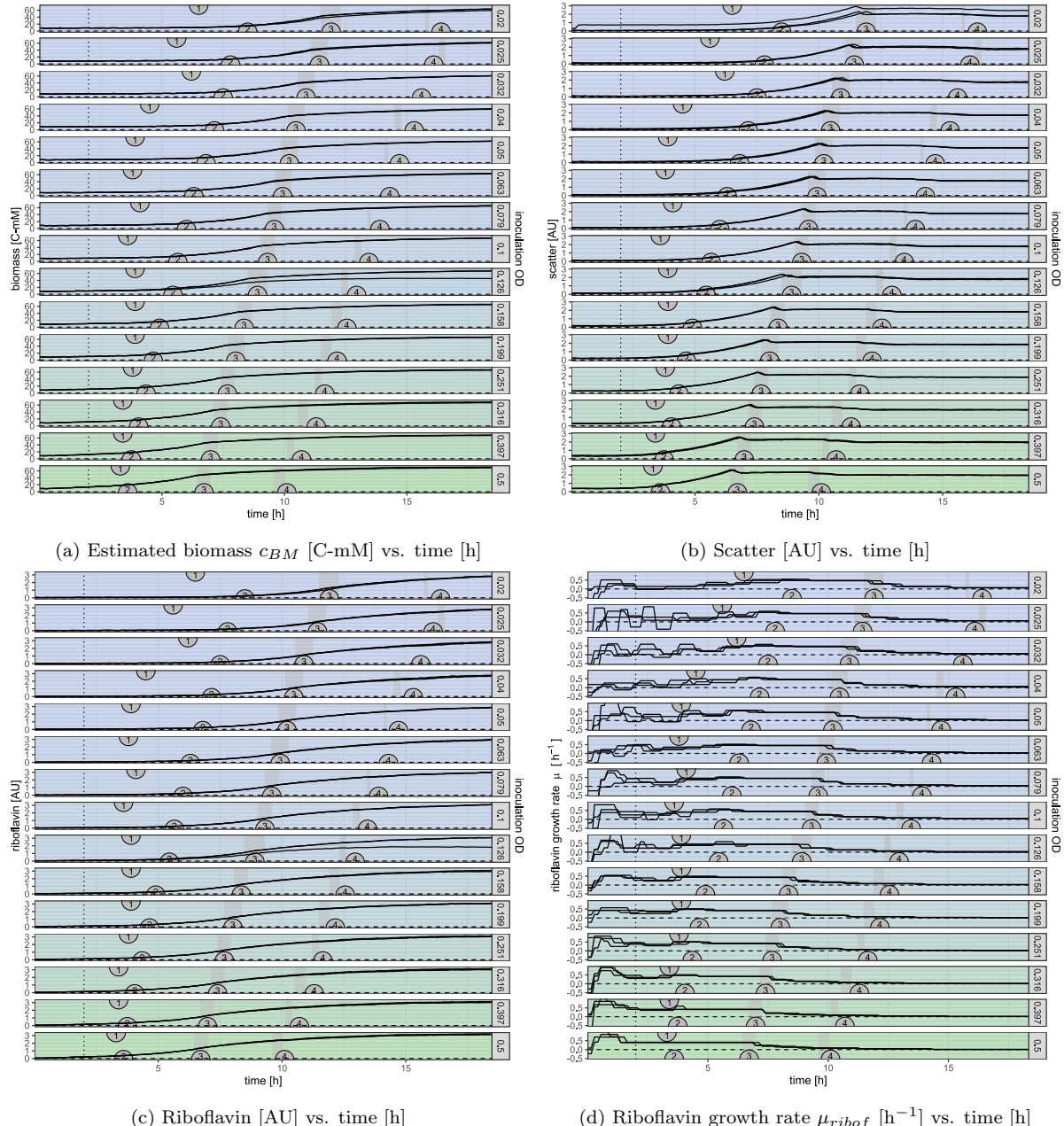


Figure S16: Selected supplementary online or derived measurements of Ex. InocG vs. time [h] for *E. coli* batch growth on 119.88 C-mM glucose with variation of the inoculation OD. Plots vertically separated by the well's OD after inoculation (logarithmic gradient: 0.02–0.5), visualized by the amount of green in the background. The constant blue tint shows the constant glucose concentration. Each OD-grouping is represented by $n = 3$ technical replicates. Grey shaded areas mark time ranges of automatically determined scatter-drops. Numbers in semicircles show the manually annotated mid points of POIs: 1) End-of-lag, 2) 5 h point, 3) Scatter-drop 1, 4) Scatter-drop 2.

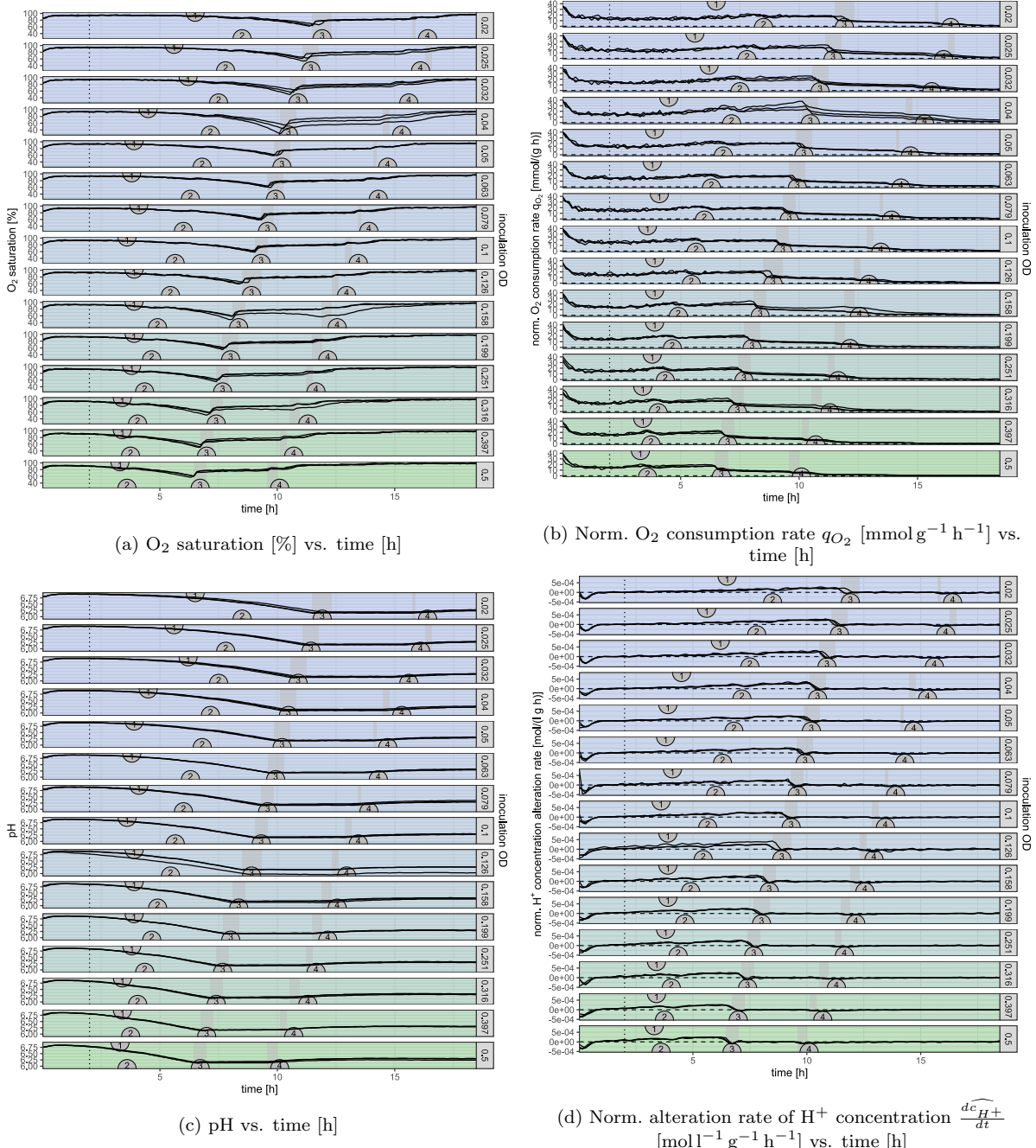


Figure S17: Selected supplementary online or derived measurements of Ex. InocG vs. time [h] for *E. coli* batch growth on 119.88 C-mM glucose with variation of the inoculation OD. Plots vertically separated by the well's OD after inoculation (logarithmic gradient: 0.02–0.5), visualized by the amount of green in the background. The constant blue tint shows the constant glucose concentration. Each OD-grouping is represented by $n = 3$ technical replicates. Grey shaded areas mark time ranges of automatically determined scatter-drops. Numbers in semicircles show the manually annotated mid points of POIs: 1) End-of-lag, 2) 5 h point, 3) Scatter-drop 1, 4) Scatter-drop 2.

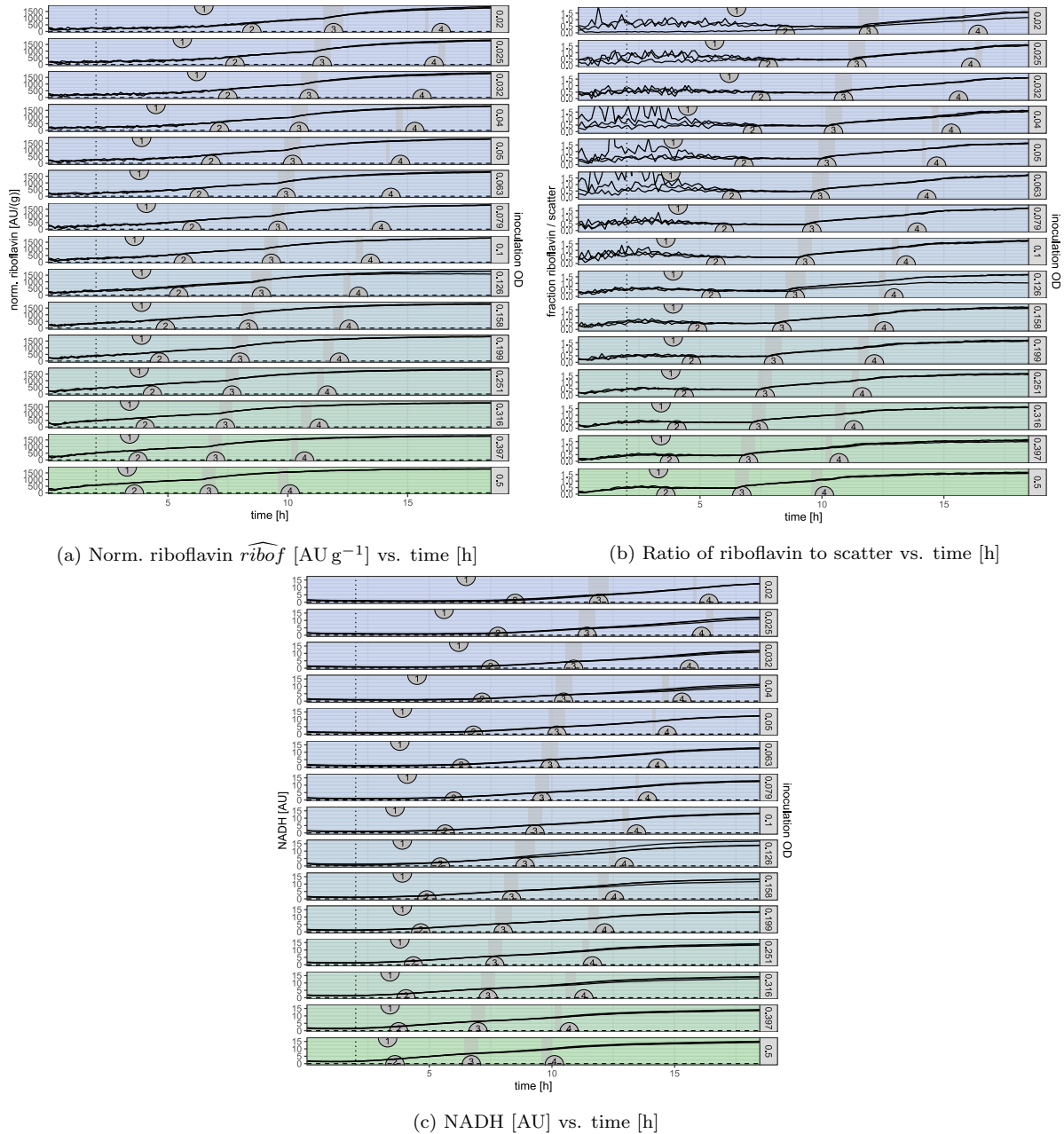


Figure S18: Selected supplementary online or derived measurements of Ex. InocG vs. time [h] for *E. coli* batch growth on 119.88 C-mM glucose with variation of the inoculation OD. Plots vertically separated by the well's OD after inoculation (logarithmic gradient: 0.02–0.5), visualized by the amount of green in the background. The constant blue tint shows the constant glucose concentration. Each OD-grouping is represented by $n = 3$ technical replicates. Grey shaded areas mark time ranges of automatically determined scatter-drops. Numbers in semicircles show the manually annotated mid points of POIs: 1) End-of-lag, 2) 5 h point, 3) Scatter-drop 1, 4) Scatter-drop 2.

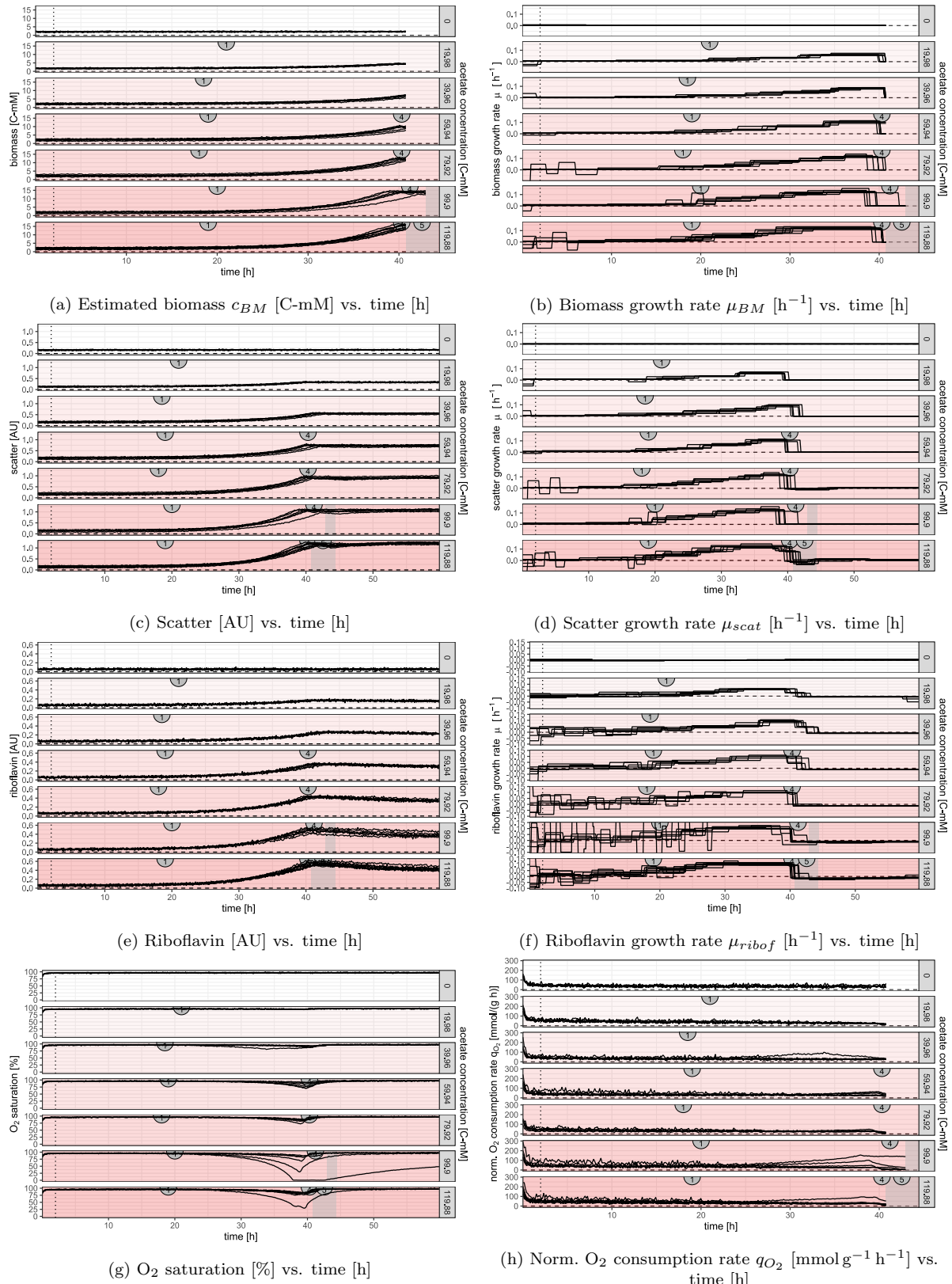


Figure S19: Selected supplementary online or derived measurements of Ex. HighA vs. time [h] for *E. coli* batch growth on acetate. Plots vertically separated by the used acetate concentration (linear gradient: 0 C-mM - 119.88 C-mM), also represented by strength of red background. Each concentration is represented by $n = 6$ technical replicates. Grey shaded areas mark the time range of an automatically determined scatter-drop. Numbers in semicircles show the manually annotated mid points of POIs: 1) end-of-lag, 2) growth increase, 3) O₂-dip, 4) growth decrease, 5) acetate scatter drop.

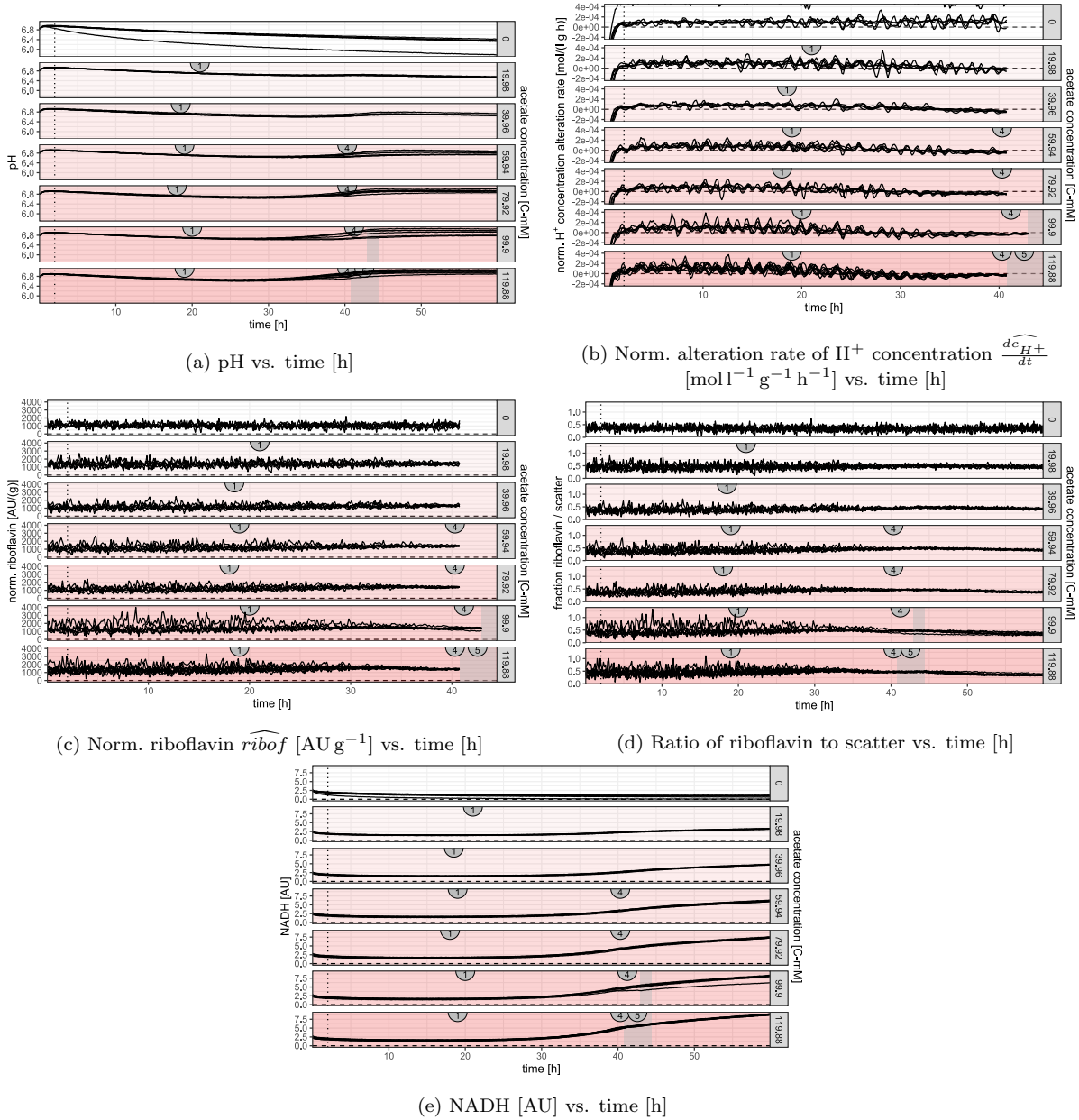


Figure S20: Selected supplementary online or derived measurements of Ex. HighA vs. time [h] for *E. coli* batch growth on acetate. Plots vertically separated by the used acetate concentration (linear gradient: 0 C-mM - 119.88 C-mM), also represented by strength of red background. Each concentration is represented by $n = 6$ technical replicates. Grey shaded areas mark time ranges of an automatically determined scatter-drop. Numbers in semicircles show the manually annotated mid points of POIs: 1) end-of-lag, 2) growth increase, 3) O_2 -dip, 4) growth decrease, 5) acetate scatter drop.

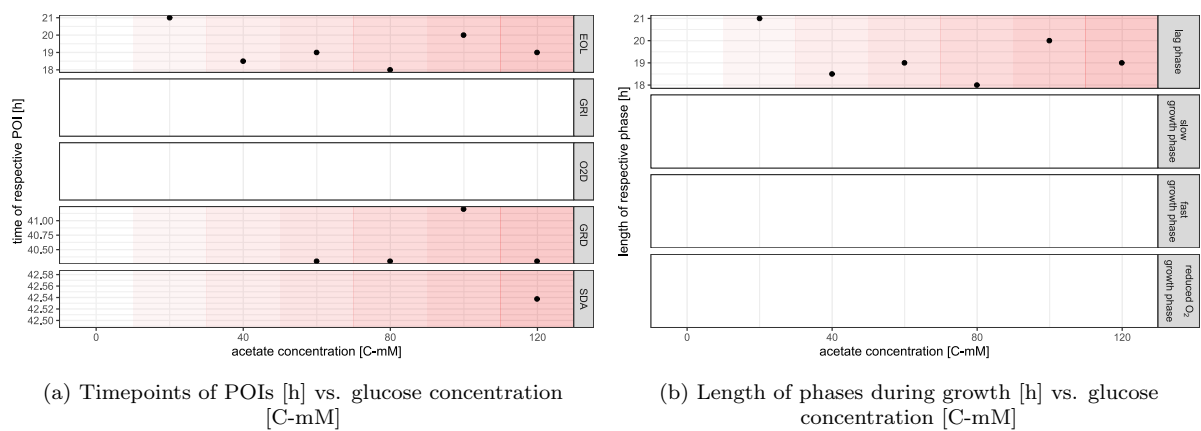


Figure S21: **Timings or lengths of POIs and phases of Ex. HighA vs. varied acetate concentration [C-mM].** The underlying timepoints were extracted from manually annotated points-of-interest and their time differences. Background color visualizes acetate concentration (strength of red). In fields with missing points and backgrounds the relevant POIs were not assigned.

Acknowledgements

Ich möchte zuerst allen lieben Menschen von QTB und SynMiBi bedanken, dass sie mich in ihre Mitte aufgenommen haben und mir ihre Unterstützung angeboten haben, als ich es brauchte. Insbesondere danke ich Ilka und Oliver, dass sie mir die Möglichkeit gaben in dieser tollen Umgebung meine Bachelorarbeit zu schreiben. Danke für die Hilfe bei jeder Art von Frage oder Problem.

Als nächstes möchte ich Rainer dafür danken, dass er mir immer mit Rat und Tat zur Seite stand. Egal ob bei der Interpretation von Ergebnissen, der Planung des Modellierens oder den spätabendlichen Probenentnahmen (mit spendiertem Essen) war auf ihn immer Verlass.

Ich danke auch Jonas, der bei vielen meiner Experimente tatkräftig mithalf und dafür sorgte, dass alles viel reibungsloser lief. Selbst als es nur darum ging mir im Labor gesellschaft zu leisten war Jonas immer bereit zu helfen.

Ich möchte auch Tim und insbesondere Nik und Alice danken, die mich in die Abläufe im Labor einführten und auf jede Frage eine Antwort wussten. Nima danke ich dafür, dass er mir Rede und Antwort stand, als ich Hilfe für mein Modell brauchte. Dann möchte ich noch Max und Lutz danken, die mir mehr als einmal halfen im Labor zurecht zu kommen.

Meinen Eltern danke ich, dass sie mich bei allem unterstützten, immer ein offenes Ohr hatten und meinen Schreibprozess mit viel Kaffe und lauter Musik tolerierten.

Zuletzt danke ich meinen Freunden Andreas, Christoph und Becky, die mir halfen einen klaren Kopf zu behalten. Für ihre Hilfe als Korrektoren kann ich nicht genug danken.

Selbstständigkeitserklärung — Declaration of Academic Honesty

Hiermit erkläre ich, dass ich die vorliegende Bachelorarbeit selbstständig verfasst und keine anderen als die angegebenen Quellen und Hilfsmittel verwendet habe. Die wörtlichen oder sinngemäß übernommenen Zitate habe ich als solche kenntlich gemacht.

I hereby declare that this Bachelor thesis was generated by myself and that I not used any other resources and references than the ones that were cited and listed. Literal or analogous quotation was designated as such.

Date: 5th of September 2020

Signature:



Tobias Pfennig